2017 Coastal Master Plan

Appendix C – Modeling

Attachment C3-25.1

Storm Surge and Risk Assessment Appendices

DRAFT

Report: DRAFT Version 1

Date: July 2015

Prepared By: Hugh Roberts and Zachary Cobell

Appendices for C3-25.1 - Storm Surge and Risk Assessment

Appendix 1: ADCIRC+SWAN Model Updates and Validation

Appendix 2: Synthetic Storm Suite Simulations

Appendix 3: Raised Feature Elevation Interpolation Sensitivity Analysis

Appendix 4: Sector-Based Wind Drag Analysis

Appendix 5: Asymmetric Hurricane Literature Review

DRAFT

Appendix 1: ADCIRC+SWAN Model Updates and Validation

Introduction

As part of the 2017 Coastal Master Plan improvement process, the CPRA2012 (Cobell et al., 2013) ADvanced CIRCulation (ADCIRC) and Simulating Waves Nearshore (SWAN) models, referred to as ADCIRC+SWAN, were updated to improve the representation of storm surge across Louisiana while maintaining the mission of providing a high-speed, physics-based modeling approach. The model geometry was updated in three critical ways: geometry enhancements to account for features that were underrepresented, additional model resolution in areas that enhance model skill, and inclusion of protected areas. With these enhancements in place, the model is now referred to as the CPRA2017 ADCIRC+SWAN model.

After applying the aforementioned updates, the model was validated using Hurricane Ike (Ike; 2008) and Hurricane Gustav (Gustav; 2008) observations like the CPRA2012 ADCIRC+SWAN model. Additionally, the CPRA2017 model was compared to observations collected during Hurricane Katrina (Katrina; 2005) and Hurricane Rita (Rita; 2005). For the purposes of validation, the geometry of the CPRA2017 model was altered to remove major features that have been constucted since the storms occurred, such as the Seabrook Gate, the Inner Harbor Navigation Canal Lake Borgne Surge Barrier, and the Gulf Intracoastal Waterway West Closure Complex.

Model Geometry Updates

Model geometry was updated to enhance the representation of Louisiana's coast in the model. The geometry was specifically updated in the following ways:

1. **Texas and the Louisiana-Texas Shelf** – Additional model resolution on the continental shelf improves SWAN model performance, specifically in transforming waves from deep water to the more shallow coastal areas. Additionally, increased model resolution in Coastal Texas improves model performance in southwestern Louisiana. Figure 1-1 shows the change in model resolution between CPRA2012 and CPRA2017.

2. **Coastal Mississippi and Alabama** – The model boundary was extended inland to mimic the extent used in the Federal Emergency Management Agency (FEMA) models developed for the Flood Insurance Rate Map (FIRM) development in this area (U.S. Army Corps of Engineers [USACE], 2008b). This allows surge to propagate inland naturally, enhancing model performance for storms and scenarios that result in high flood levels in these areas. Figure 1-2 shows the model with and without the extended model boundary.

3. **Protected Areas** – Areas that were previously excluded from the model in order to reduce computational costs have been introduced to provide both additional numerical accuracy and better visual understanding of model outputs. With the protected areas included, a more accurate head differential across the protection system can be computed in ADCIRC, thereby enhancing the exterior calculation while providing results on the interior as well. (Note: The Coastal Louisiana Risk Assessment [CLARA] model does not directly use ADCIRC results in protected areas.) Figure 1-3 shows the model with and without the protected areas included.

4. **West Shore of Lake Pontchartrain** – Under high sea level rise conditions, the CPRA2012 model boundary was near the edge of surge inundation limits. To prevent possible

boundary effects, the boundary was extended further to the west, and the Mississippi River was extended north to Baton Rouge. Figures 1-1 and 1-3 show this model extension.

5. **Feedback** – Relatively minor changes were made to select areas that were specifically recommended for updates by individuals familiar with the CPRA2012 model or as part of CPRA studies since the 2012 Coastal Master Plan. Updates were based upon available survey and satellite images. The most noteworthy update is near Des Allemandes, which was upgraded as part of a separate CPRA study in the Upper Barataria Basin.

Upon completion of these updates, the CPRA2017 model contained 1.39 million vertices. This is a significant reduction from the current high-resolution model in Louisiana, SL18, which contains 6.9 million vertices. In the following sections, validation results for the CPRA2017 model are analyzed and compared to the SL16 model, the predecessor to SL18. The SL16 model contains 5.0 million vertices, and its validation has been published in multiple journal articles (Dietrich et al., 2011 ; Dietrich et al., 2012).

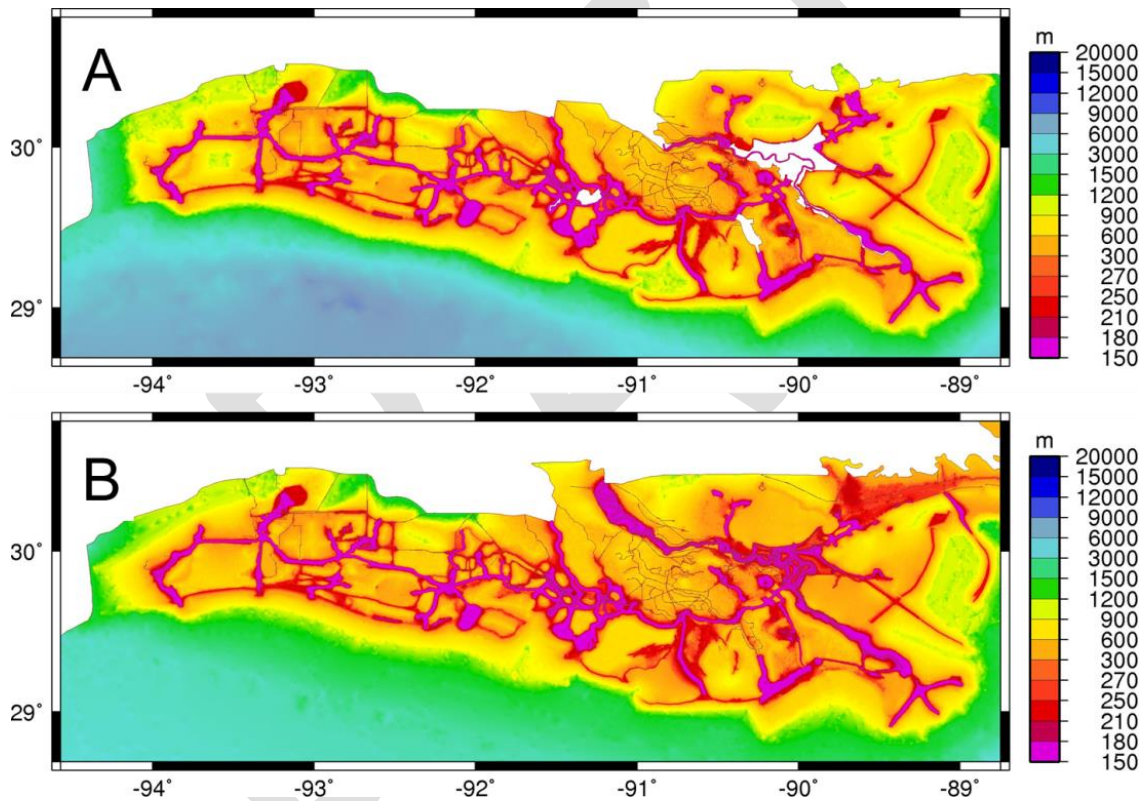

Figure 1-1: (A) CPRA2012 model resolution and (B) CPRA2017 model resolution. Warmer colors indicate greater model resolution.

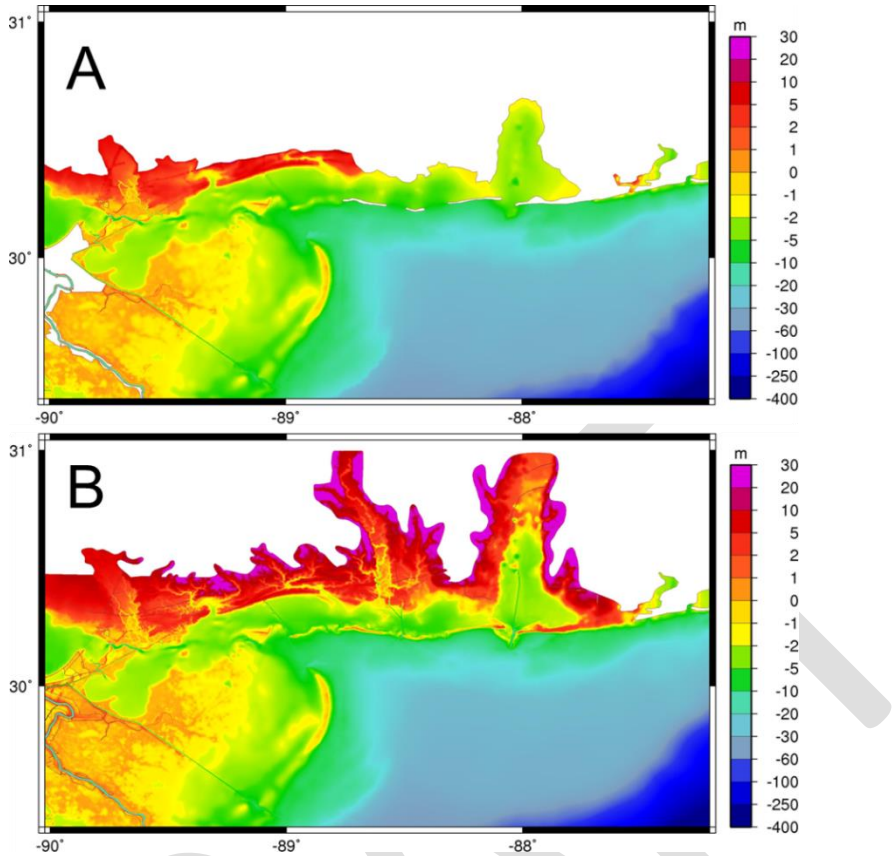

Figure 1-2: Model domain in Mississippi and Alabama for the (A) CPRA2012 and (B) CPRA2017 models. Warmer colors indicate greater elevations.

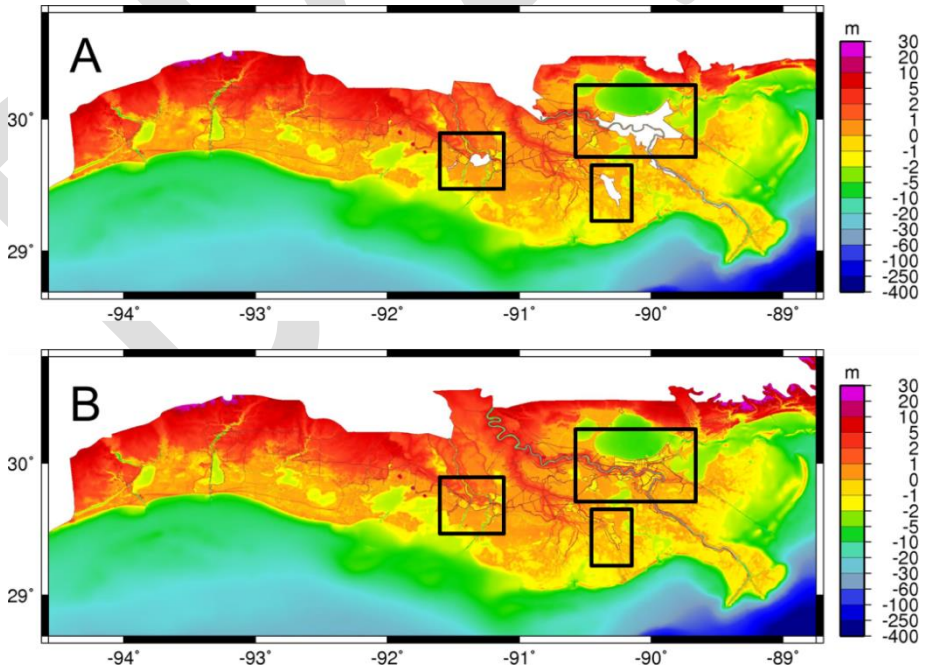

Figure 1-3: Protected areas in the (A) CPRA2012 and (B) CPRA2017 models. Warmer colors indicate greater elevations. Black boxes identify areas of model improvement for CPRA2017.

Model Validation

The 2017CPRA model validation was conducted using the same two storms as were used for the 2012 Coastal Master Plan, Gustav and Ike, as well as two additional storms, Katrina and Rita. Oceanweather, Inc., produced data-assimilated wind, and pressure fields were applied. These Katrina and Rita wind and pressure fields were created during the 2007 FEMA Flood Insurance Study (FIS) in Louisiana, and the Gustav and Ike wind and pressure fields were created during the 2011 FEMA FIS in Texas. The studies were conducted to develop coastal FIRMs in both states (USACE, 2008a; USACE, 2008b; USACE, 2008c; USACE, 2011).

Tidal forcing for the model was provided by the Oregon State University Tidal Database (TPXO 7.2). The constituents Q1, O1, P1, K1, N2, M2, S2, and K2 were used to force the model open boundary as well as tidal potential forcing throughout the model.

River discharges were applied for both the Mississippi and Atchafalaya Rivers. Currently, the ADCIRC model only allows a single flow rate to be applied for the entire simulation and, therefore, an averaged flow rate was applied from measured discharges during the individual events. The Mississippi River discharge was applied at Baton Rouge, Louisiana with measurement from USGS station 07374000. The Atchafalaya River flowrate was applied near Splice Island with the discharge measurement at Simmesport, Louisiana from USGS station 07381490.

The model tidal and river forcings were allowed to reach a dynamic equilibrium for a minimum of 18 days before wind and pressure forcing was applied, during which time the SWAN wave model was not active. Once the wind and pressure information was applied to the model, ADCIRC and SWAN computed hydrodynamic and wave calculations, respectively, passing information between the models every 10 minutes. The wind velocity vectors were applied to the water surface in both the ADCIRC and SWAN model using the wind drag formulation described in Appendix 4.

Note that the 2005 and 2008 model versions removed various newly constructed protection features to reflect the conditions under which these storms occurred.

The model was validated with data from the following sources:

- National Oceanographc and Atmospheric Administration (NOAA) water level measurement time series;
- USACE water level measurement time series;
- Coastal Studies Institute (CSI) wave information and water level information;
- Andrew Kennedy (Kennedy et al., 2011) deployed gages in the path of both Gustav and Ike in 2008. These gages measure both wave information and water level information;
- United States Geological Survey (USGS) water level measurement time series;
- Coastwide Reference Monitoring System (CRMS) water level measurement time series; and
- High water mark measurements collected post-storm by FEMA, USACE, and their contractors.

Unless otherwise noted, the data used in this study are the same as used in Dietrich et al., 2012.

Hurricane Katrina (2005)

Katrina entered the Gulf of Mexico (Gulf) and quickly became a Category 5 storm while approaching Louisiana. Shortly after weakening to a Category 3 storm, Katrina turned north across the Mississippi River Delta, making landfall and building surge against the Mississippi River levees and the Greater New Orleans hurricane protection system. The storm continued north before making another landfall in Mississippi and eventually degrading while moving north across the southern United States.

The CPRA2017 model simulation of Katrina began on August 7, 2005, and concluded on August 31, 2005. River discharges of 171,000 cubic feet per second (cfs) and 73,000 cfs were applied for the Mississippi and Atchafalaya River model boundaries, respectively. Other freshwater inputs such as the Pearl River are not included in the model setup due to model resolution limitations. The lack of freshwater inputs may impact water surface elevation calculations locally. However, the Mississippi and Atchafalaya Rivers are included to ensure that regional impacts from the large river basins are included in the analyses.

Katrina provides an excellent test for the updated model, particularly because of the observed storm surge elevations in Missiissippi and Alabama, which can be used to validate the recently added portions of the model domain. Many of the measured high water marks are concentrated in this region.

Figure 1-4 shows the maximum computed surge from the ADCIRC+SWAN model, and Figure 1-5 shows the maximum computed significant wave height. Figures 1-6 through 1-8 show gage locations used for the validation of all four storms. Table 1-1 reflects the station names as they relate to the numbers shown in these figures. Figures 1-9 through 1-11 show the comparison to National Data Buoy Center (NDBC) wave gages. Figures 1-12 and 1-13 show the water level comparisons to gage data. Comparisons to high water mark information are shown in Figures 1-14 and 1-15. For this storm, high water mark data were available in Mississippi as well as Louisiana. Figures 1-14 and 1-15 include high water marks west of High 110 near Biloxi, Mississippi. The ADCIRC model resolution east of Biloxi Bay is more coarse than areas west of the bay in order to minimize computational costs. Previous studies, including analyses of a barrier from New Orleans to the Pearl River Basin, have shown that projects in Louisiana have very limited, if any, impacts on storm surge levels east of Biloxi Bay (Ben C. Gerwick, Inc., 2012).

DRAFT

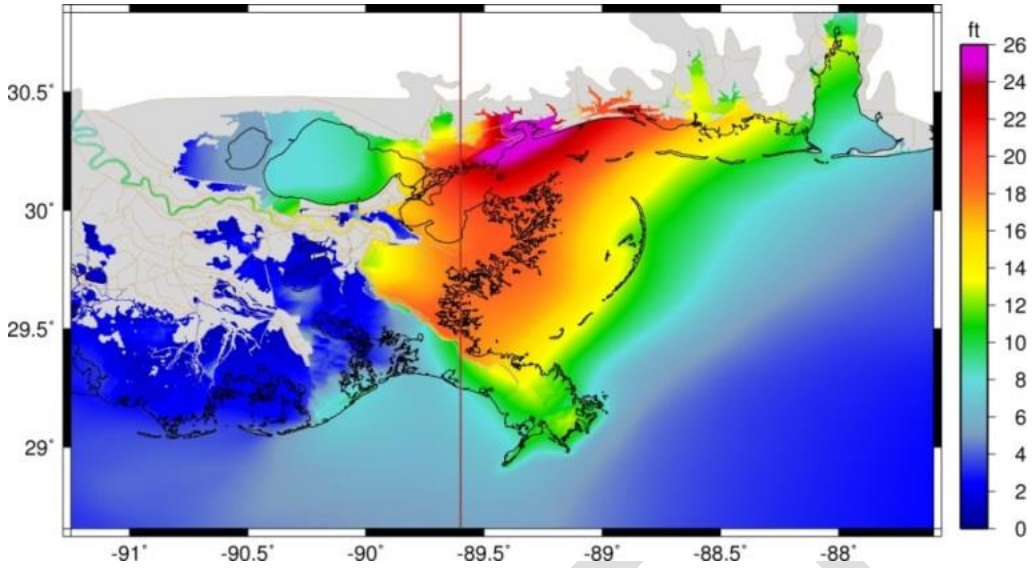

Figure 1-4: Maximum storm surge elevation (ft, NAVD88) during the 2017CPRA Hurricane Katrina simulation. Storm track shown in brown.

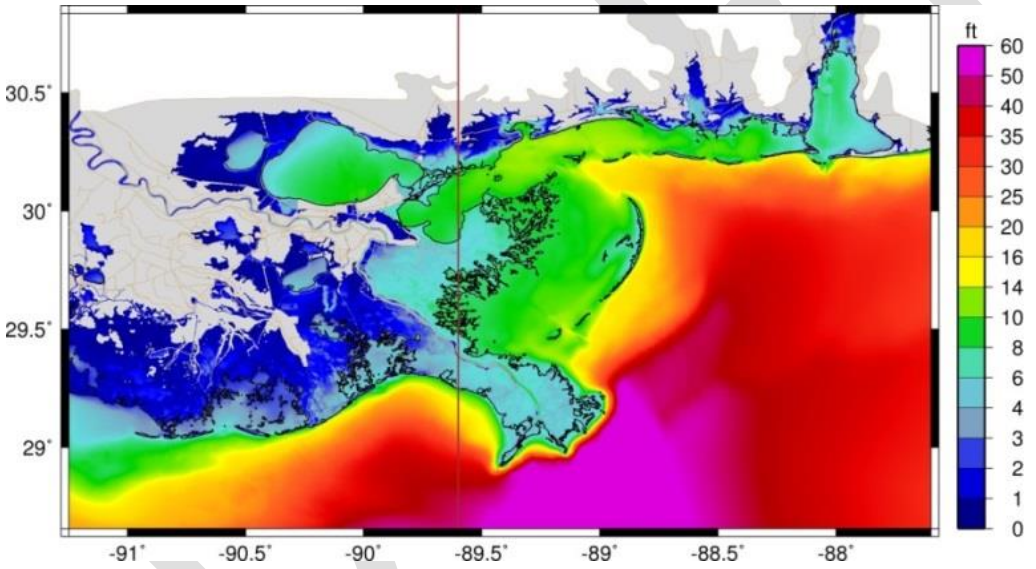

Figure 1-5: Maximum significant wave height (ft) during the 2017CPRA Hurricane Katrina simulation. Storm track shown in brown.

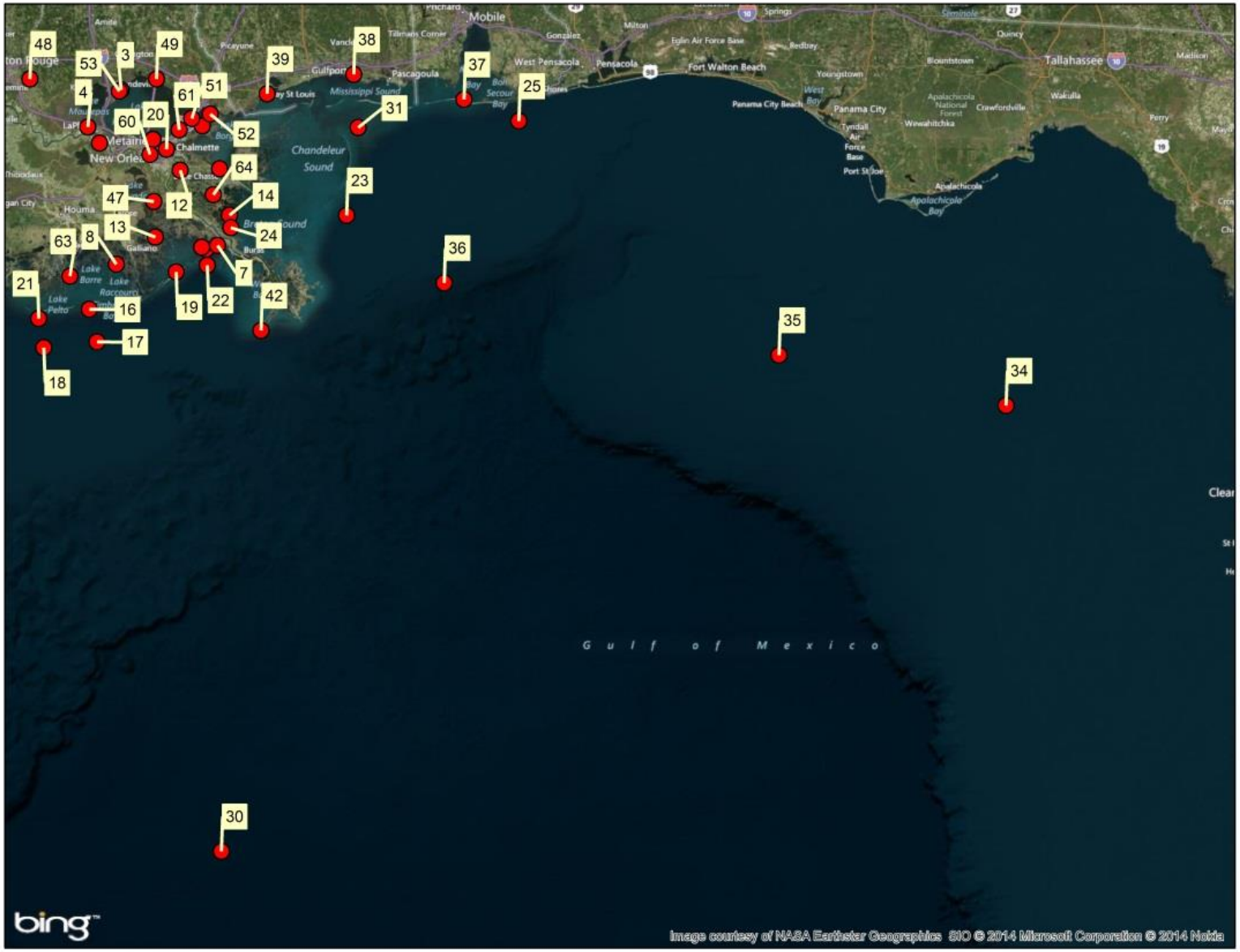

Figure 1-6: Gage locations used for CPRA2017 model validation.

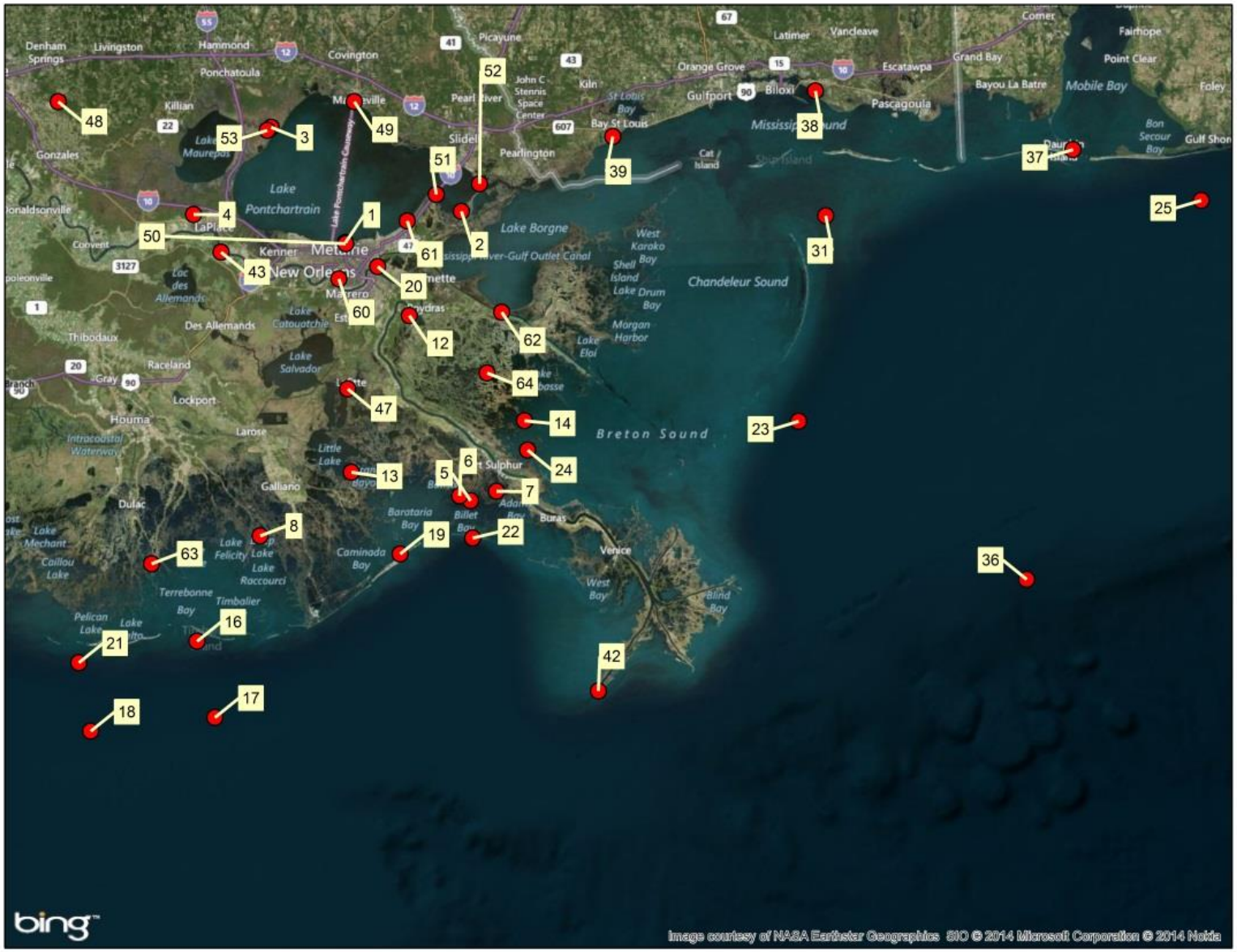

Figure 1-7: Gage locations used for the CPRA2017 model validation.

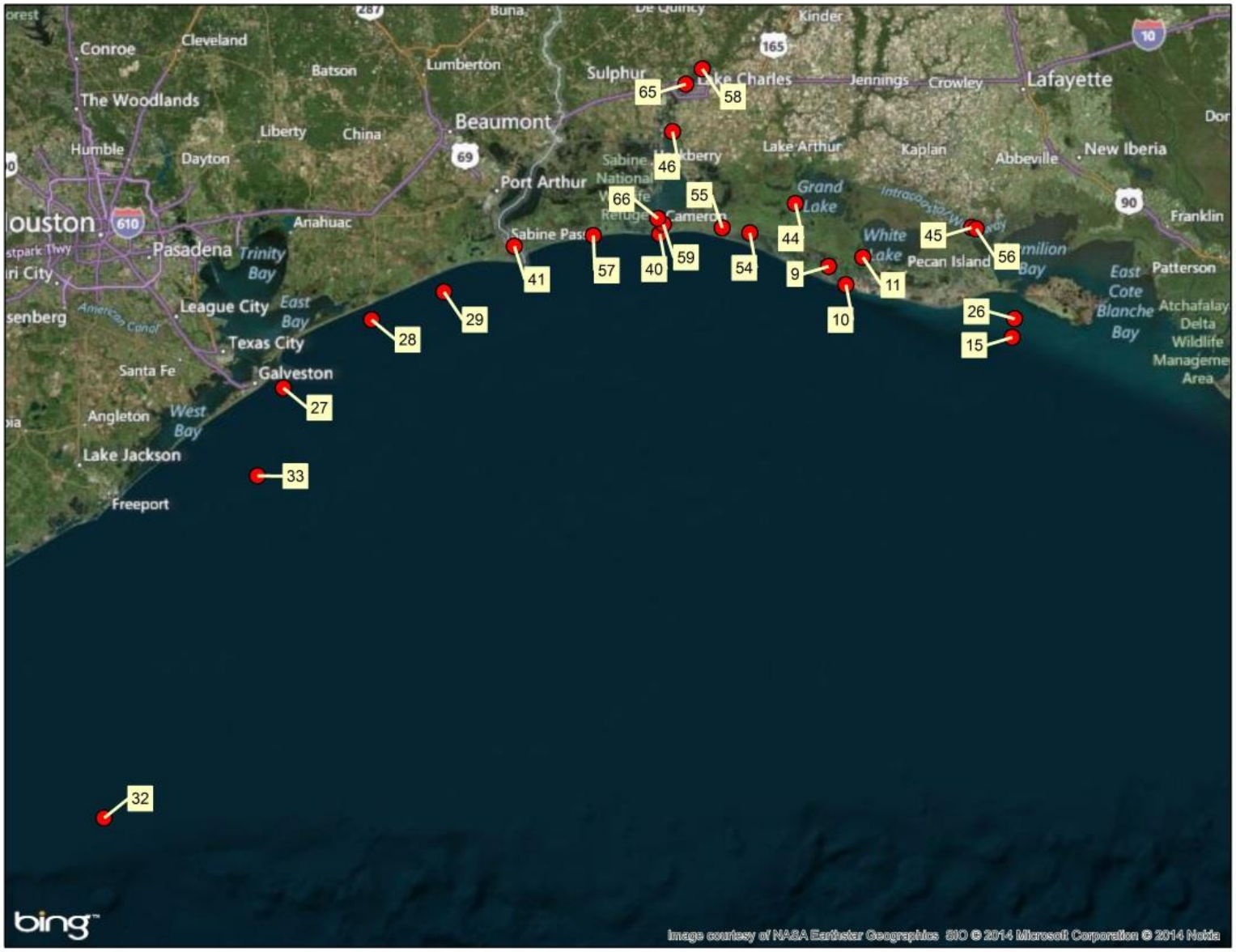

Figure 1-8: Gage locations used for the CPRA2017 model validation.

Table 1-1: CPRA2017 Validation Gages

Station Number	Longitude	Latitude	Name
1	-90.117000	30.025000	17th Street Canal (USACE)
2	-89.791547	30.100333	CRMS 0002-H01
3	-90.325165	30.303964	CRMS 0030-H01
4	-90.543070	30.093135	CRMS 0059-W01
5	-89.765495	29.397287	CRMS 0174-H01
6	-89.796239	29.408751	CRMS 0176-H01
7	-89.692874	29.419984	CRMS 0272-H01
8	-90.355854	29.311394	CRMS 0337-H01
9	-92.728166	29.665219	CRMS 0581-H01
10	-92.665070	29.606958	CRMS 0599-H01
11	-92.604395	29.693726	CRMS 0626-W01
12	-89.937500	29.847779	CRMS BS08-30
13	-90.100000	29.466667	CRMS DCPBA07
14	-89.614445	29.592222	CRMS DCPBS03
15	-92.061333	29.441167	CSI 03
16	-90.533333	29.053333	CSI 05
17	-90.483333	28.866667	CSI 06
18	-90.832000	28.833167	CSI 15
19	-89.963300	29.267100	Grand Isle (NOAA)
20	-90.026397	29.966639	IHNC Lock(USACE)
21	-90.865100	29.001033	Kennedy 1
22	-89.759817	29.306183	Kennedy 11
23	-88.844850	29.590567	Kennedy 12
24	-89.605633	29.520317	Kennedy 13
25	-87.715150	30.127117	Kennedy 19
26	-92.053183	29.499367	Kennedy 6
27	-94.708950	29.281267	Kennedy X
28	-94.388400	29.496333	Kennedy Y
29	-94.125333	29.584683	Kennedy Z
30	-89.667000	25.900000	NDBC 42001
31	-88.769000	30.090000	NDBC 42007
32	-95.360000	27.913000	NDBC 42019
33	-94.803000	29.003000	NDBC 42035
34	-84.517000	28.500000	NDBC 42036
35	-86.008000	28.791000	NDBC 42039
36	-88.205000	29.205000	NDBC 42040
37	-88.075000	30.250000	NOAA 8735180
38	-88.798330	30.391670	NOAA 8743281

DRAFT

Station Number	Longitude	Latitude	Name
39	-89.366700	30.281700	NOAA 8747766
40	-93.341670	29.766670	NOAA 8768094
41	-93.870000	29.728330	NOAA 8770570
42	-89.406700	28.931700	Southwest Pass (NOAA)
43	-90.466131	30.001667	USACE 01275
44	-92.849242	29.862933	USACE 70750
45	-92.209250	29.787019	USACE 76800
46	-93.294886	30.088719	USACE 76960
47	-90.110556	29.669444	USACE 82875
48	-90.922888	30.365797	USACE 85575
49	-90.092289	30.365797	USACE 85575
50	-90.115644	30.022164	USACE 85625
51	-89.861900	30.141700	USGS 300830089515000
52	-89.740600	30.166900	USGS 301001089442600
53	-90.336000	30.296400	USGS 301748090200900
54	-93.014730	29.770570	USGS DEP-LA11
55	-93.114940	29.786100	USGS DEP-LA12
56	-92.192500	29.783110	USGS DEP-LA9B
57	-93.582580	29.761980	USGS DEP-LC11
58	-93.187500	30.284920	USGS DEP-LC2B
59	-93.328860	29.797640	USGS DEP-LC8A
60	-90.135430	29.936750	USGS DEP-SSS-LA-ORL-001
61	-89.943340	30.077170	USGS DEP-SSS-LA-ORL-014
62	-89.678340	29.855790	USGS DEP-SSS-LA-STB-004
63	-90.660810	29.243140	USGS DEP-SSS-LA-TER-024
64	-89.719444	29.708056	USGS PERM-73745257
65	-93.247222	30.236944	USGS PERM-8017044
66	-93.348800	29.815500	USGS PERM-8017118

DRAFT

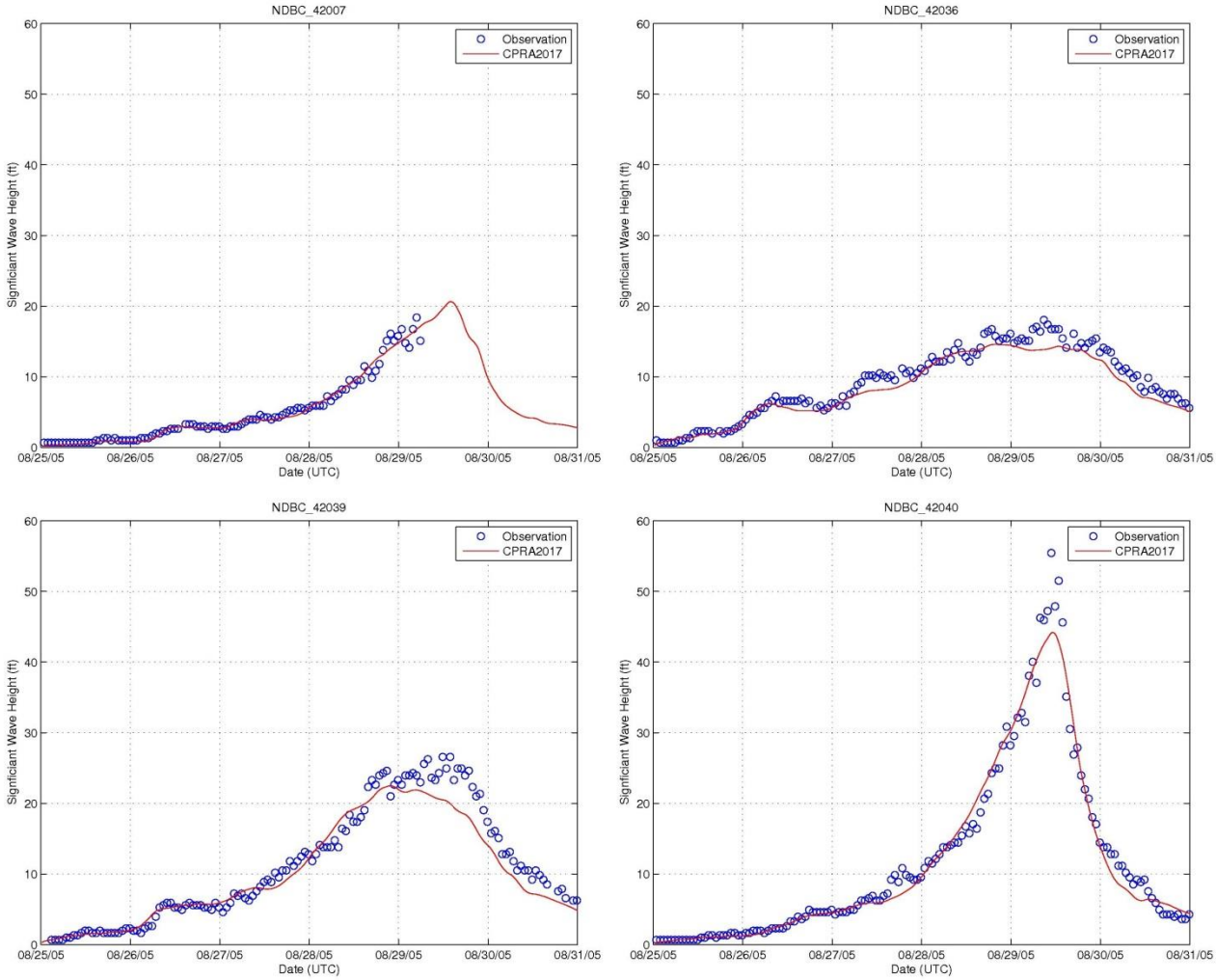

Figure 1-9: NDBC significant wave height comparisons for Hurricane Katrina. Observations are in blue; CPRA2017 model results are in red.

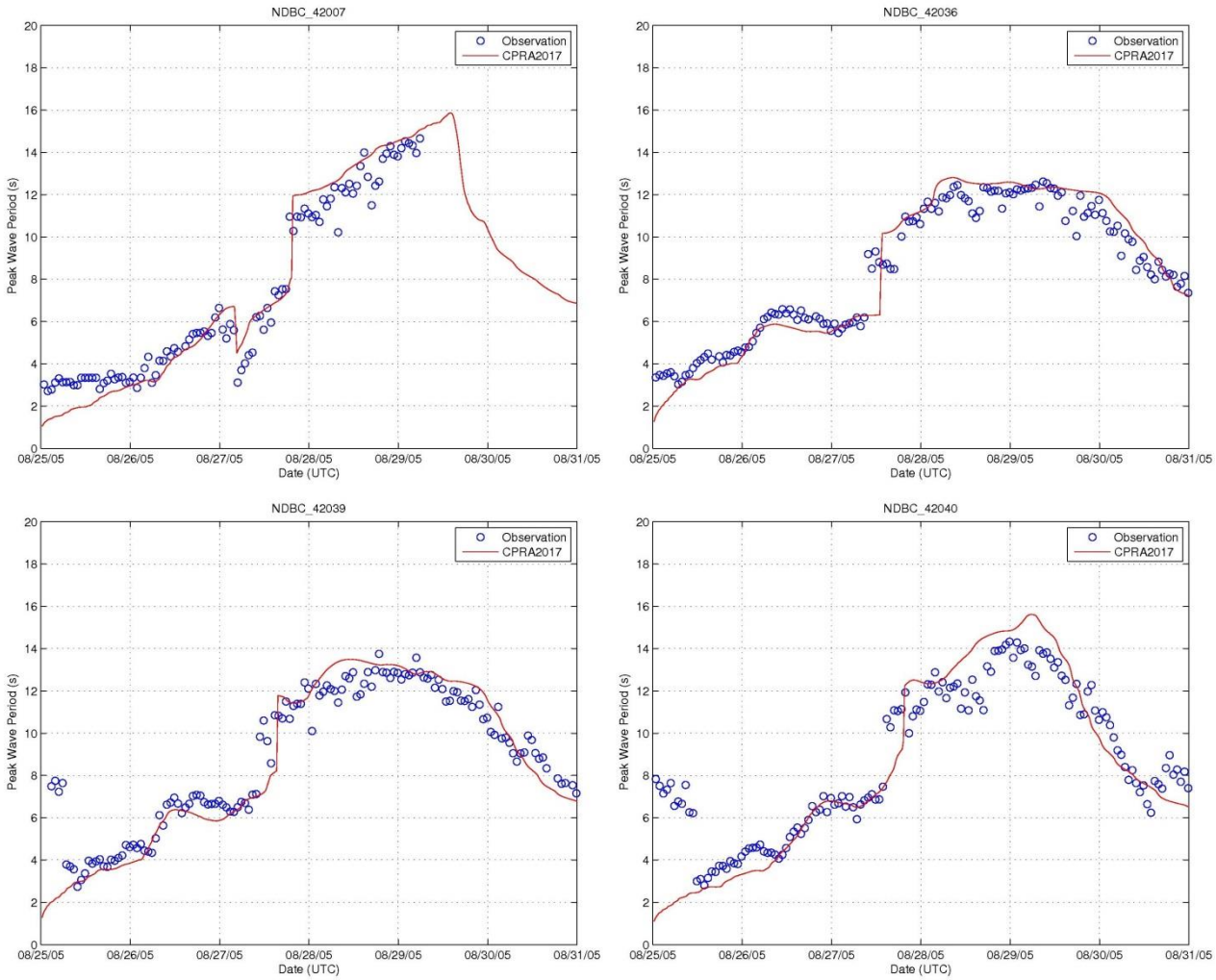

Figure 1-10: NDBC peak wave period comparisons for Hurricane Katrina. Observations are in blue; CPRA2017 model results are in red.

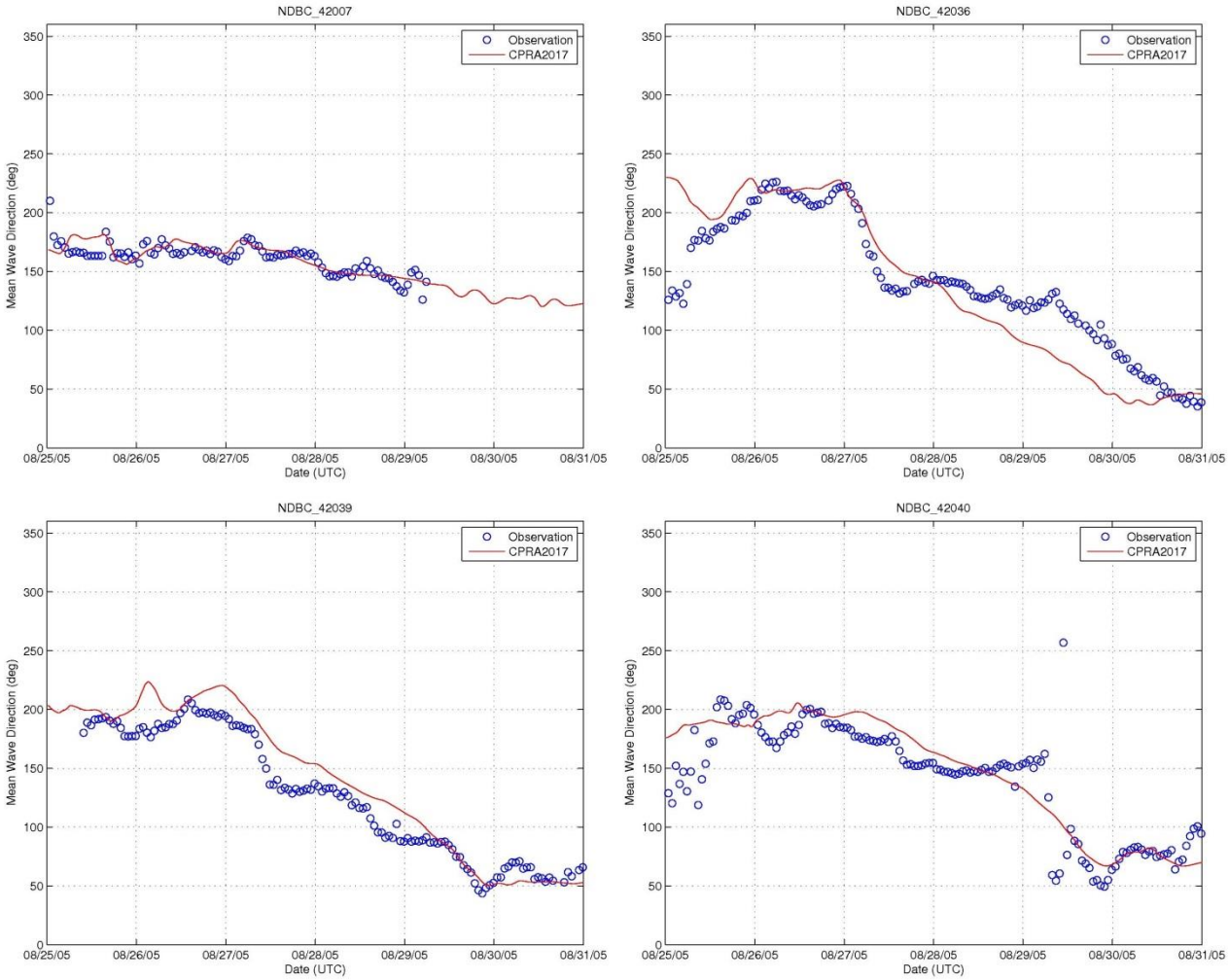

Figure 1-11: NDBC mean wave direction comparisons for Hurricane Katrina. Observations are in blue; CPRA2017 model results are in red.

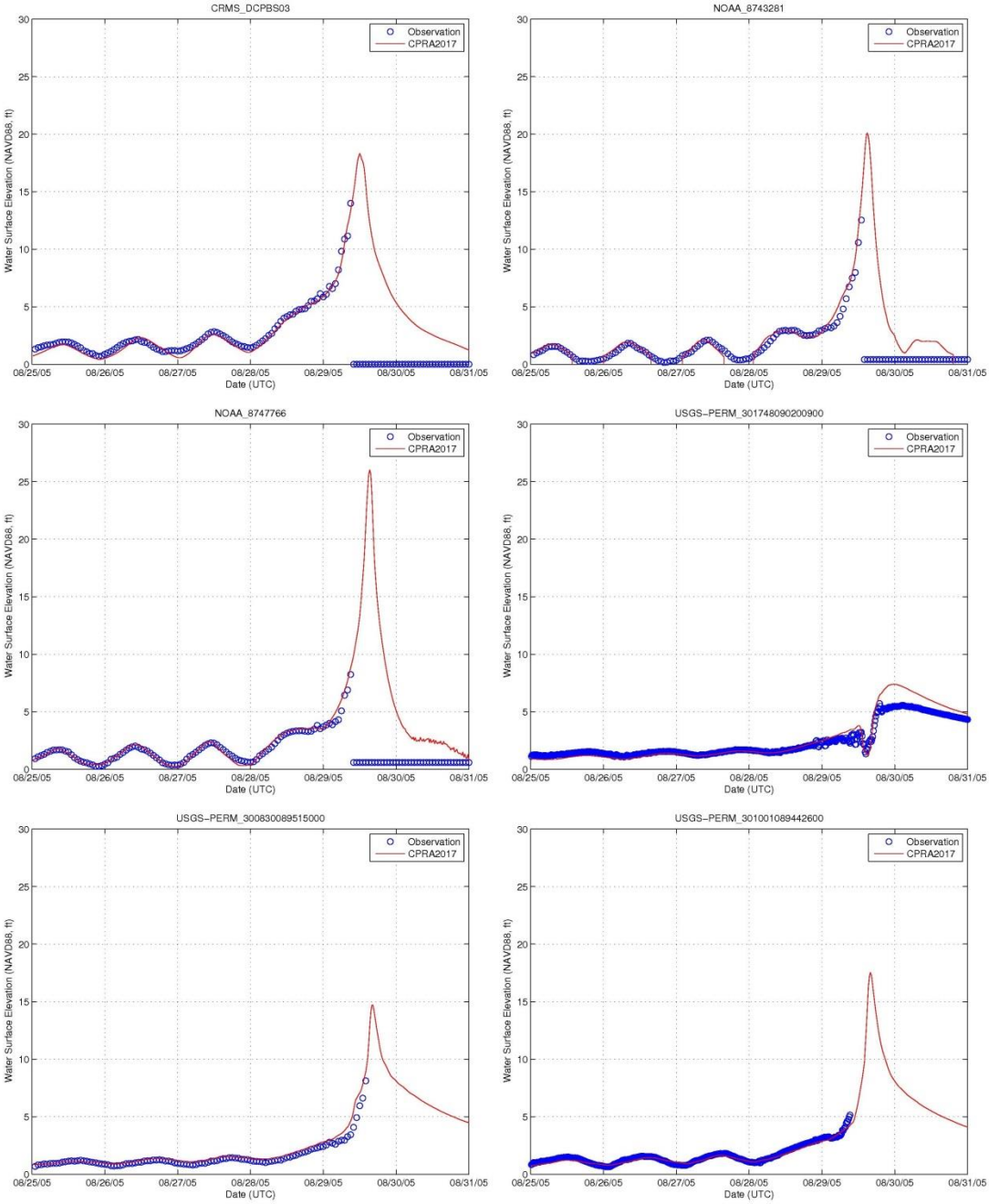

Figure 1-12: Water elevation (ft, NAVD88) comparisons for Hurricane Katrina. Observations are in blue; CPRA2017 model results are in red.

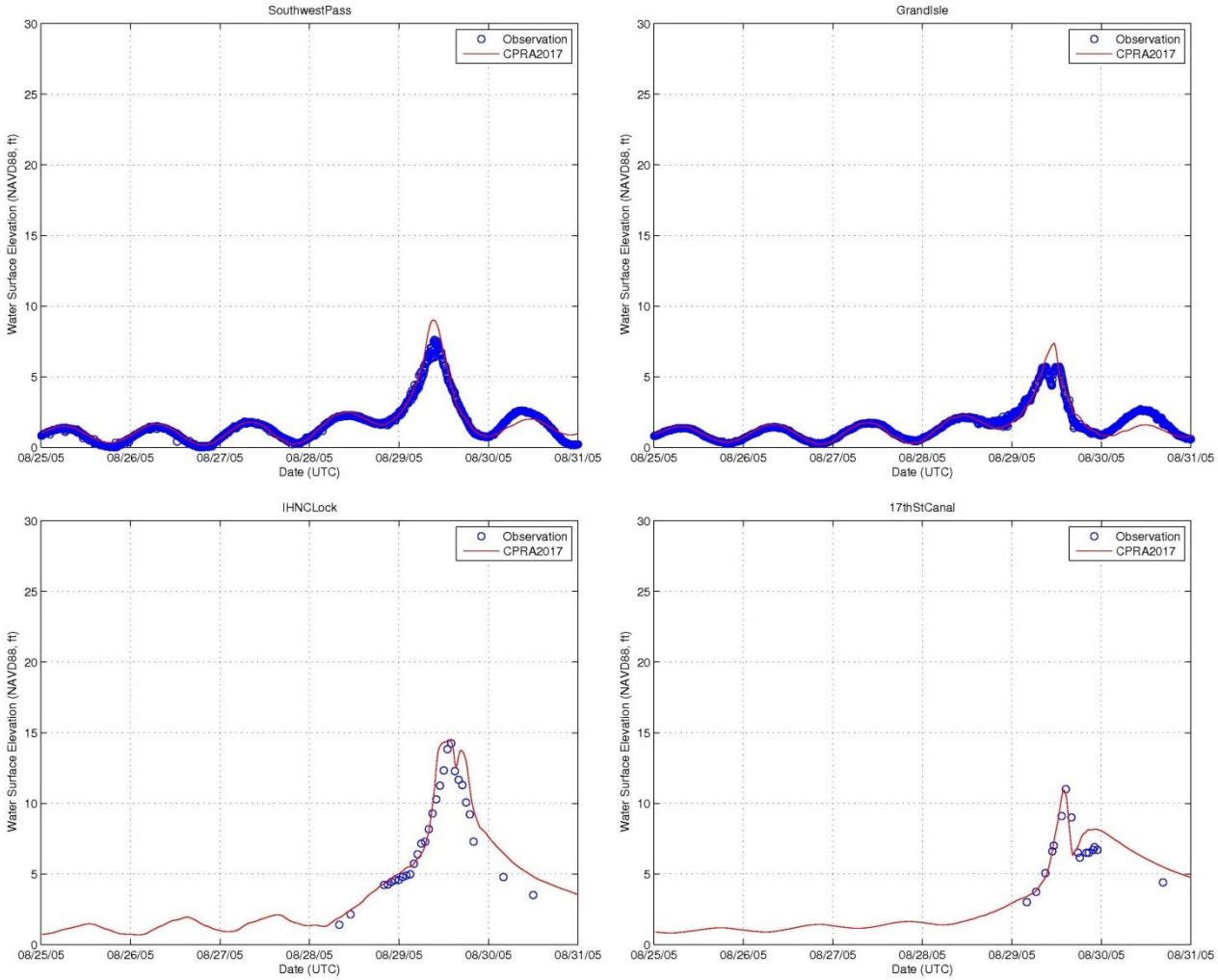

Figure 1-13: Water elevation (ft, NAVD88) comparisons for Hurricane Katrina. Observations are in blue; CPRA2017 model results are in red.

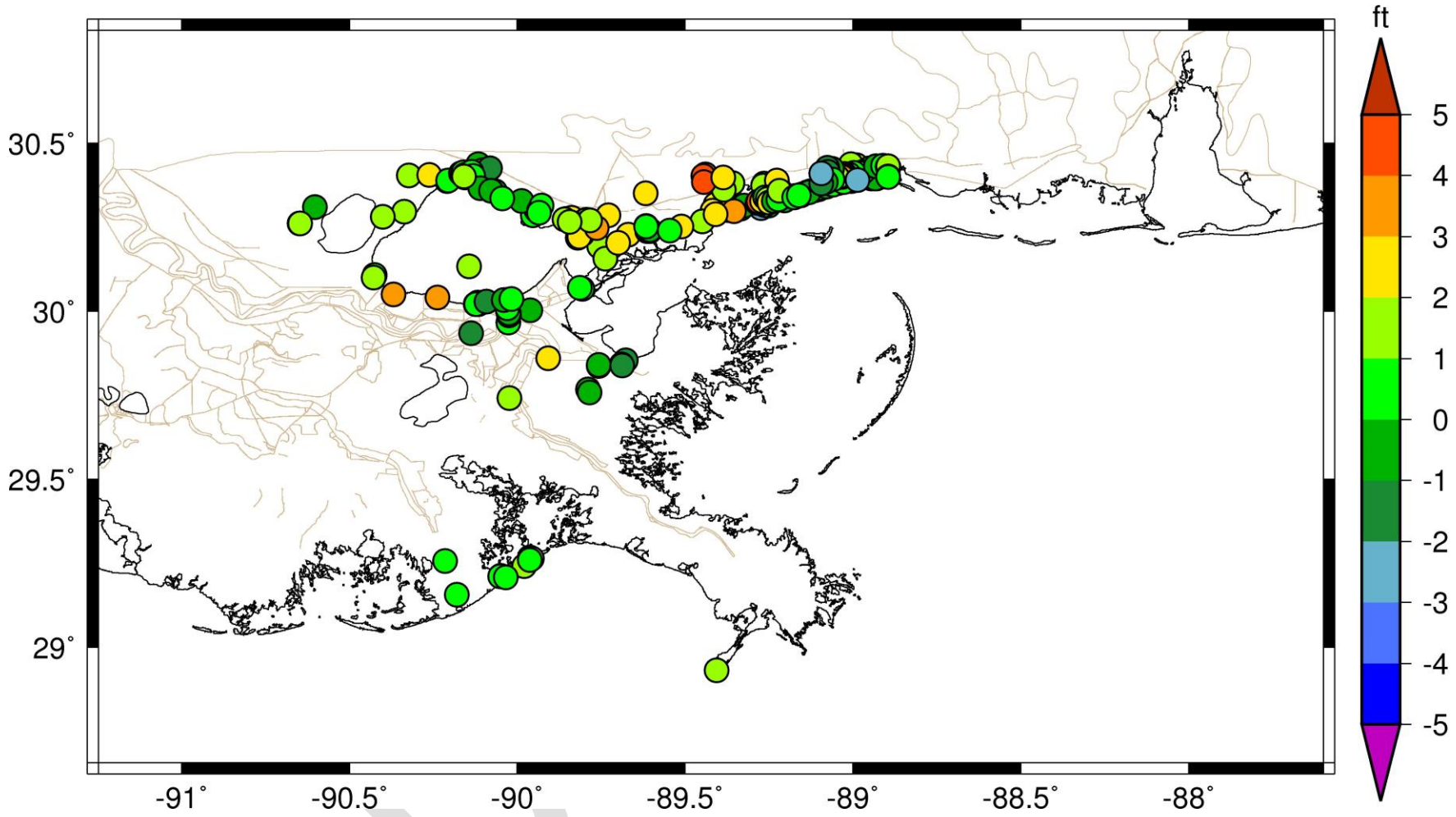

Figure 1-14: CPRA2017 model Hurricane Katrina comparison to measured high water marks. Warm colors indicate the model results are greater than measurement; cool colors indicate the model results are lower than measurement.

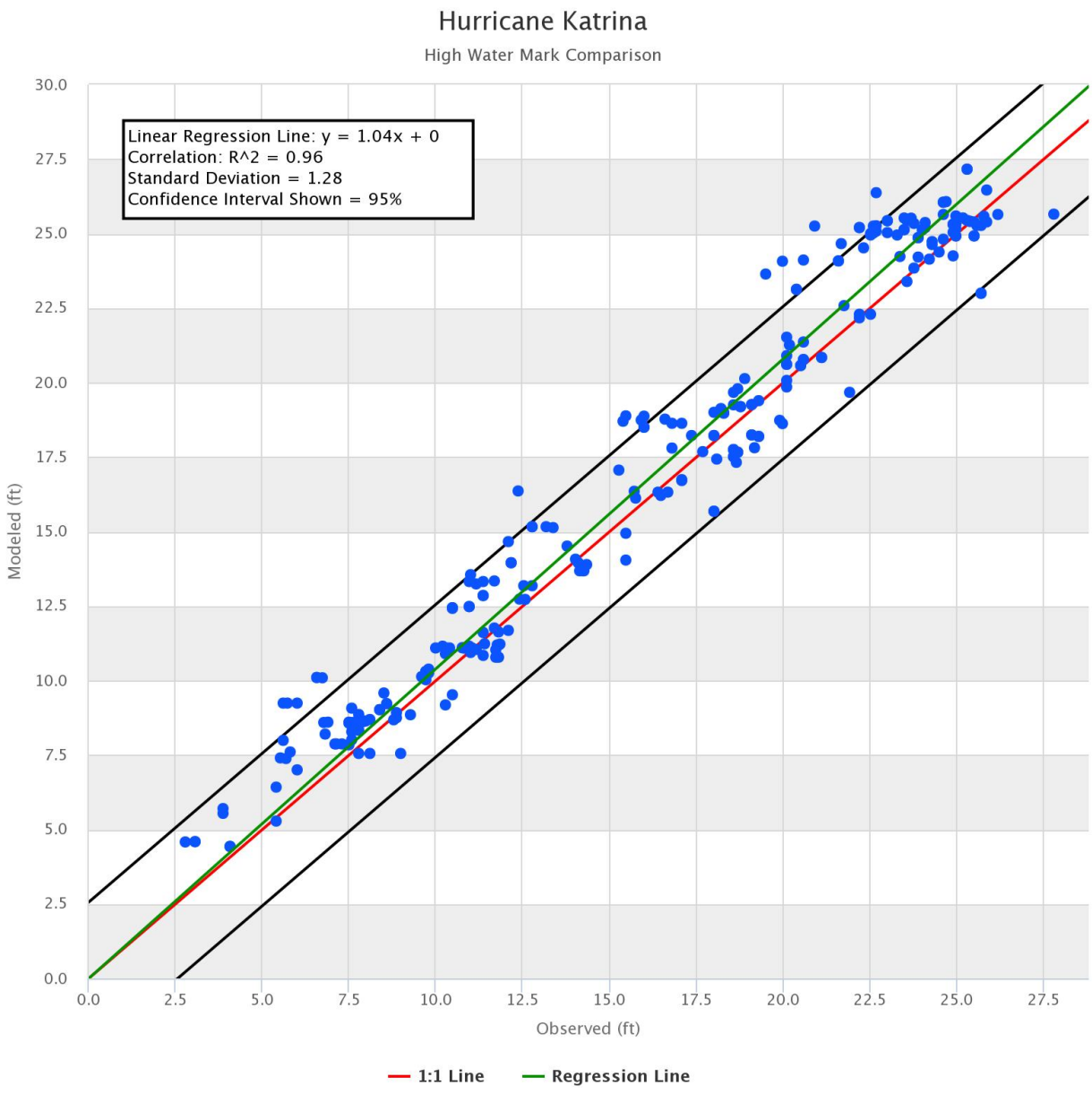

Figure 1-15: Hurricane Katrina regression plot comparing measured high water marks to CPRA2017 model results.

Hurricane Rita (2005)

Rita entered the Gulf, passing between Florida and Cuba. While moving northwest toward Louisiana, warm waters strengthened the storm to Category 5 intensity. However, the storm weakened to a Category 3 before making landfall in western Louisiana near Sabina Pass approximately one month after Katrina.

The CPRA2017 model simulation of Rita began on August 31, 2005, and concluded September 5, 2005. River discharges of 192,000 cfs and 82,000 cfs were used for the Mississippi and Atchafalaya River model boundaries, respectively. Other freshwater inputs such as the Calcasieu River are not included in the model setup due to model resolution limitations.

Figure 1-16 shows the maximum computed surge from the ADCIRC+SWAN model, and Figure 1-17 shows the maximum computed significant wave height. Figures 1-18 through 1-20 show the comparisons to wave measurements. Figure 1-21 shows the comparison to water level measurements. Finally, Figures 1-22 and 1-23 show the comparisons to measured high water marks. One notable deviation from the measurement is seen in the high water mark comparisons west of Lake Calcasieu near where the eye of the storm made landfall. Previous studies have shown simliar trends (Dietrich et al., 2012) The overpredicted water levels have been attributed to wind speeds greater than those which actually occurred during the storm. Unlike the other storms applied for model calibration, the best available Hurricane Rita winds were not developed using data assimilaton in the eye of the storm. Instead parametric wind fields have been applied, which are generally less accurate than data assimilated winds.

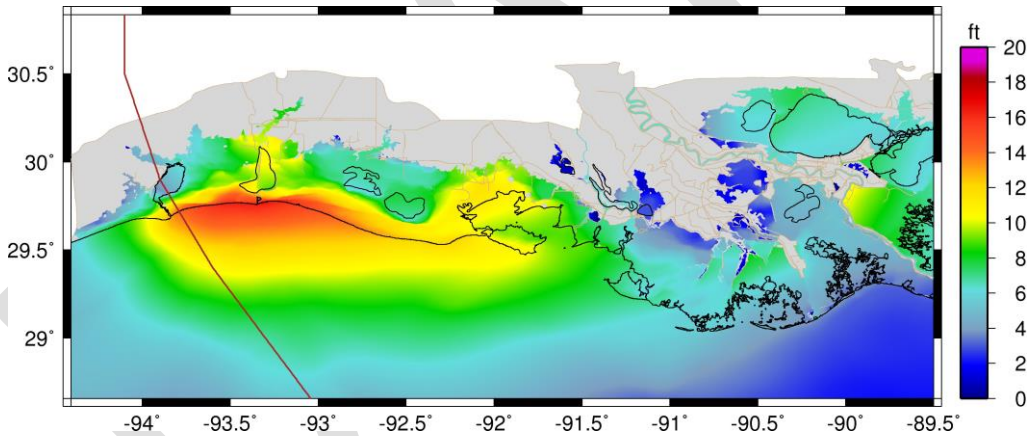

Figure 1-16: Maximum storm surge elevation (ft, NAVD88) during the 2017CPRA Hurricane Rita simulation. Storm track shown in brown.

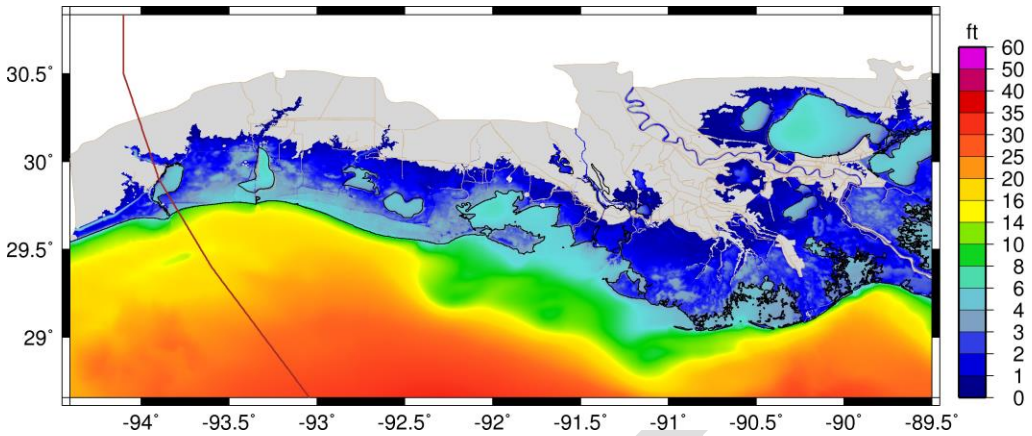

Figure 1-17: Maximum significant wave height (ft) during the 2017CPRA Hurricane Rita simulation. Storm track shown in brown.

DRAFT

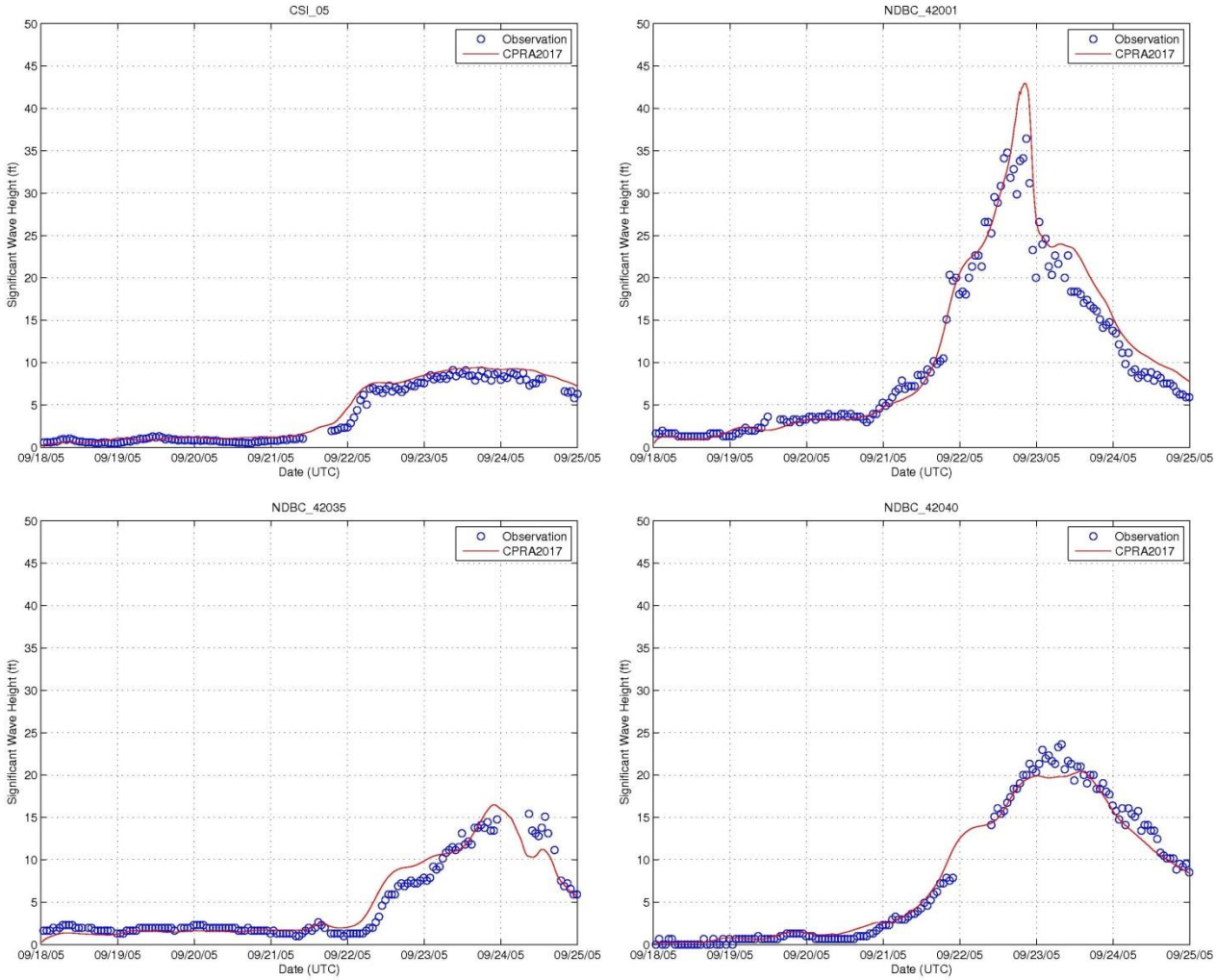

Figure 1-18: NDBC significant wave height comparisons for Hurricane Rita. Observations are in blue; CPRA2017 model results are in red.

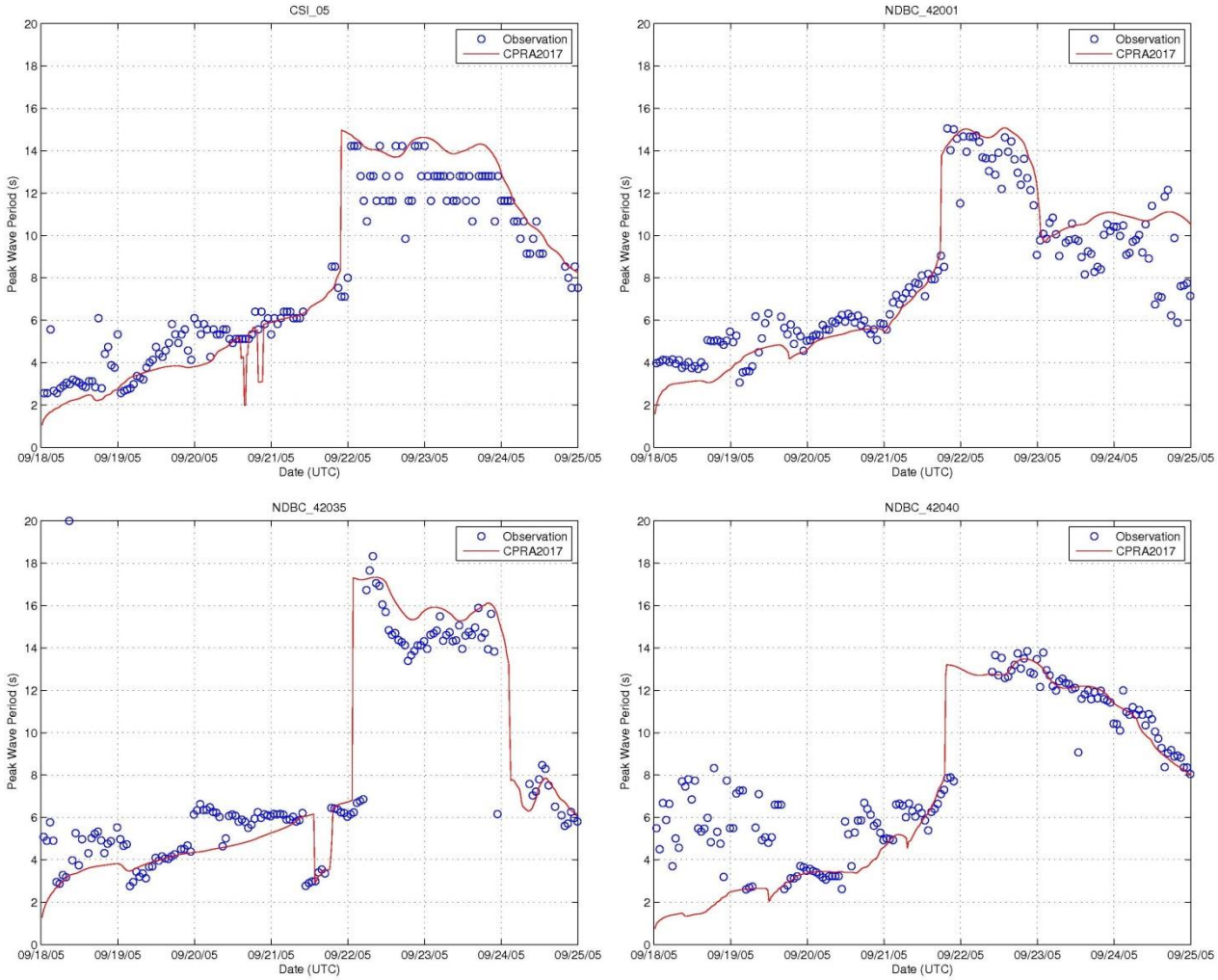

Figure 1-19: NDBC peak wave period comparisons for Hurricane Rita. Observations are in blue; CPRA2017 model results are in red.

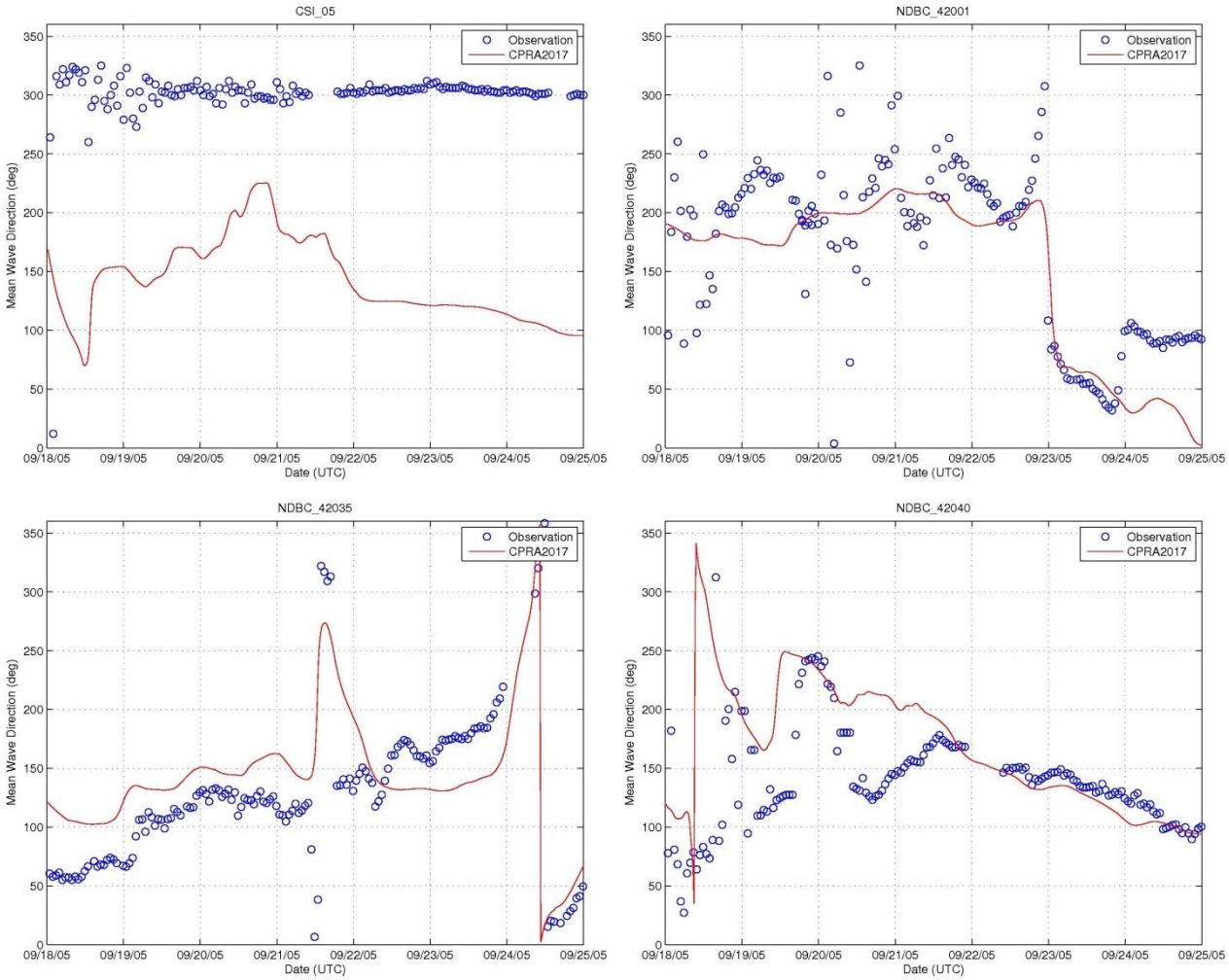

Figure 1-20: NDBC mean wave direction comparisons for Hurricane Rita. Observations are in blue; CPRA2017 model results are in red. Note that observed wave directions at CSI_05 are believed to be a result of incorrect measurement.

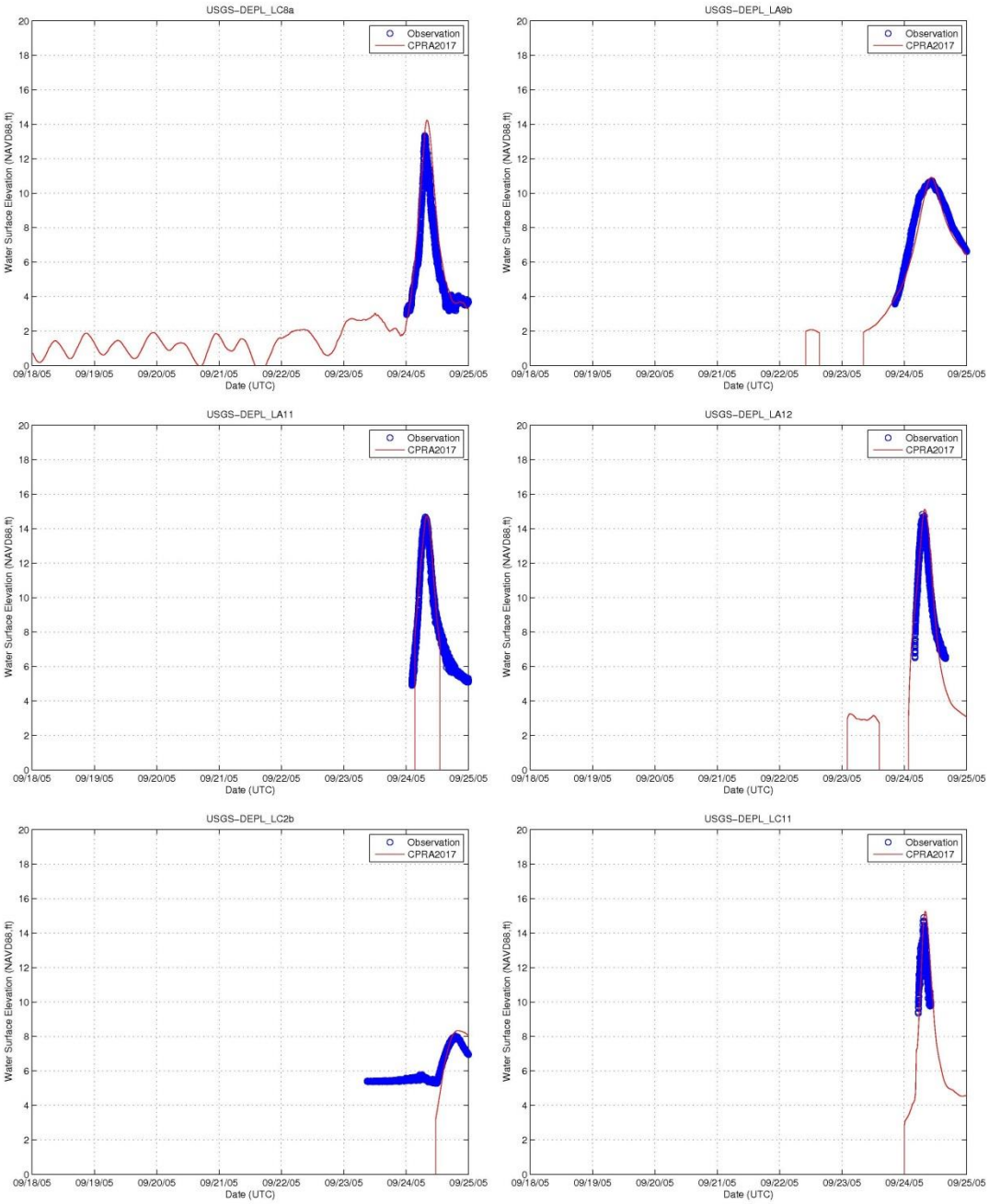

Figure 1-21: Water elevation (ft, NAVD88) comparisons for Hurricane Rita. Observations are in blue; CPRA2017 model results are in red.

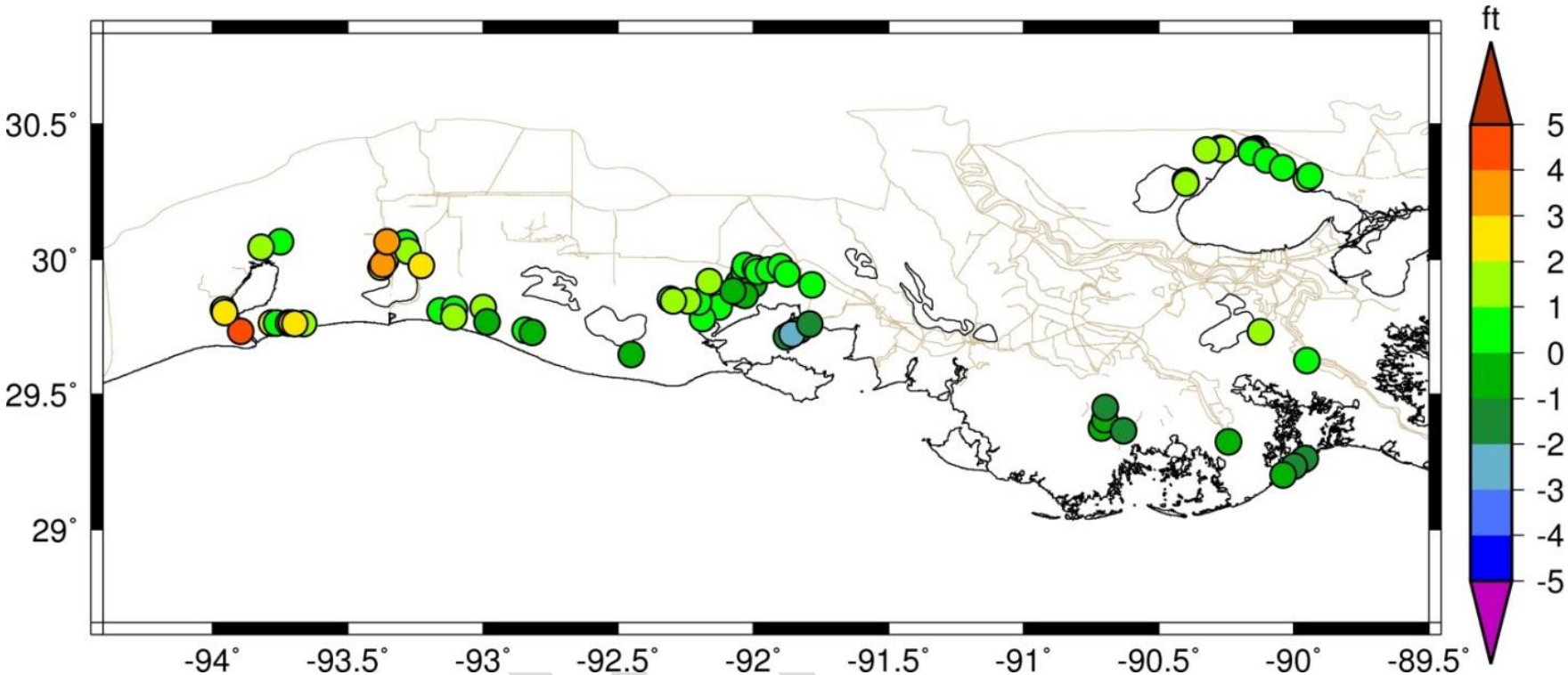

Figure 1-22: CPRA2017 model Hurricane Rita comparison to measured high water marks. Warm colors indicate the model results are greater than measurement; cool colors indicate the model results are lower than measurement.

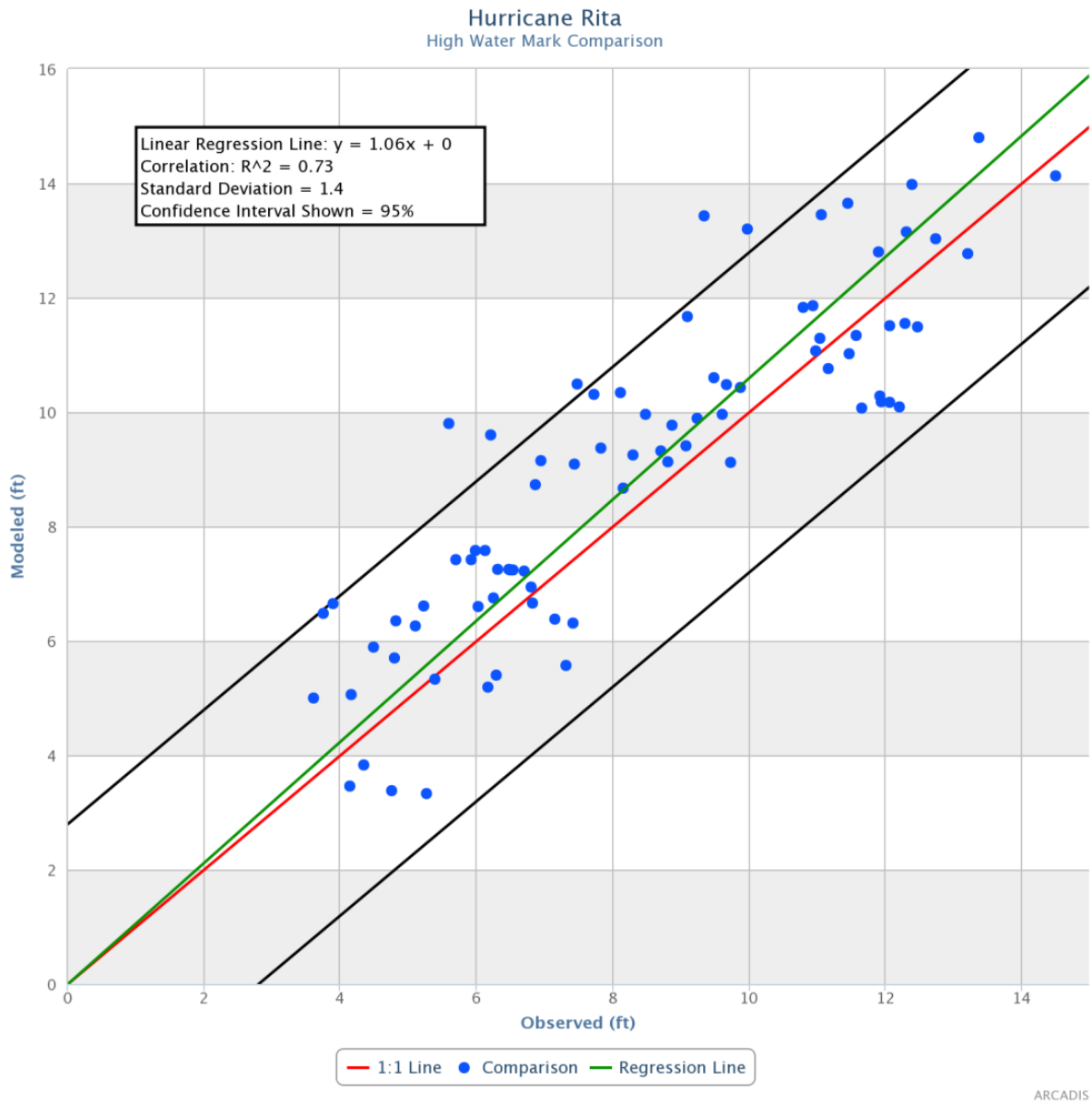

Figure 1-23: Hurricane Rita regression plot comparing measured high water marks to CPRA2017 model results.

Hurricane Gustav (2008)

Gustav spent a short time as a Category 4 hurricane before weakening as it crossed Cuba. On August 31, 2008, three years and two days after Katrina made landfall, Gustav weakened to a Category 2 storm and made landfall near Terrebonne Bay. Gustav continued its northwestern track across the state as a tropical storm until finally making a turn toward the northeast over Arkansas as a tropical depression.

The CPRA2017 model simulation of Gustav began on July 21, 2008, and concluded on September 4, 2008. River discharges of 167,000 cfs and 70,000 cfs were applied to the Mississippi and Atchafalaya River model boundaries, respectively. Other freshwater inputs are not included in the model setup due to model resolution limitations.

Figure 1-24 shows the maximum computed surge from the ADCIRC+SWAN model, and Figure 1-25 shows the maximum computed significant wave height. Figures 1-26 through 1-30 show the time series comparisons of wave data. Figures 1-31 and 1-32 show the comparisons to measured time series water level measurements. Finally, Figures 1-33 and 1-34 show the comparisons to measured high water marks.

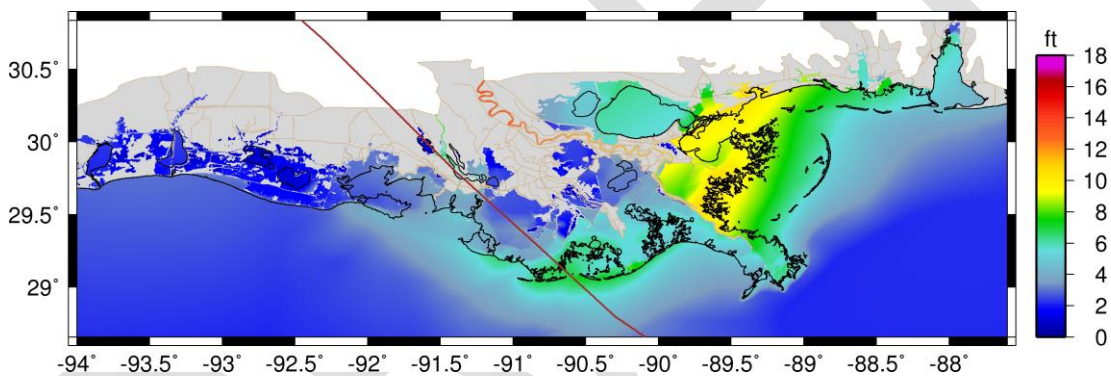

Figure 1-24: Maximum storm surge elevation (ft, NAVD88) during the 2017CPRA Hurricane Gustav simulation. Storm track shown in brown.

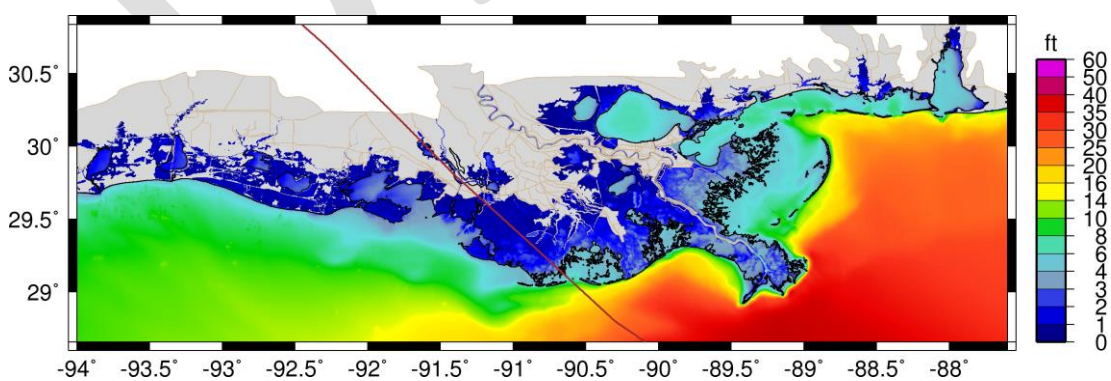

Figure 1-25: Maximum significant wave height (ft) during the 2017CPRA Hurricane Gustav simulation. Storm track shown in brown.

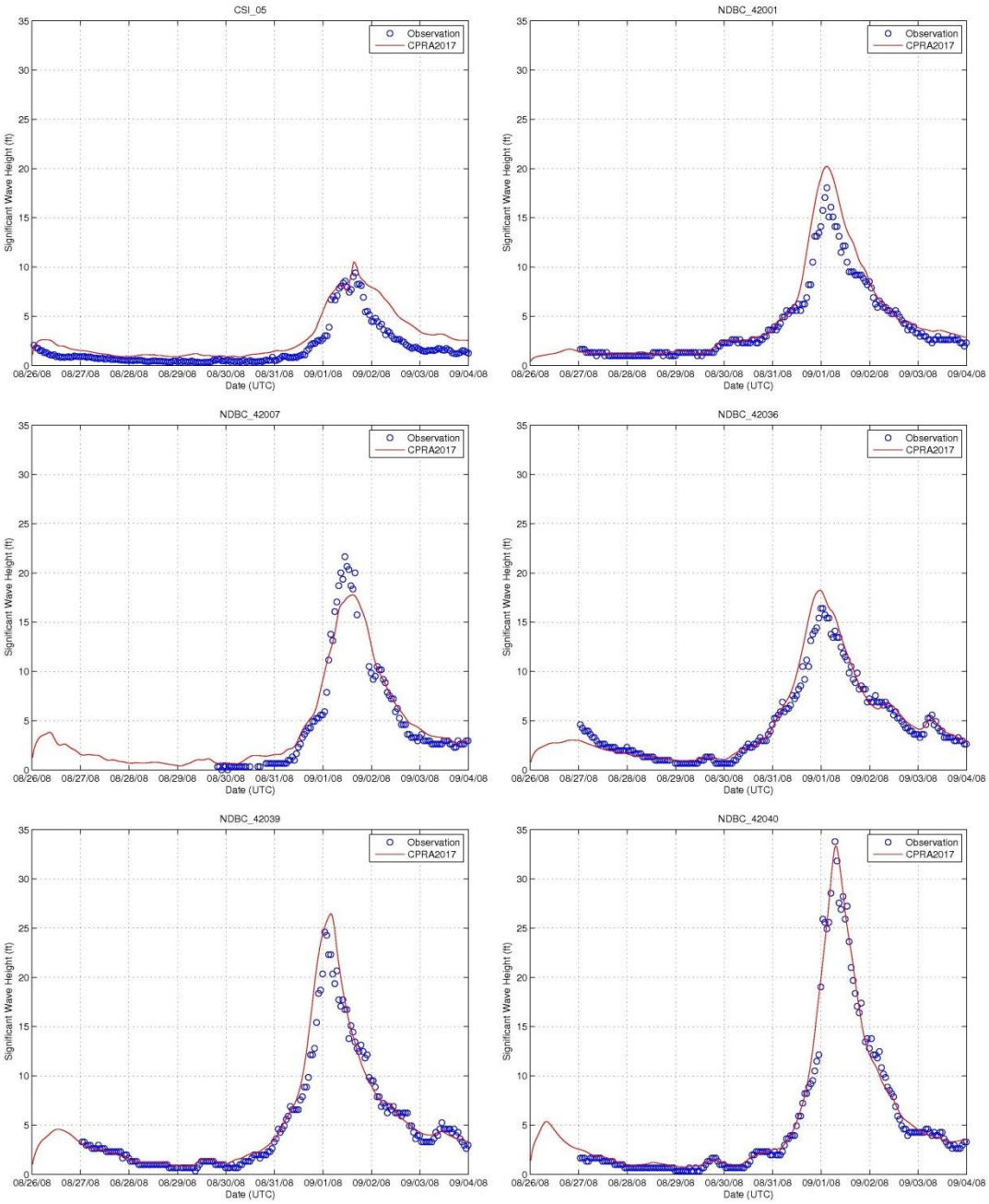

Figure 1-26: NDBC and CSI significant wave height comparisons for Hurricane Gustav. Observations are in blue; CPRA2017 model results are in red.

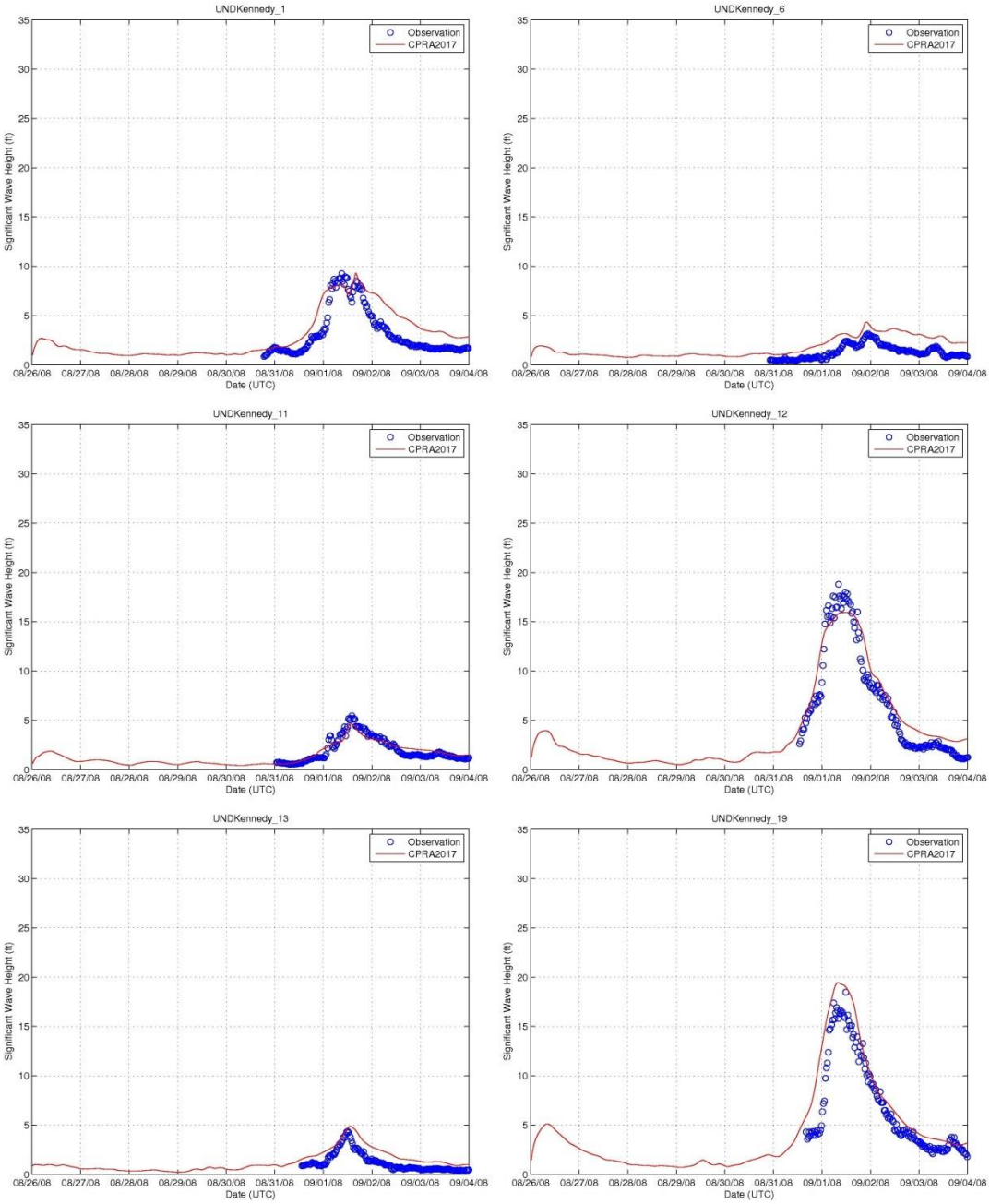

Figure 1-27: Significant wave height comparisons at Andrew Kennedy locations for Hurricane Gustav. Observations are in blue; CPRA2017 model results are in red.

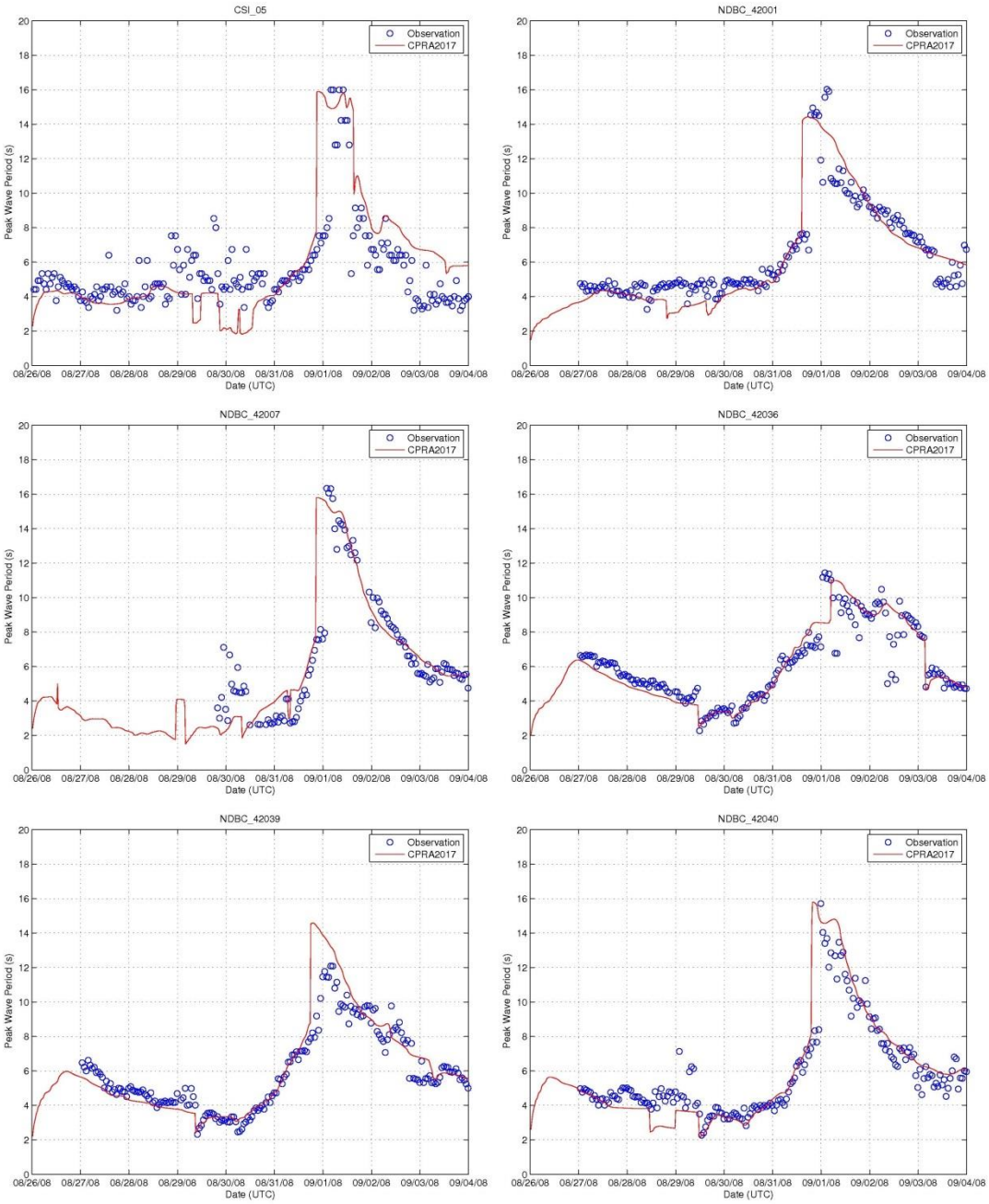

Figure 1-28: NDBC and CSI peak wave period comparisons for Hurricane Gustav. Observations are in blue; CPRA2017 model results are in red.

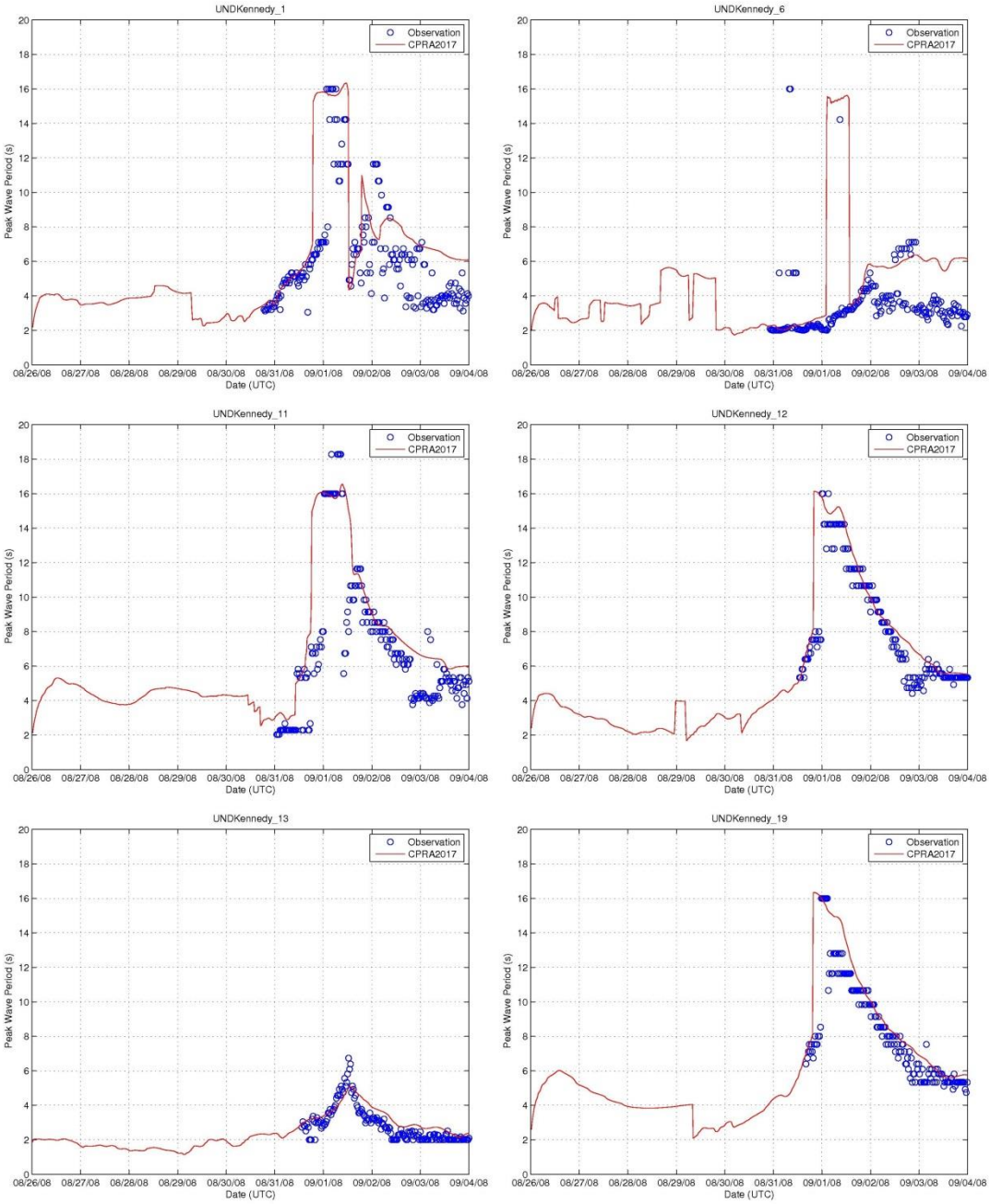

Figure 1-29: Peak wave period comparisons at Andrew Kennedy locations for Hurricane Gustav. Observations are in blue; CPRA2017 model results are in red.

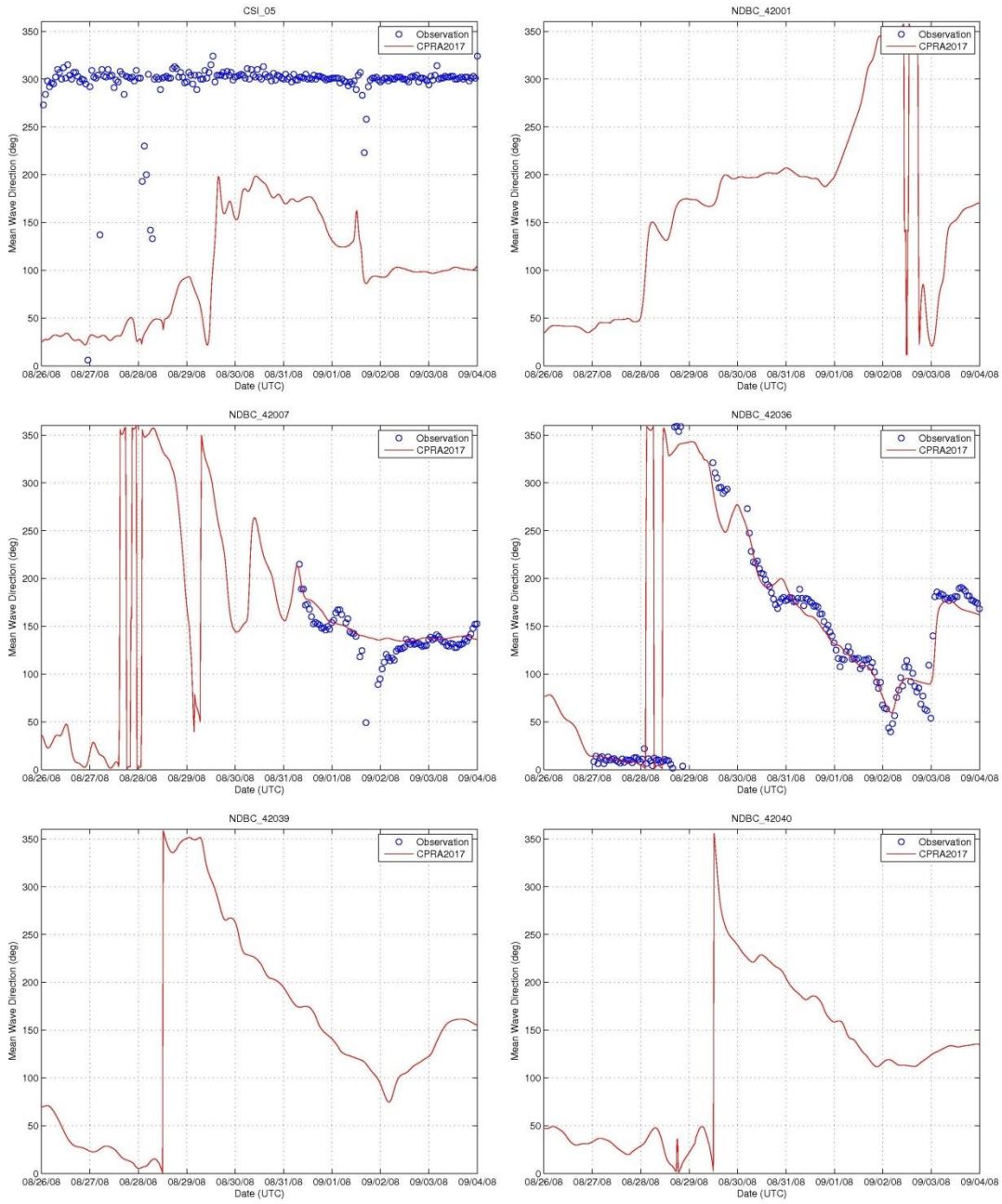

Figure 1-30: NDBC and CSI mean wave direction comparisons for Hurricane Gustav. Observations are in blue; CPRA2017 model results are in red. Note that observed wave directions at CSI_05 are believed to be a result of incorrect measurement.

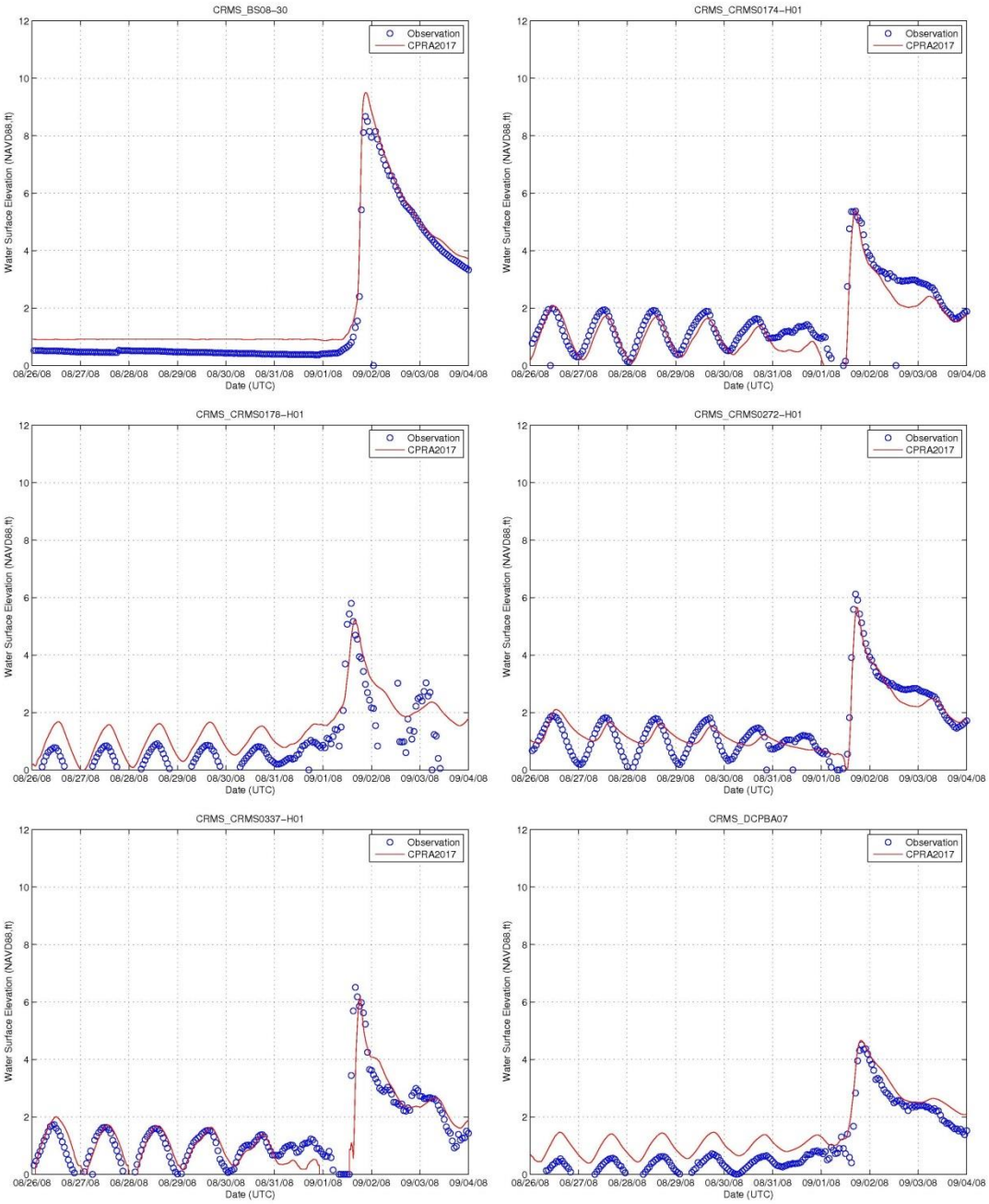

Figure 1-31: Water elevation (ft, NAVD88) comparisons at CRMS stations for Hurricane Gustav. Observations are in blue; CPRA2017 model results are in red.

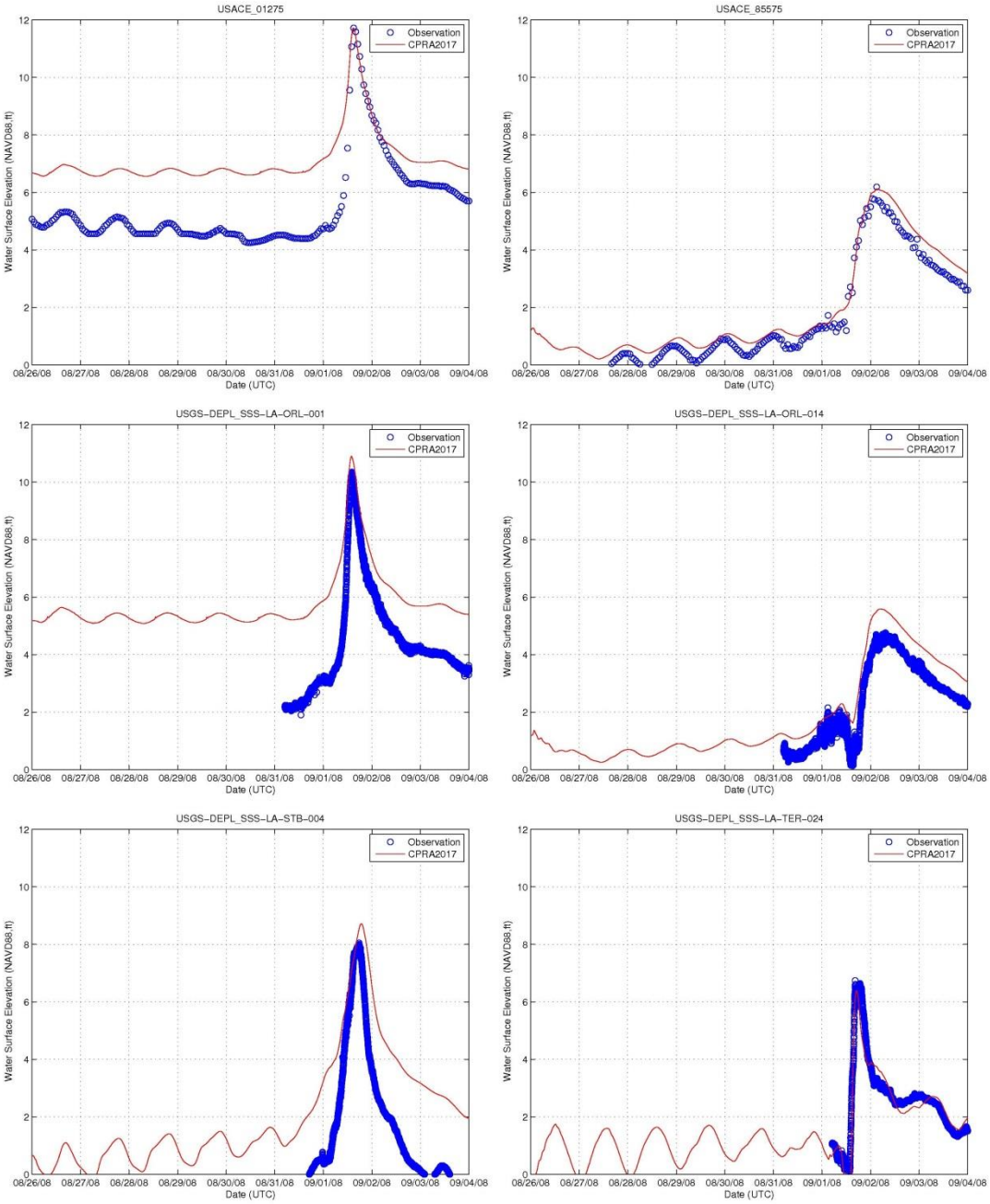

Figure 1-32: Water elevation (ft, NAVD88) comparisons at USGS and USACE stations for Hurricane Gustav. Observations are in blue; CPRA2017 model results are in red. Note that station 01275 and SSS-LA-ORL-001 lie in the Mississippi River. Since a constant flow rate is used, the pre-storm river stage is not captured, however, an accurate maximum water level is maintained once the surge overwealms the river flow.

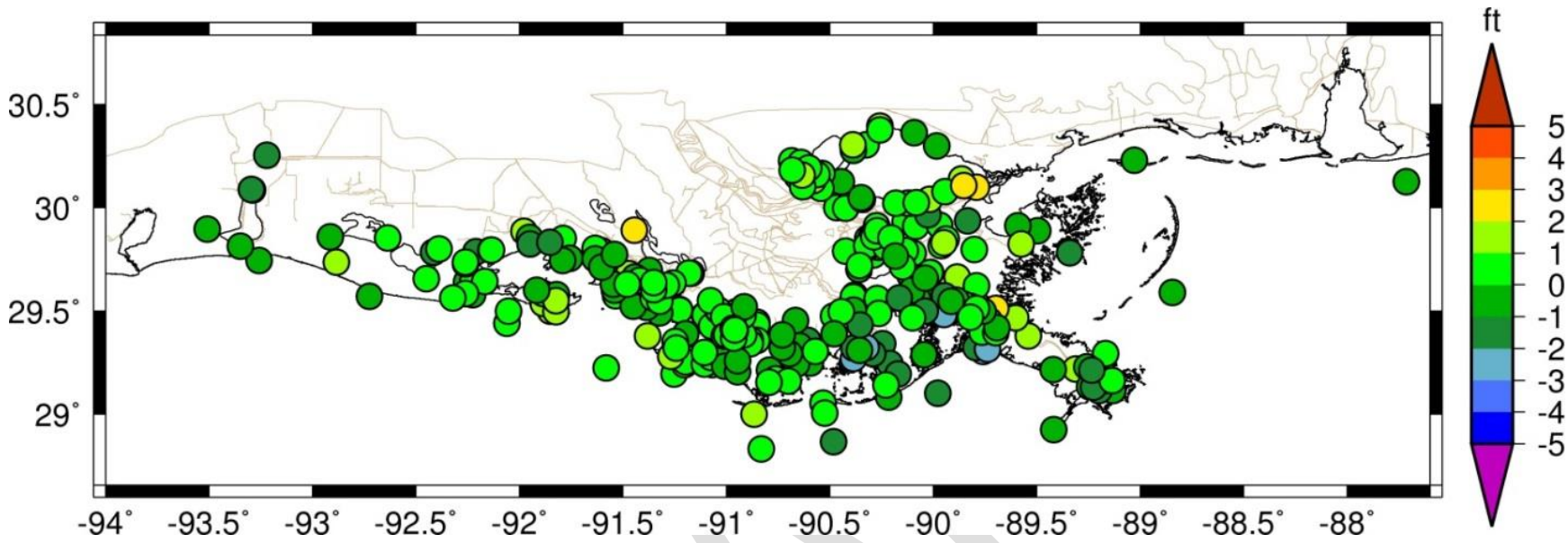

Figure 1-33: CPRA2017 model Hurricane Gustav comparison to measured high water marks. Warm colors indicate the model results are greater than measurement; cool colors indicate the model results are lower than measurement.

DRAFT

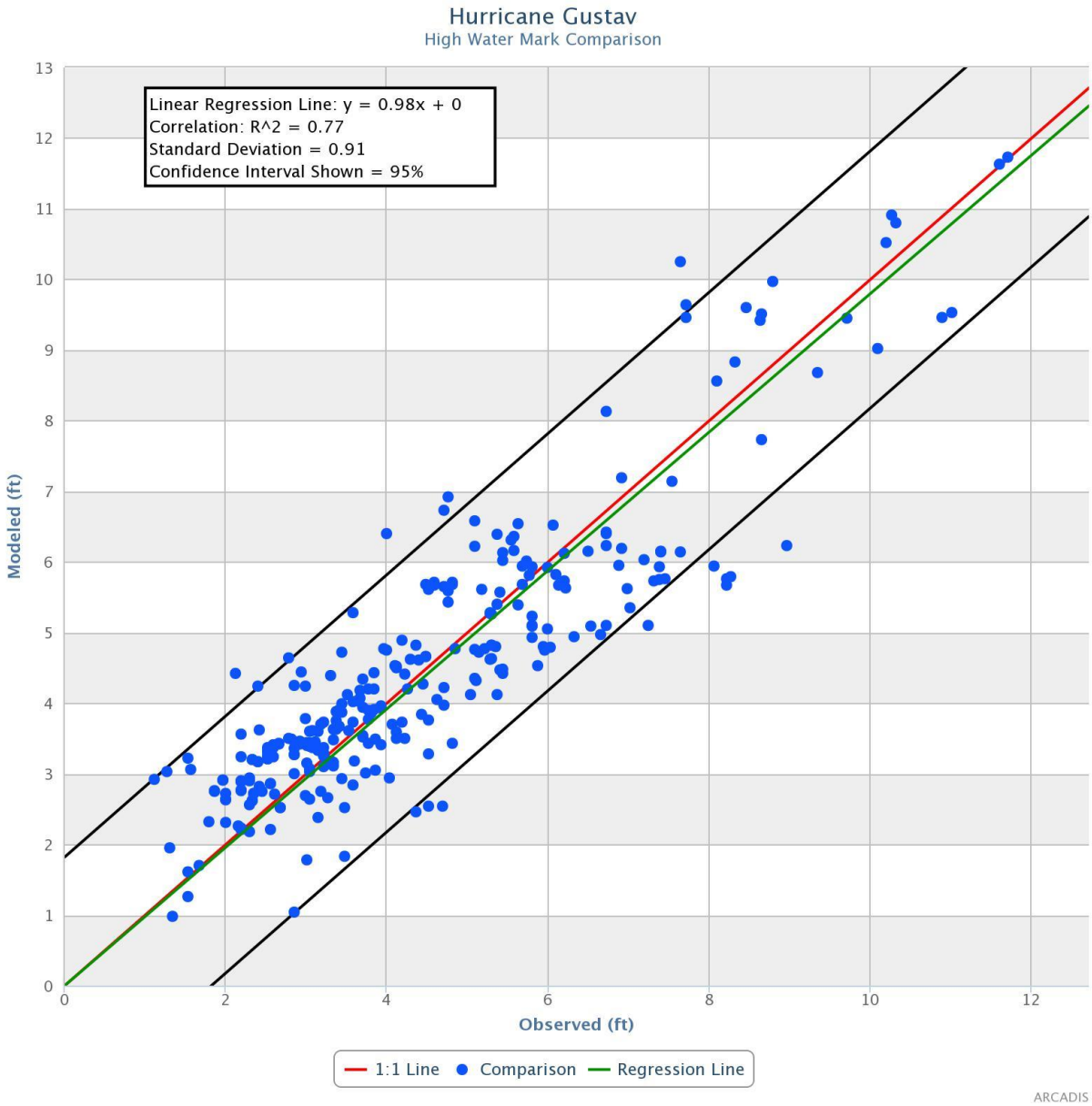

Figure 1-34: Hurricane Gustav regression plot comparing measured high water marks to CPRA2017 model results.

Hurricane Ike (2008)

Before Ike entered the Gulf and made landfall in Cuba, it was a Category 4 hurricane. By the time it entered the Gulf, however, it was a Category 1 storm. Warm currents in the Gulf reintensified the storm to a Category 2 hurricane before making landfall on September 13, 2008, in Galveston, Texas, just two weeks after Gustav made landfall in Louisiana.

Ike provides an interesting test of model ability. Shore parallel currents caused waters to rise nearly a full day before landfall in western Louisiana and Texas. This can be attributed to an Ekman setup (Kennedy et al., 2011). This extra setup is driven by a combination of the Coriolis force and current velocities. As Kennedy points out, these velocities, especially in shallower waters like those on the Louisiana-Texas shelf, are highly dependent upon properly selected bottom friction coefficients and are very difficult to determine, given the size and inaccessibility of the Louisiana-Texas shelf. However, applying a similar model setup as Kennedy et al (2011). and Hope et al. (2013), much of this extra setup is achieved. Figure 1-35 shows the water level as measured by the NOAA gage at Sabine Lake, the computed surge in the CPRA2017 model, and the computed surge from the newly developed 9.1 million vertex SL18+TX model used by Hope et al. (2013) for validation of Ike. The plot shows much of the forerunner is captured by CPRA2017 between midnight on September 12, 2008, and midnight on September 13, 2008. The plot additinally shows excellent agreement with the state-of-the-art SL18+TX model. Notice that the surge hits the first peak during the forerunner, followed by a small dip. Then a second, larger peak is observed as the storm passes through the area. This early forerunner provides the initial water level necessary to generate the measured surge.

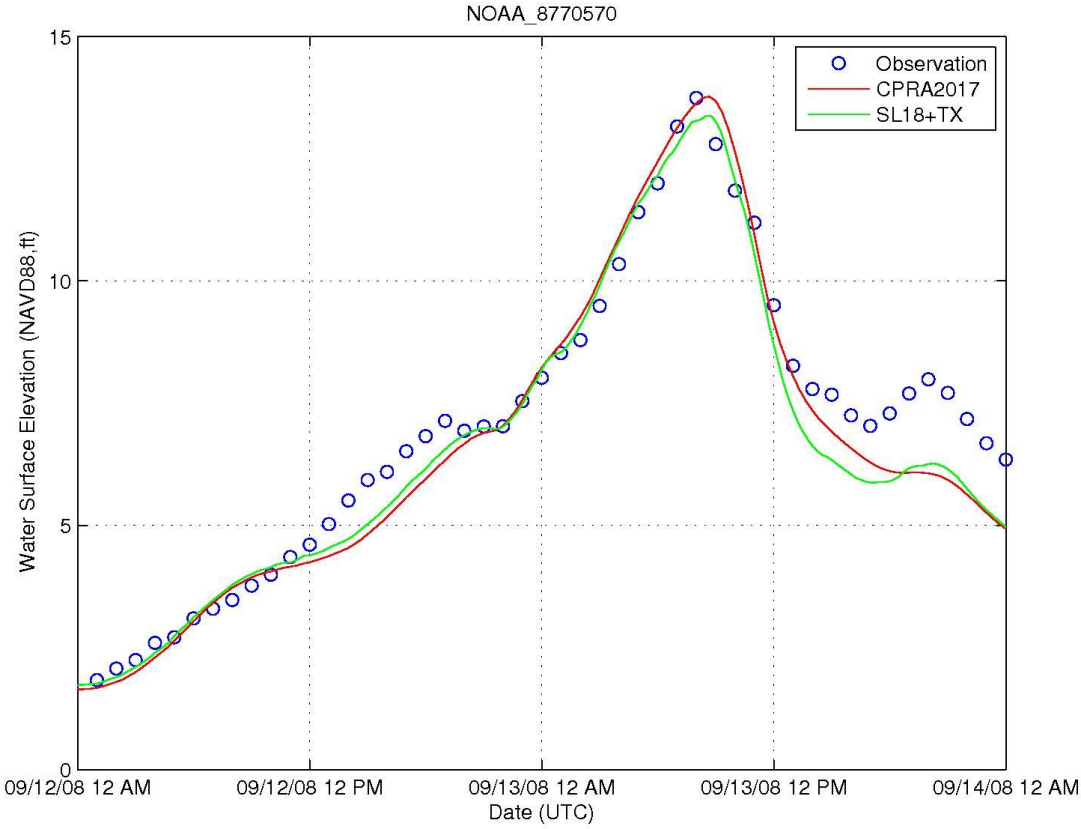

Figure 1-35: Hurricane Ike forerunner surge (ft, NAVD88) (Hope et al., 2013). Observations are shown in blue; CPRA2017 is shown in red; SL18+TX is shown in green

The simulation of Ike uses Gustav as an initial condition. Since the storms occur so near each other in time, the dynamic solution already computed from Gustav creates the initial condition for Ike. The initial conditions for both circulation and waves are applied. The simulation concludes on September 14, 2008.

River flow rates from Gustav are carried forward and used during the Ike simulation.

Figure 1-36 shows the maximum computed surge from the ADCIRC+SWAN model, and Figure 1-37 shows the maximum computed significant wave height during the simulation of Ike. Figures 1-38 through 1-42 show the wave comparisons to measured data. Figures 1-43 through 1-45 show the water level comparisons to measured data. Finally, Figures 1-46 and 1-47 show the comparisons to measured high water marks.

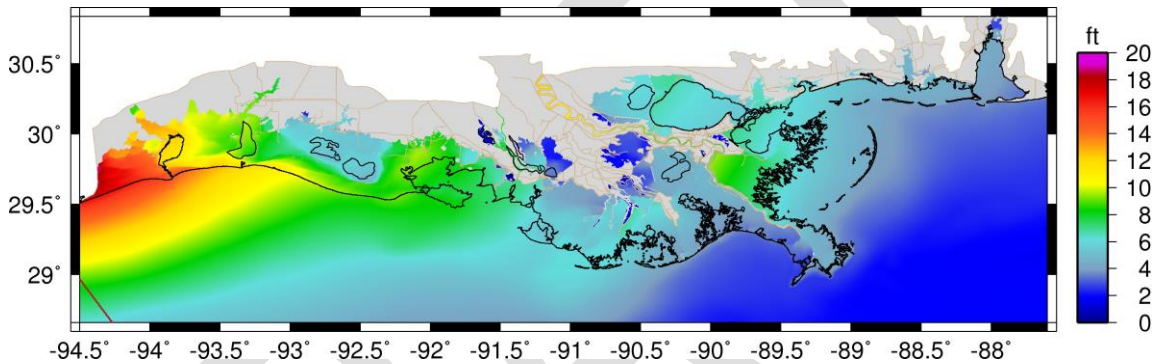

Figure 1-36: Maximum storm surge elevation (ft, NAVD88) during the 2017CPRA Hurricane Ike simulation. Storm track shown in brown.

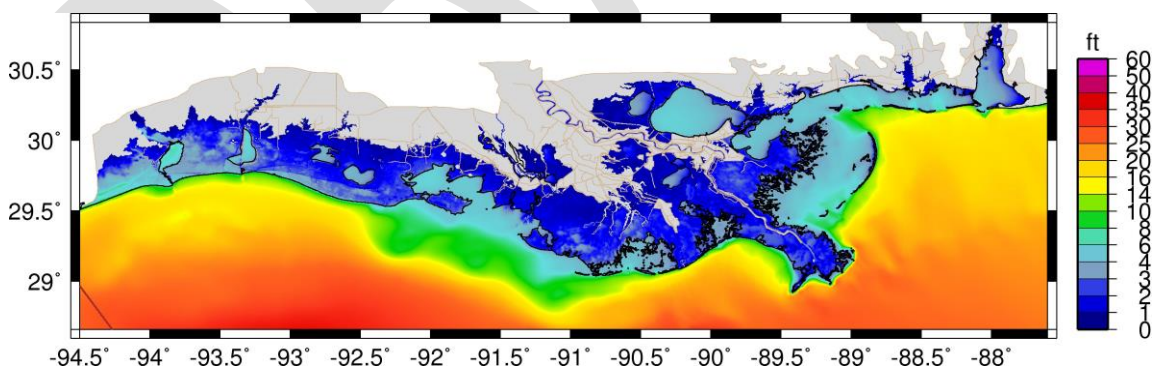

Figure 1-37: Maximum significant wave height (ft) during the 2017CPRA Hurricane Ike simulation. Storm track shown in brown.

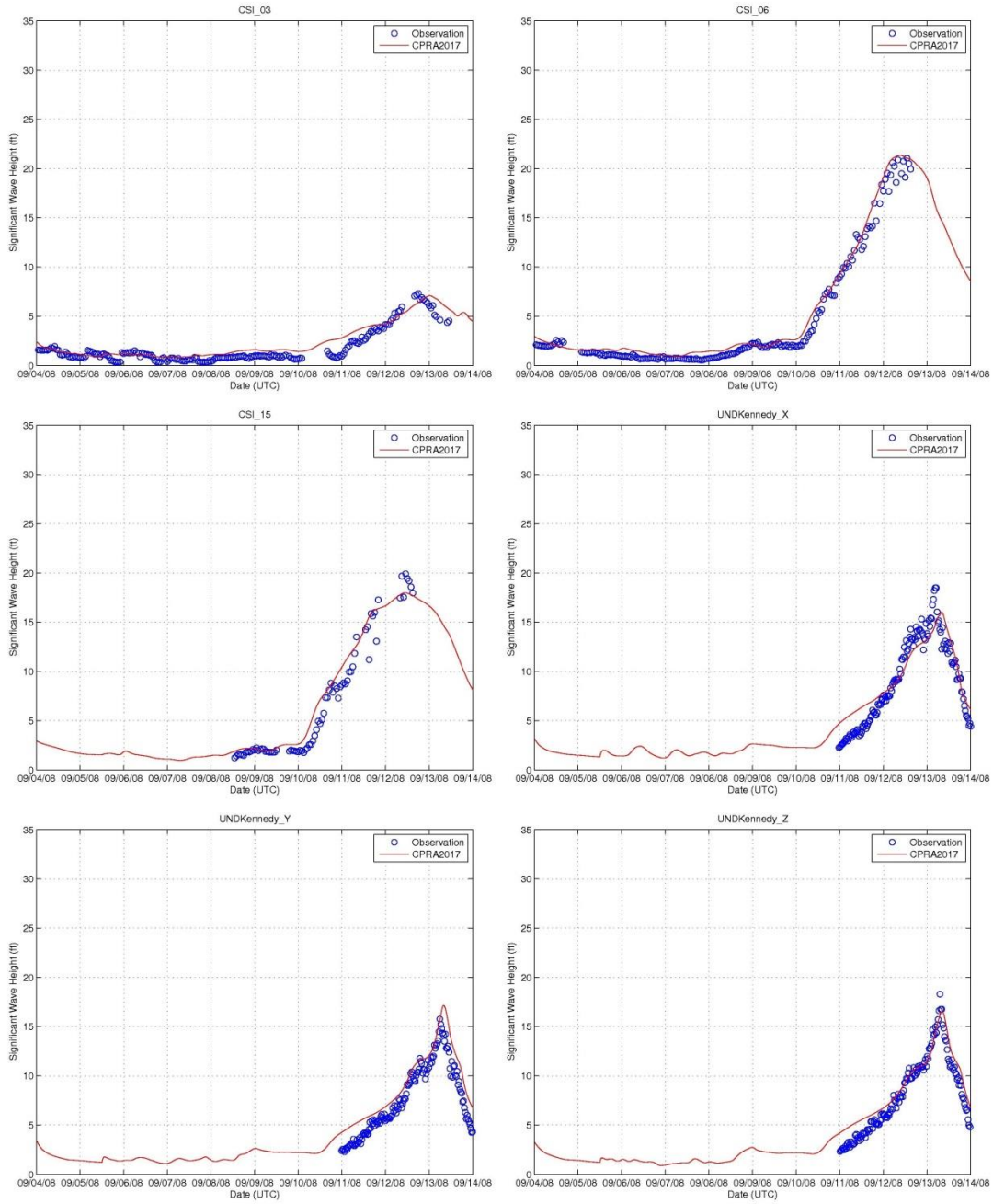

Figure 1-38: Significant wave height comparisons at CSI and Andrew Kennedy locations for Hurricane Ike. Observations are in blue; CPRA2017 model results are in red.

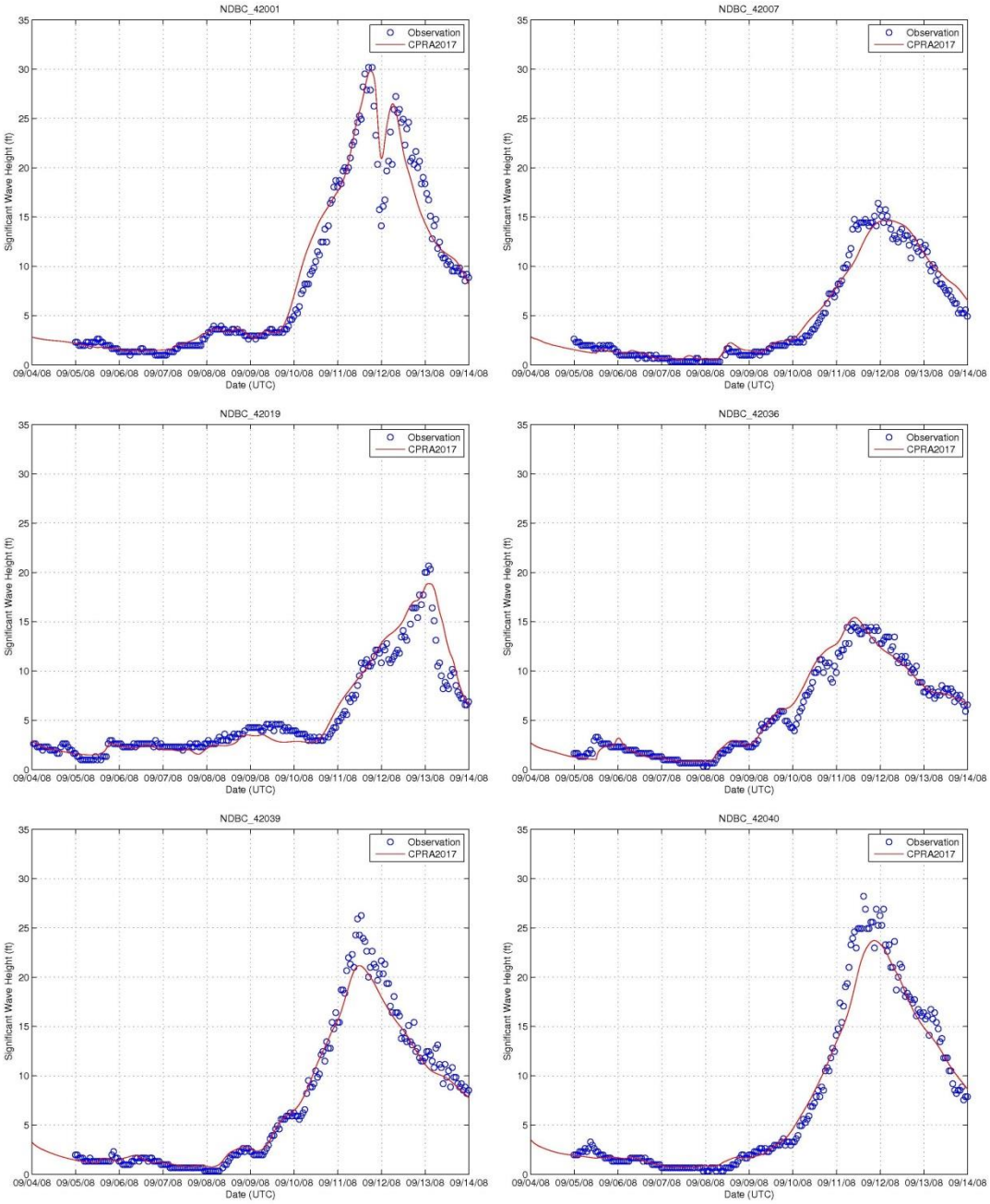

Figure 1-39: Significant wave height comparisons at NDBC locations for Hurricane Ike. Observations are in blue; CPRA2017 model results are in red.

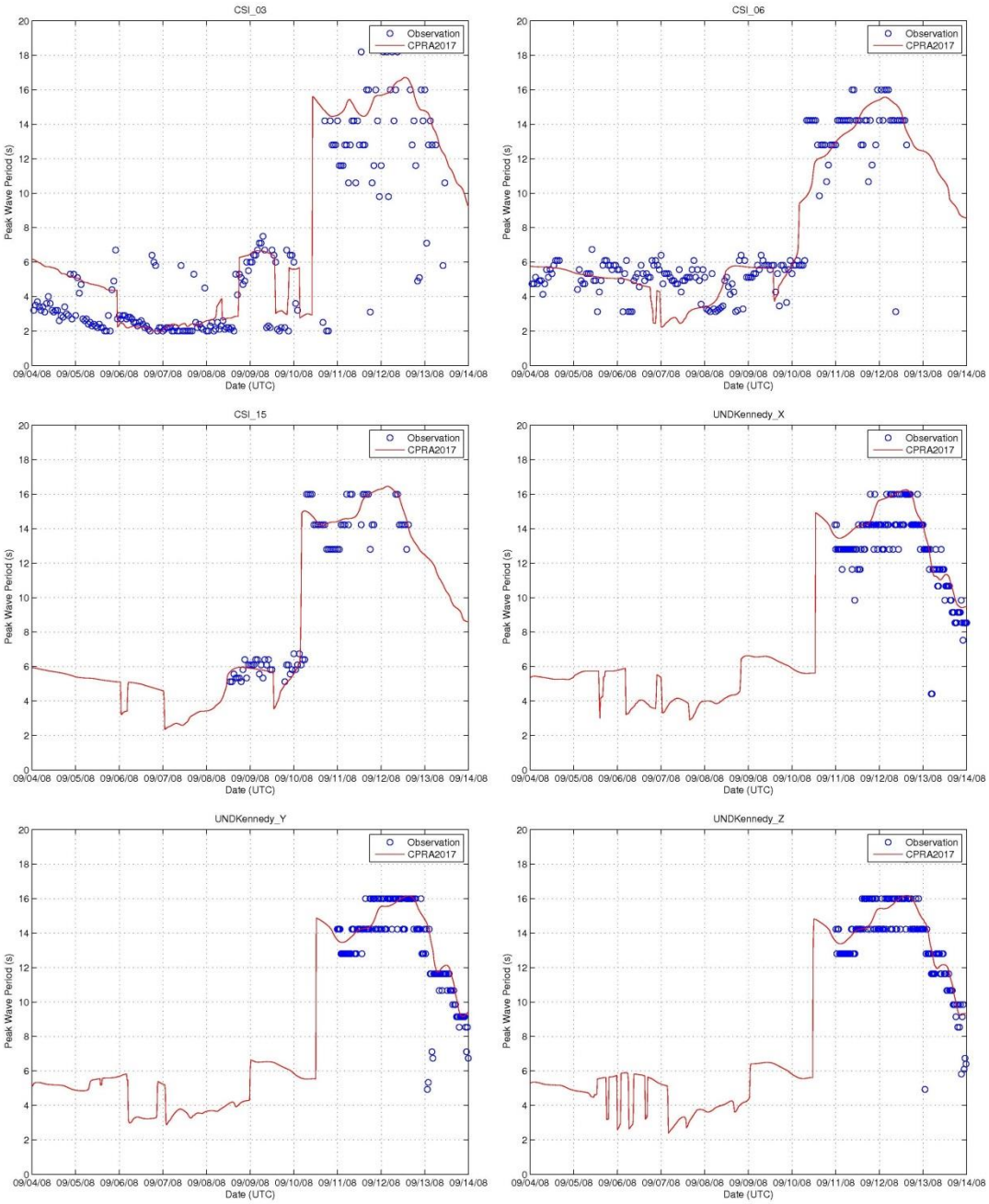

Figure 1-40: Peak wave period comparisons at CSI and Andrew Kennedy locations for Hurricane Ike. Observations are in blue; CPRA2017 model results are in red.

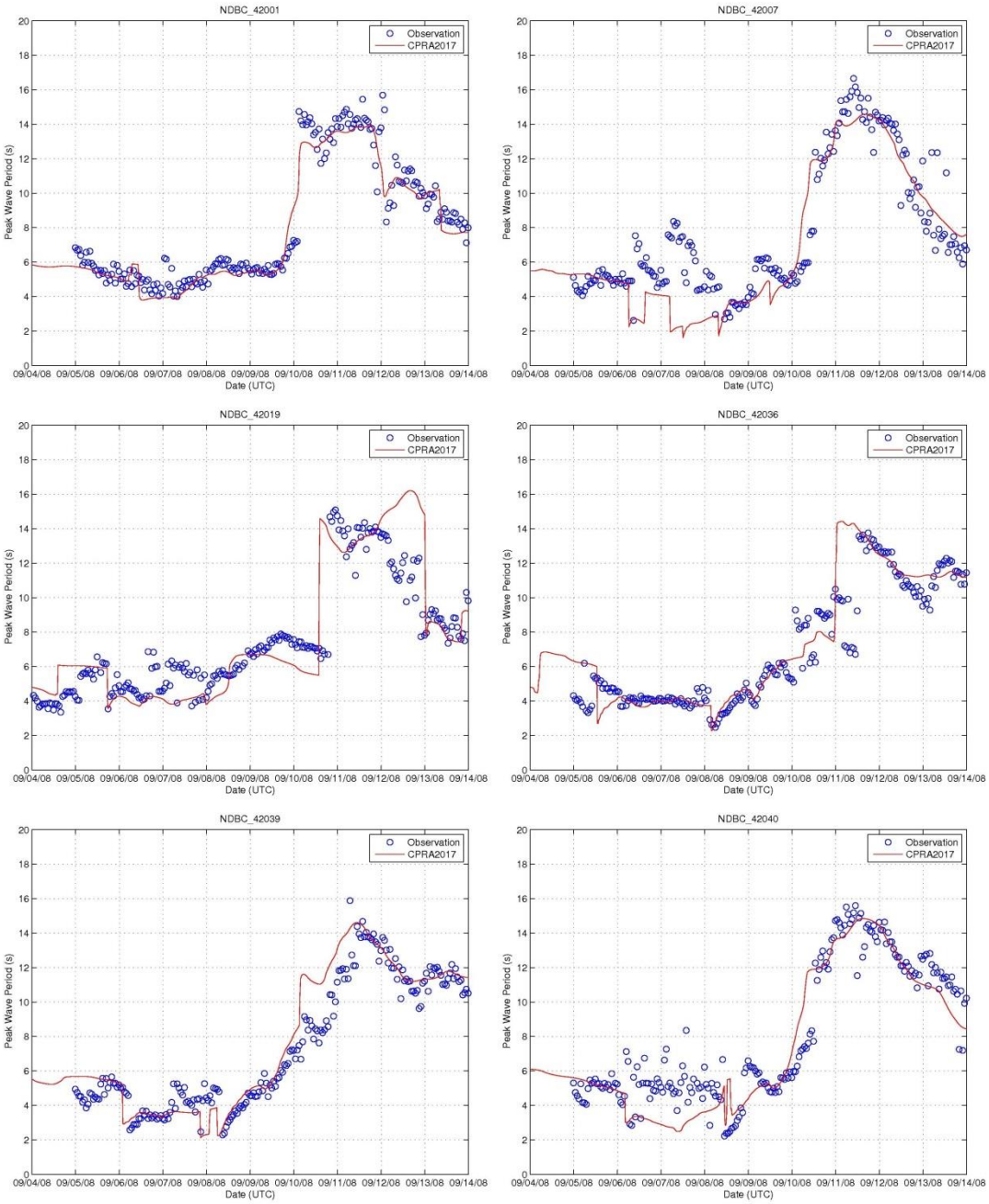

Figure 1-41: Peak wave period comparisons at NDBC locations for Hurricane Ike. Observations are in blue; CPRA2017 model results are in red.

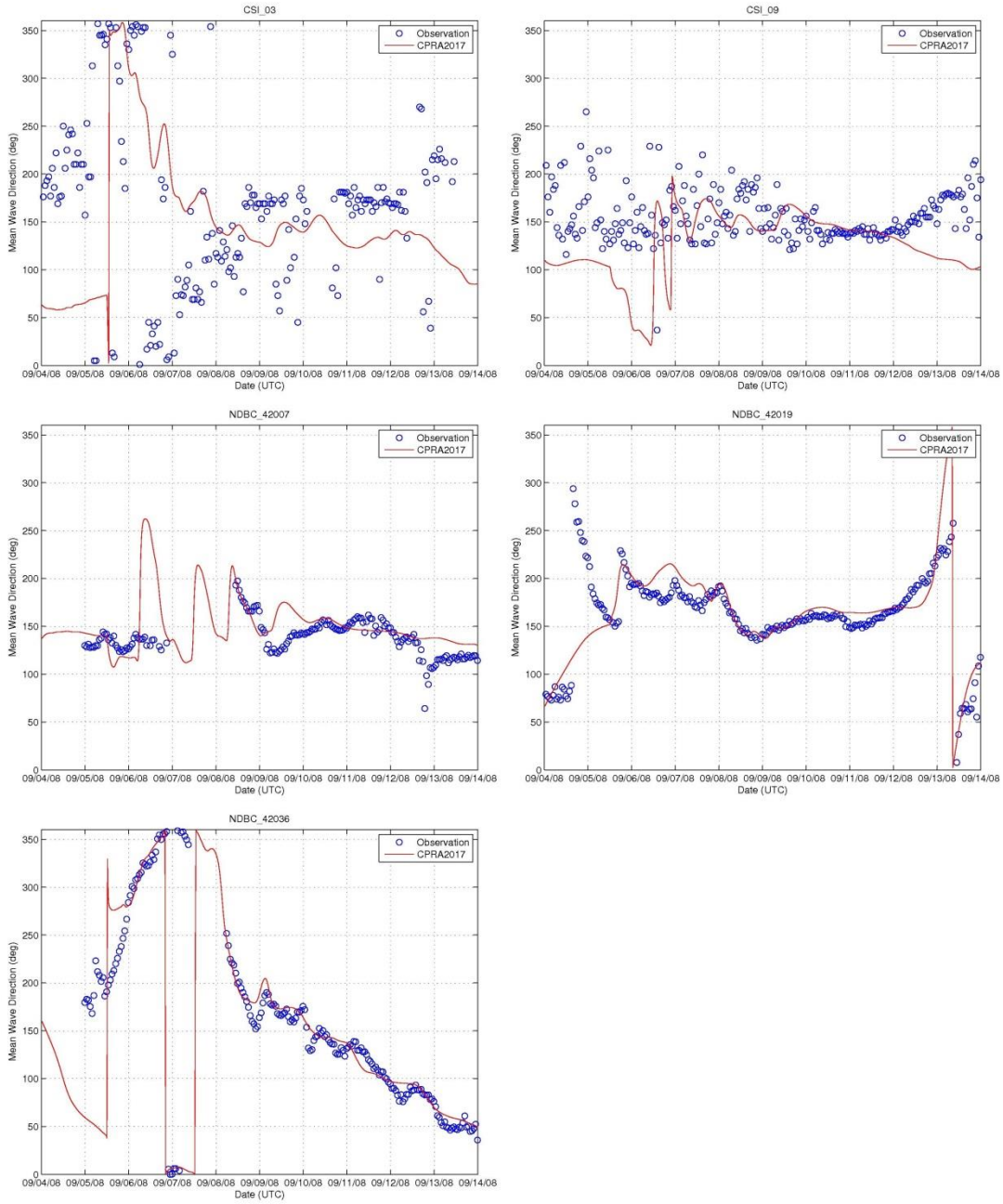

Figure 1-42: Mean wave direction comparisons for Hurricane Ike at NDBC and CSI locations. Observations are in blue; CPRA2017 model results are in red.

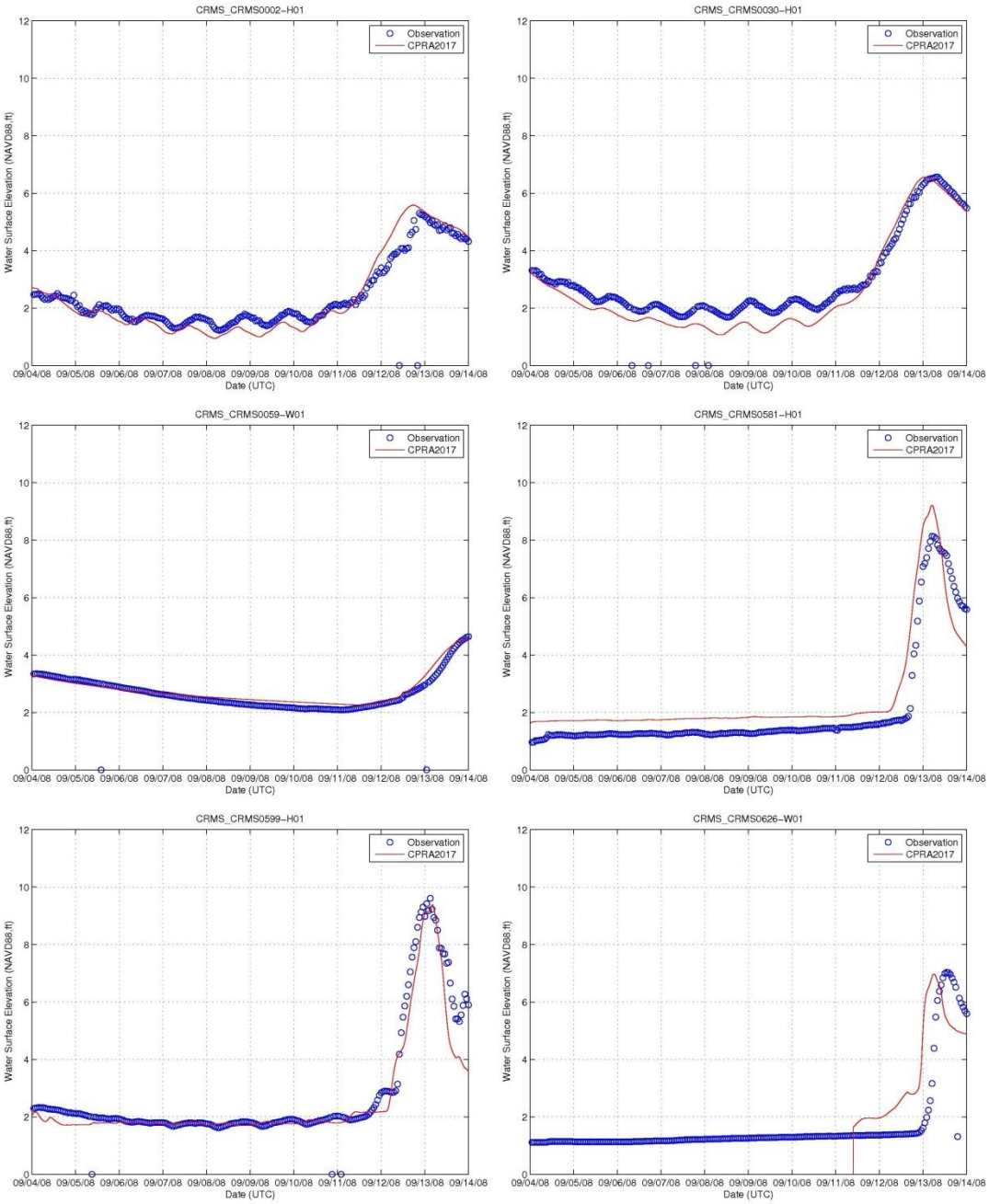

Figure 1-43: Water elevation (ft, NAVD88) comparisons for Hurricane Ike at CRMS locations. Observations are in blue; CPRA2017 model results are in red.

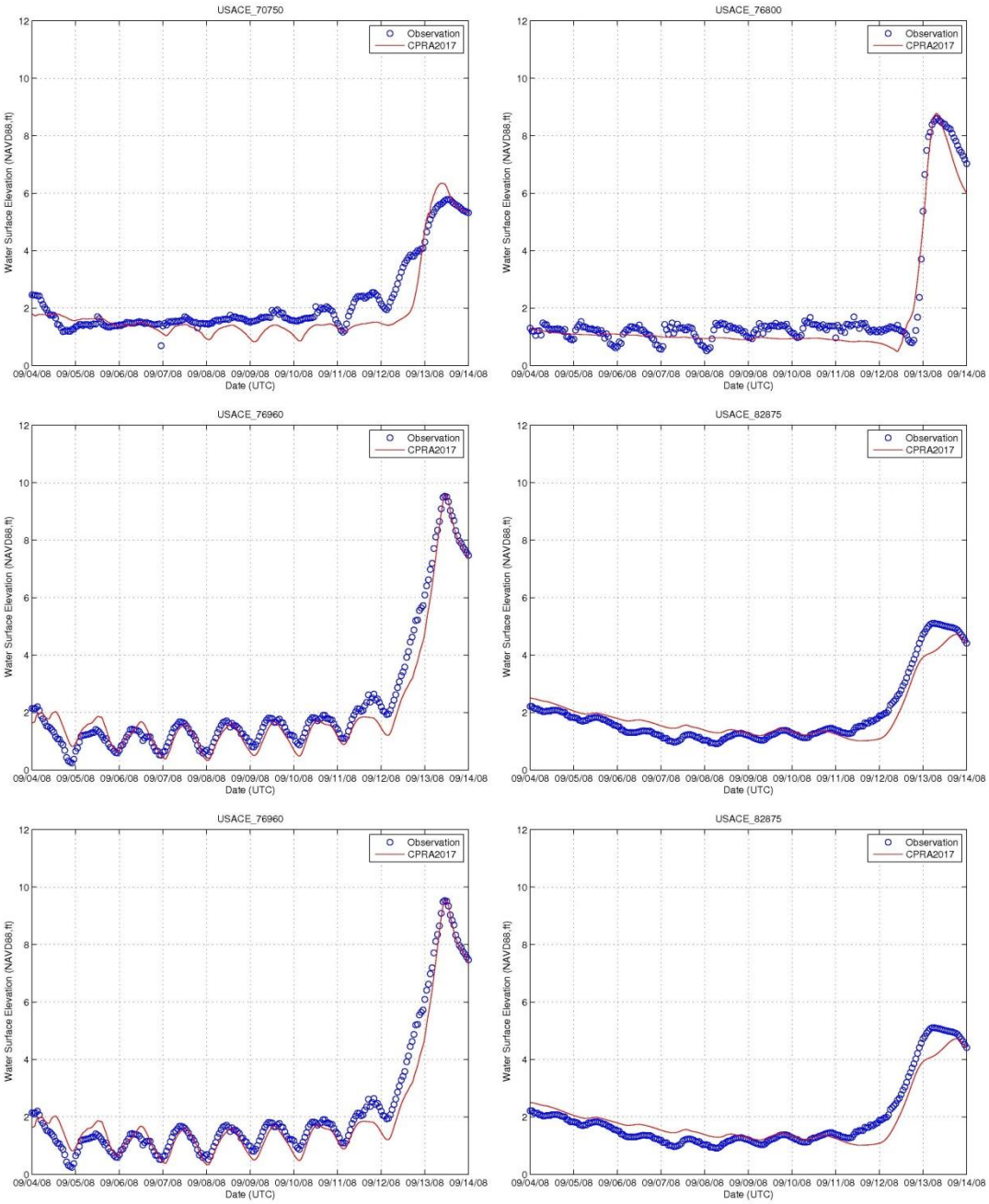

Figure 1-44: Water elevation (ft, NAVD88) comparisons for Hurricane Ike at USACE locations. Observations are in blue; CPRA2017 model results are in red.

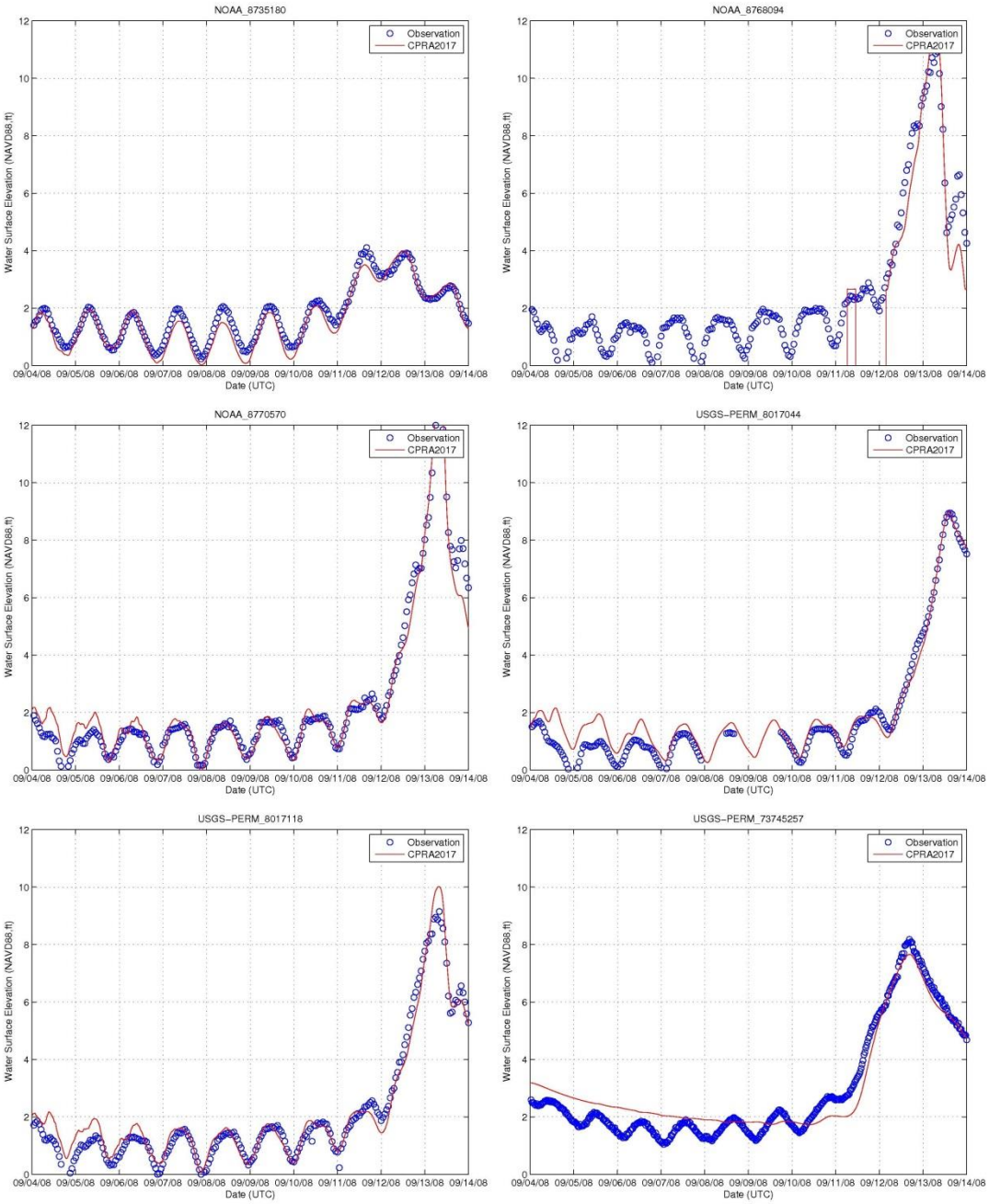

Figure 1-45: Water elevation (ft, NAVD88) comparisons for Hurricane Ike at NOAA and USGS locations. Observations are in blue; CPRA2017 model results are in red.

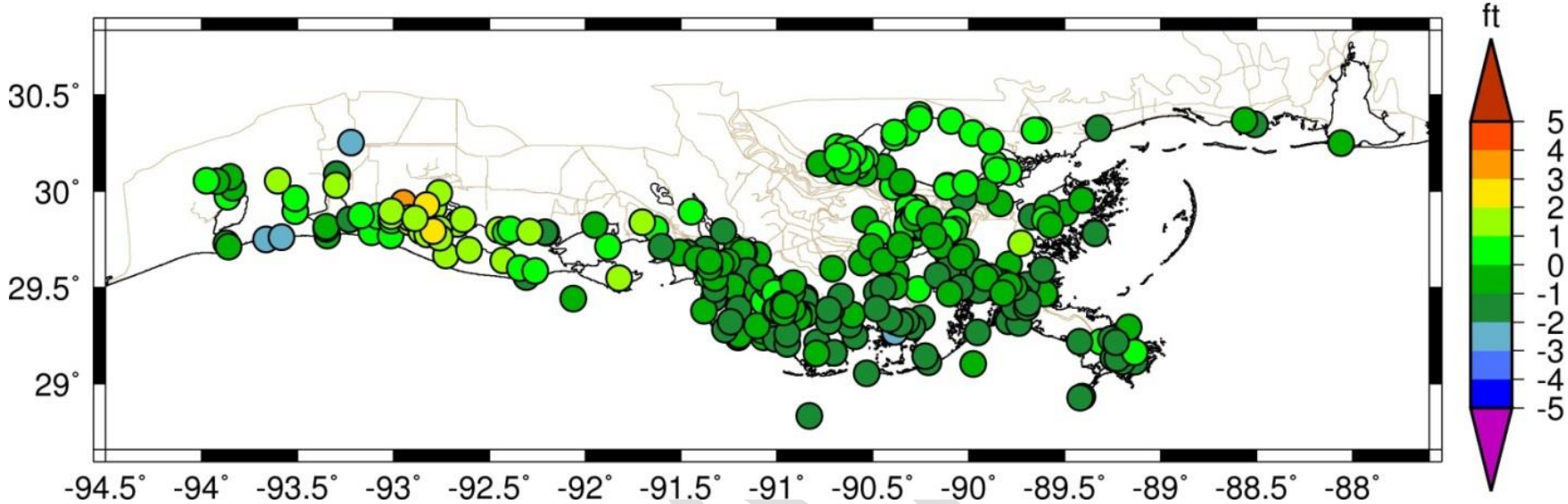

Figure 1-46: CPRA2017 model Hurricane Ike comparison to measured high water marks. Warm colors indicate the model results are greater than measurement; cool colors indicate the model results are lower than measurement.

DRAFT

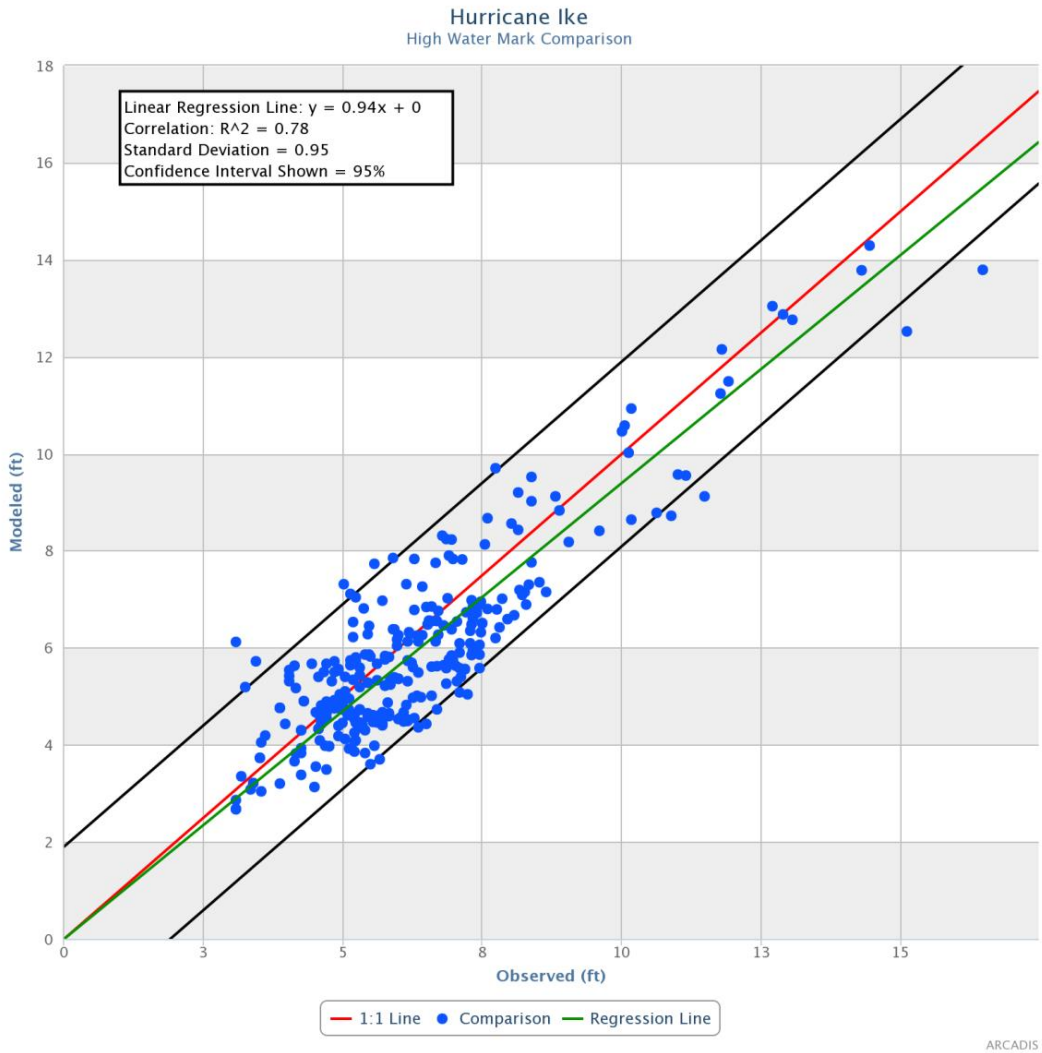

Figure 1-47: Hurricane Ike regression plot comparing measured high water marks to CPRA2017 model results.

Validation Simulations Performance Summary

2017CPRA model comparisons to high water marks are summarized in Table 1-2. The 2017CPRA model demonstrates a high skill level simlar to the Dietrich et al. study performed on the five million vertex SL16 mesh (2012). Figure 1-48 shows a regression plot for all four storms combined. When comparing measured high water marks to model results for all four storms, the overall regression slope is 1.02, the correlation coefficient is 0.97, and the standard deviation is 1.18 feet.

Table 1-2: Summary of High Water Mark Comparisons

	CPRA2017		*Dietrich et al. 2012*	
Storm	**Regression Slope**	**Correlation Coefficient**	**Regression Slope**	**Correlation Coefficient**
Katrina	1.04	0.96	1.00	0.93
Rita	1.06	0.73	1.08	0.79
Gustav	0.98	0.77	0.95	0.80
Ike*	0.94	0.78	0.93	0.77

***Note: Not compared to Hope et al. (2013) because domain coverage is significantly different.**

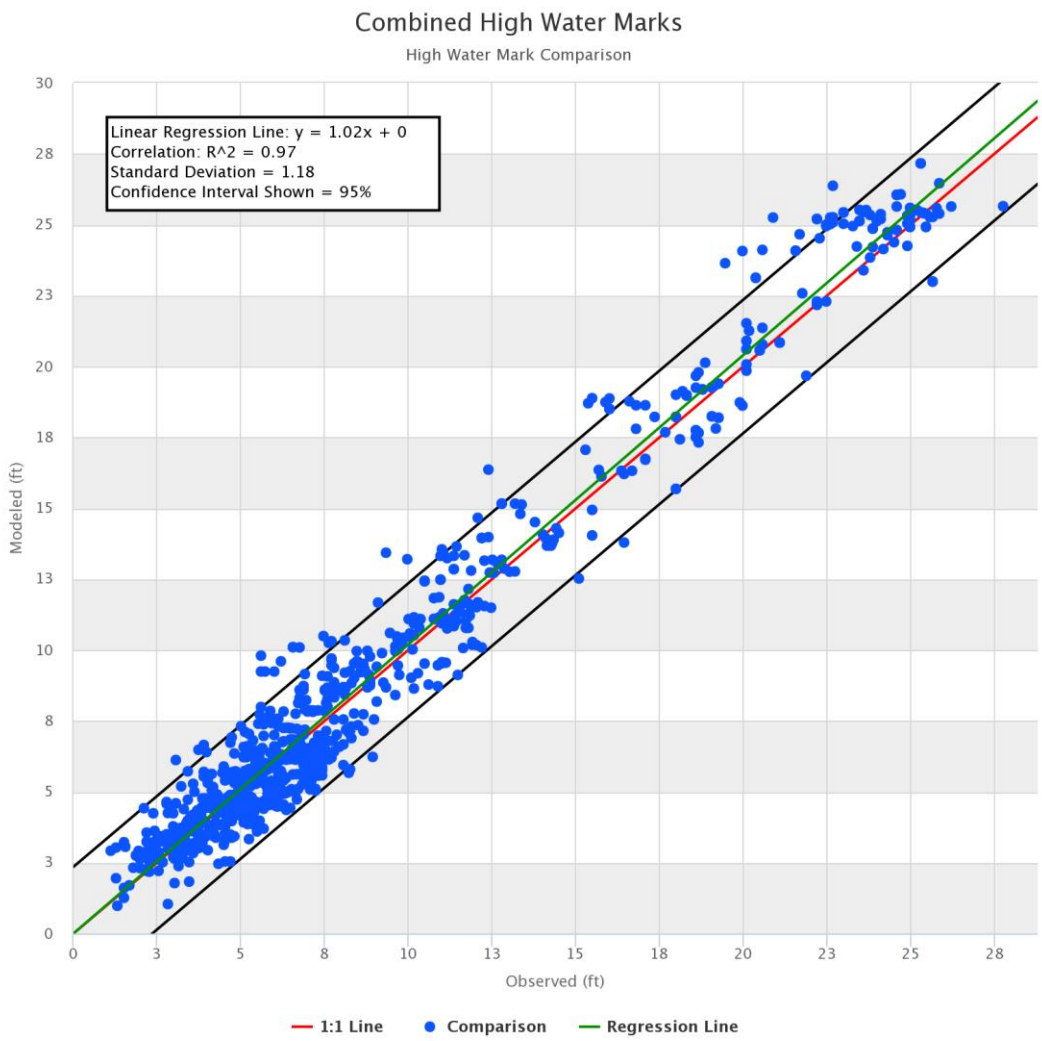

Figure 1-48: Regression plot comparing measured high water marks for all four storms to CPRA2017 model results.

References

Cobell, Z., H. Zhao, H.J. Roberts, F.R. Clark, S. Zou. (2013). Surge and Wave Modeling for the Louisiana 2012 Coastal Master Plan. Journal of Coastal Research: Special Issue 67 – Louisiana's 2012 Coastal Master Plan Technical Analysis, pp. 88-108.

Dietrich, J.C., Westerink, J.J., Kennedy, A.B., Smith, J.M., Jensen, R., Zijlema, M., Holthuijsen, L.H., Dawson, C., Luettich, Jr., R.A., Powell, M.D., Cardone, V.J., Cox, A.T., Stone, G.W., Pourtaheri, H., Hope, M.E., Tanaka, S., Westerink, L.G., Westerink, H.J., Z. Cobell, Z. (2011) Hurricane Gustav Waves and Storm Surge: Hindcast, Synoptic Analysis and Validation in Southern Louisiana. Monthly Weather Review, Volume 139, pp. 2488-2522, DOI 10.1175/2011MWR3611.1.

Dietrich, J.C., Tanaka, S., Westerink, J.J., Dawson, C.N.,Luettich, Jr., R.A., Zijlema, M.,Holthuijsen, L.H., Smith, J.M., Westerink, L.G., H.J. Westerink, H.J. (2012) Performance of the Unstructured-Mesh, SWAN+ADCIRC Model in Computing Hurricane Waves and Surge. Journal of Scientific Computing, Volume 52, Issue 2, pp. 468-497.

Ben C. Gerwick, Inc. (2012). Southeast Louisiana Flood Protection Authority – East: New Orleans East Land Bridge Study. Oakland, CA. 228pp.

Hope, M.E., Westerink, J.J., Kennedy, A.B., Kerr, P.C., Dawson, C., Bender, C.J., Smith, J.M., Jensen, R.E., Zijlema, M., Holthuijsen, L.H.,Luettich, Jr., R.A., Powell, M.D., Cardone, V.J., A.T. Cox, A.T., Pourtaheri, H., Roberts, H.J.,Atkinson, J.H., Tanaka, S., Westerink, H.J., Westerink, L.G., (2013) Hindcast and Validation of Hurricane Ike Waves, Forerunner, and Storm Surge. Journal of Geophysical Research: Oceans, Volume 118, pp. 4424-4460.

Kennedy, A.B., Gravois, U., Zachry, B.C., Westerink, J.J, Hope, M.E., Dietrich, J.C.,Powell, M.D., Cox, A.T., R.A. Luettich, Jr.,R.A., Dean, R.G.(2011) Origin of the Hurricane Ike Forerunner Surge. Geophysical Research Letters, Volume 38, Issue 8, L08608, DOI 10.1029/2011GL047090.

USACE (2008a). Louisiana Coastal Protection and Restoration Technical Report. Vicksburg, Mississippi: USACE, 98 pp.

USACE (2008b). Flood Insurance Study: Southeastern Parishes, Louisiana. Intermediate Submission 2: Offshore Water Levels and Waves. Vicksburg, Mississippi: USACE, 152 pp.

USACE (2008c). Flood Insurance Study: Southwestern Parishes, Louisiana. Intermediate Submission 2. Vicksburg, Mississippi: USACE, 697 pp.

USACE (2011). Flood Insurance Study: Coastal Counties, Texas Intermediate Submission 2, Vicksburg, Mississippi: USACE, 150 pp.

DRAFT

Appendix 2: Synthetic Storm Suite Simulations

In order to supply ADvanced CIRCulation (ADCIRC)+Simulating Waves Nearshore (SWAN) model results for Coastal Louisiana Risk Assessment (CLARA) model improvements, the CPRA2017 model was used to simulate all 446 synthetic storms that were developed as part of the Federal Emergency Management Agency Flood Insurance Rate Map studies in Louisiana (U.S. Army Corps of Engineers [USACE], 2008b; USACE, 2008c). The storm tracks are shown in Figure 2-1. For each storm track, there are multiple storm parameters. These parameters are shown in Table 2-1. This storm suite includes both the FEMA low-frequency storms, which are the most powerful and generate the largest surge levels but happen more rarely, and the FEMA high-frequency storms, which are relatively less powerful and generate lower surge levels but happen more frequently. These simulations were completed on both the Current Conditions geometry from the 2012 Coastal Master Plan and the Less Optimistic (S13) future without action (FWOA) scenario 50 years into the future which takes into account future sea level rise (1.5 feet) and landscape changes.

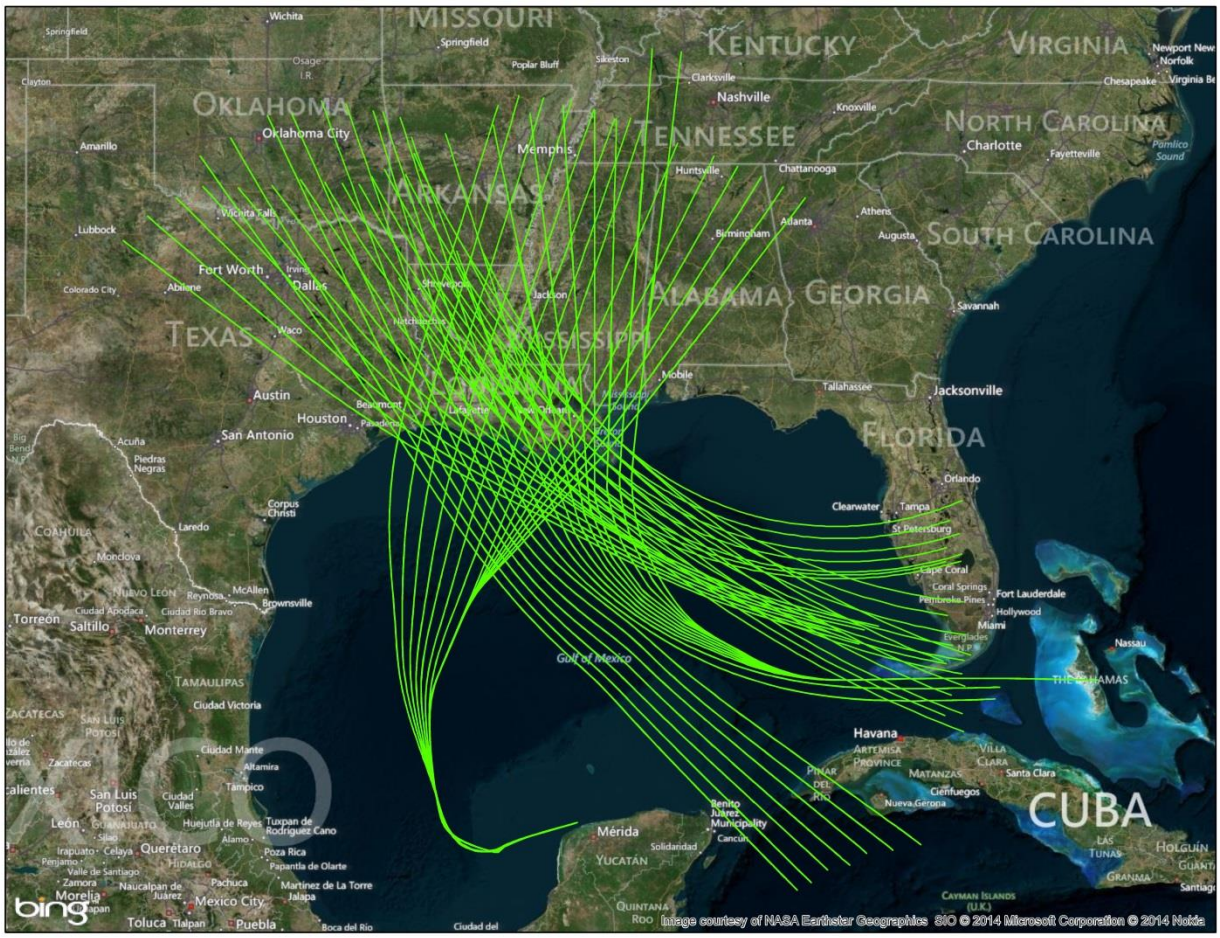

Figure 2-1: Synthetic storm tracks for Louisiana. Note that more than one storm lies on each track.

Model setup for these simulations mirrored that of the 2012 Coastal Master Plan with only a few changes:

1. Wave coupling occurred every 10 minutes as opposed to every 20 minutes. This provides a more detailed wave solution and quicker wave model numerical convergence;

2. The Powell (2006) wind drag formulation was used in ADCIRC and SWAN. More details about this can be found in Appendix 4; and

3. The ADCIRC model used was release version 50 where version 49 was used during the 2012 Coastal Master Plan.

Table 2-1: Louisiana Synthetic Storm Parameters.

Storm Number	Minimum Central Pressure (mb)	Radius To Maximum Winds (nmi)	Track	Forward Velocity (kt)	Angle (°)	Landfall Location	
						Longitude	Latitude
1	960	11	E1	11	0	-91.2111	29.5000
2	960	21	E1	11	0	-91.2111	29.5000
3	960	35.6	E1	11	0	-91.2111	29.5000
4	930	8	E1	11	0	-91.2111	29.5000
5	930	17.7	E1	11	0	-91.2111	29.5000
6	930	25.8	E1	11	0	-91.2111	29.5000
7	900	6	E1	11	0	-91.2111	29.5000
8	900	14.9	E1	11	0	-91.2111	29.5000
9	900	21.8	E1	11	0	-91.2111	29.5000
10	960	11	E2	11	0	-90.4511	29.5000
11	960	21	E2	11	0	-90.4511	29.5000
12	960	35.6	E2	11	0	-90.4511	29.5000
13	930	8	E2	11	0	-90.4511	29.5000
14	930	17.7	E2	11	0	-90.4511	29.5000
15	930	25.8	E2	11	0	-90.4511	29.5000
16	900	6	E2	11	0	-90.4511	29.5000
17	900	14.9	E2	11	0	-90.4511	29.5000
18	900	21.8	E2	11	0	-90.4511	29.5000
19	960	11	E3	11	0	-89.8479	29.5000
20	960	21	E3	11	0	-89.8479	29.5000
21	960	35.6	E3	11	0	-89.8479	29.5000
22	930	8	E3	11	0	-89.8479	29.5000
23	930	17.7	E3	11	0	-89.8479	29.5000
24	930	25.8	E3	11	0	-89.8479	29.5000
25	900	6	E3	11	0	-89.8479	29.5000
26	900	14.9	E3	11	0	-89.8479	29.5000

DRAFT

Storm Number	Minimum Central Pressure (mb)	Radius To Maximum Winds (nmi)	Track	Forward Velocity (kt)	Angle (°)	Landfall Location	
						Longitude	Latitude
27	900	21.8	E3	11	0	-89.8479	29.5000
28	960	11	E4	11	0	-89.2758	29.5000
29	960	21	E4	11	0	-89.2758	29.5000
30	960	35.6	E4	11	0	-89.2758	29.5000
31	930	8	E4	11	0	-89.2758	29.5000
32	930	17.7	E4	11	0	-89.2758	29.5000
33	930	25.8	E4	11	0	-89.2758	29.5000
34	900	6	E4	11	0	-89.2758	29.5000
35	900	14.9	E4	11	0	-89.2758	29.5000
36	900	21.8	E4	11	0	-89.2758	29.5000
37	960	11	E5	11	0	-88.6467	29.5000
38	960	21	E5	11	0	-88.6467	29.5000
39	960	35.6	E5	11	0	-88.6467	29.5000
40	930	8	E5	11	0	-88.6467	29.5000
41	930	17.7	E5	11	0	-88.6467	29.5000
42	930	25.8	E5	11	0	-88.6467	29.5000
43	900	6	E5	11	0	-88.6467	29.5000
44	900	14.9	E5	11	0	-88.6467	29.5000
45	900	21.8	E5	11	0	-88.6467	29.5000
46	960	18.2	E1	11	-45	-91.3677	29.5000
47	960	24.6	E1	11	-45	-91.3677	29.5000
48	900	12.5	E1	11	-45	-91.3677	29.5000
49	900	18.4	E1	11	-45	-91.3677	29.5000
50	960	18.2	E2	11	-45	-90.7238	29.5000
51	960	24.6	E2	11	-45	-90.7238	29.5000
52	900	12.5	E2	11	-45	-90.7238	29.5000
53	900	18.4	E2	11	-45	-90.7238	29.5000
54	960	18.2	E3	11	-45	-89.9208	29.5000
55	960	24.6	E3	11	-45	-89.9208	29.5000
56	900	12.5	E3	11	-45	-89.9208	29.5000
57	900	18.4	E3	11	-45	-89.9208	29.5000
58	960	18.2	E4	11	-45	-89.1054	29.5000
59	960	24.6	E4	11	-45	-89.1054	29.5000
60	900	12.5	E4	11	-45	-89.1054	29.5000
61	900	18.4	E4	11	-45	-89.1054	29.5000
66	960	18.2	E1	11	45	-90.9941	29.5000

DRAFT

Storm Number	Minimum Central Pressure (mb)	Radius To Maximum Winds (nmi)	Track	Forward Velocity (kt)	Angle (°)	Landfall Location	
						Longitude	Latitude
67	960	24.6	E1	11	45	-90.9941	29.5000
68	900	12.5	E1	11	45	-90.9941	29.5000
69	900	18.4	E1	11	45	-90.9941	29.5000
70	960	18.2	E2	11	45	-90.2138	29.5000
71	960	24.6	E2	11	45	-90.2138	29.5000
72	900	12.5	E2	11	45	-90.2138	29.5000
73	900	18.4	E2	11	45	-90.2138	29.5000
74	960	18.2	E3	11	45	-89.6380	29.5000
75	960	24.6	E3	11	45	-89.6380	29.5000
76	900	12.5	E3	11	45	-89.6380	29.5000
77	900	18.4	E3	11	45	-89.6380	29.5000
78	960	18.2	E4	11	45	-89.0471	29.5000
79	960	24.6	E4	11	45	-89.0471	29.5000
80	900	12.5	E4	11	45	-89.0471	29.5000
81	900	18.4	E4	11	45	-89.0471	29.5000
82	960	17.7	E1	6	0	-91.1978	29.5000
83	900	17.7	E1	6	0	-91.1978	29.5000
84	960	17.7	E2	6	0	-90.4540	29.5000
85	900	17.7	E2	6	0	-90.4540	29.5000
86	960	17.7	E3	6	0	-89.8470	29.5000
87	900	17.7	E3	6	0	-89.8470	29.5000
88	960	17.7	E4	6	0	-89.2700	29.5000
89	900	17.7	E4	6	0	-89.2700	29.5000
90	960	17.7	E5	6	0	-88.6490	29.5000
91	900	17.7	E5	6	0	-88.6490	29.5000
92	930	17.7	E1	6	-45	-91.3729	29.5000
93	930	17.7	E2	6	-45	-90.7129	29.5000
94	930	17.7	E3	6	-45	-89.9200	29.5000
95	930	17.7	E4	6	-45	-89.0971	29.5000
97	930	17.7	E1	6	45	-90.9920	29.5000
98	930	17.7	E2	6	45	-90.2100	29.5000
99	930	17.7	E3	6	45	-89.6425	29.5000
100	930	17.7	E4	6	45	-89.0500	29.5000
101	930	17.7	E1	17	0	-91.2177	29.5000
102	930	17.7	E2	17	0	-90.4437	29.5000
103	930	17.7	E3	17	0	-89.8476	29.5000

DRAFT

Storm Number	Minimum Central Pressure (mb)	Radius To Maximum Winds (nmi)	Track	Forward Velocity (kt)	Angle (°)	Landfall Location	
						Longitude	Latitude
104	930	17.7	E4	17	0	-89.2743	29.5000
105	930	17.7	E5	17	0	-88.6455	29.5000
106	930	17.7	E1	17	-45	-91.3730	29.5000
107	930	17.7	E2	17	-45	-90.7265	29.5000
108	930	17.7	E3	17	-45	-89.9205	29.5000
109	930	17.7	E4	17	-45	-89.1060	29.5000
111	930	17.7	E1	17	45	-90.9923	29.5000
112	930	17.7	E2	17	45	-90.2108	29.5000
113	930	17.7	E3	17	45	-89.6386	29.5000
114	930	17.7	E4	17	45	-89.0571	29.5000
115	960	17.7	E1B	11	0	-90.8224	29.5000
116	900	17.7	E1B	11	0	-90.8224	29.5000
117	960	17.7	E2B	11	0	-90.1267	29.5000
118	900	17.7	E2B	11	0	-90.1267	29.5000
119	960	17.7	E3B	11	0	-89.6000	29.5000
120	900	17.7	E3B	11	0	-89.6000	29.5000
121	960	17.7	E4B	11	0	-88.9500	29.5000
122	900	17.7	E4B	11	0	-88.9500	29.5000
123	960	17.7	E1B	11	-45	-91.0508	29.5000
124	960	17.7	E2B	11	-45	-90.3192	29.5000
125	960	17.7	E3B	11	-45	-89.5123	29.5000
126	900	17.7	E1B	11	-45	-91.0508	29.5000
127	900	17.7	E2B	11	-45	-90.3192	29.5000
128	900	17.7	E3B	11	-45	-89.5123	29.5000
131	960	17.7	E1B	11	45	-90.6000	29.5000
132	900	17.7	E1B	11	45	-90.6000	29.5000
133	960	17.7	E2B	11	45	-89.9267	29.5000
134	900	17.7	E2B	11	45	-89.9267	29.5000
135	960	17.7	E3B	11	45	-89.3457	29.5000
136	900	17.7	E3B	11	45	-89.3457	29.5000
137	960	17.7	E1B	6	0	-90.8100	29.5000
138	900	17.7	E1B	6	0	-90.8100	29.5000
139	960	17.7	E2B	6	0	-90.1380	29.5000
140	900	17.7	E2B	6	0	-90.1380	29.5000
141	960	17.7	E3B	6	0	-89.6000	29.5000
142	900	17.7	E3B	6	0	-89.6000	29.5000

DRAFT

Storm Number	Minimum Central Pressure (mb)	Radius To Maximum Winds (nmi)	Track	Forward Velocity (kt)	Angle (°)	Landfall Location	
						Longitude	Latitude
143	960	17.7	E4B	6	0	-88.9520	29.5000
144	900	17.7	E4B	6	0	-88.9520	29.5000
145	930	17.7	E1B	6	-45	-91.0486	29.5000
146	930	17.7	E2B	6	-45	-90.3243	29.5000
147	930	17.7	E3B	6	-45	-89.5057	29.5000
149	930	17.7	E1B	6	45	-90.6050	29.5000
150	930	17.7	E2B	6	45	-89.9233	29.5000
151	930	17.7	E3B	6	45	-89.3500	29.5000
152	930	17.7	E1B	17	0	-90.8207	29.5000
153	930	17.7	E2B	17	0	-90.1300	29.5000
154	930	17.7	E3B	17	0	-89.6000	29.5000
155	930	17.7	E4B	17	0	-88.9548	29.5000
156	930	17.7	E1B	17	-45	-91.0470	29.5000
157	930	17.7	E2B	17	-45	-90.3185	29.5000
158	930	17.7	E3B	17	-45	-89.5195	29.5000
160	930	17.7	E1B	17	45	-90.6068	29.5000
161	930	17.7	E2B	17	45	-89.9217	29.5000
162	930	17.7	E3B	17	45	-89.3445	29.5000
201	960	11	W1	11	0	-94.2200	29.5000
202	960	21	W1	11	0	-94.2200	29.5000
203	960	35.6	W1	11	0	-94.2200	29.5000
204	930	8	W1	11	0	-94.2200	29.5000
205	930	17.7	W1	11	0	-94.2200	29.5000
206	930	25.8	W1	11	0	-94.2200	29.5000
207	900	6	W1	11	0	-94.2200	29.5000
208	900	14.9	W1	11	0	-94.2200	29.5000
209	900	21.8	W1	11	0	-94.2200	29.5000
210	960	11	W2	11	0	-93.5575	29.5000
211	960	21	W2	11	0	-93.5575	29.5000
212	960	35.6	W2	11	0	-93.5575	29.5000
213	930	8	W2	11	0	-93.5575	29.5000
214	930	17.7	W2	11	0	-93.5575	29.5000
215	930	25.8	W2	11	0	-93.5575	29.5000
216	900	6	W2	11	0	-93.5575	29.5000
217	900	14.9	W2	11	0	-93.5575	29.5000
218	900	21.8	W2	11	0	-93.5575	29.5000

DRAFT

Storm Number	Minimum Central Pressure (mb)	Radius To Maximum Winds (nmi)	Track	Forward Velocity (kt)	Angle (°)	Landfall Location	
						Longitude	Latitude
219	960	11	W3	11	0	-92.9641	29.5000
220	960	21	W3	11	0	-92.9641	29.5000
221	960	35.6	W3	11	0	-92.9641	29.5000
222	930	8	W3	11	0	-92.9641	29.5000
223	930	17.7	W3	11	0	-92.9641	29.5000
224	930	25.8	W3	11	0	-92.9641	29.5000
225	900	6	W3	11	0	-92.9641	29.5000
226	900	14.9	W3	11	0	-92.9641	29.5000
227	900	21.8	W3	11	0	-92.9641	29.5000
228	960	11	W4	11	0	-92.3165	29.5000
229	960	21	W4	11	0	-92.3165	29.5000
230	960	35.6	W4	11	0	-92.3165	29.5000
231	930	8	W4	11	0	-92.3165	29.5000
232	930	17.7	W4	11	0	-92.3165	29.5000
233	930	25.8	W4	11	0	-92.3165	29.5000
234	900	6	W4	11	0	-92.3165	29.5000
235	900	14.9	W4	11	0	-92.3165	29.5000
236	900	21.8	W4	11	0	-92.3165	29.5000
237	960	11	W5	11	0	-91.6535	29.5000
238	960	21	W5	11	0	-91.6535	29.5000
239	960	35.6	W5	11	0	-91.6535	29.5000
240	930	8	W5	11	0	-91.6535	29.5000
241	930	17.7	W5	11	0	-91.6535	29.5000
242	930	25.8	W5	11	0	-91.6535	29.5000
243	900	6	W5	11	0	-91.6535	29.5000
244	900	14.9	W5	11	0	-91.6535	29.5000
245	900	21.8	W5	11	0	-91.6535	29.5000
246	960	18.2	W1	11	-45	-94.2600	29.5000
247	960	24.6	W1	11	-45	-94.2600	29.5000
248	900	12.5	W1	11	-45	-94.2600	29.5000
249	900	18.4	W1	11	-45	-94.2600	29.5000
250	960	18.2	W2	11	-45	-93.2636	29.5000
251	960	24.6	W2	11	-45	-93.2636	29.5000
252	900	12.5	W2	11	-45	-93.2636	29.5000
253	900	18.4	W2	11	-45	-93.2636	29.5000
254	960	18.2	W3	11	-45	-92.3845	29.5000

DRAFT

Storm Number	Minimum Central Pressure (mb)	Radius To Maximum Winds (nmi)	Track	Forward Velocity (kt)	Angle (°)	Landfall Location	
						Longitude	Latitude
255	960	24.6	W3	11	-45	-92.3845	29.5000
256	900	12.5	W3	11	-45	-92.3845	29.5000
257	900	18.4	W3	11	-45	-92.3845	29.5000
258	960	18.2	W4	11	-45	-91.7515	29.5000
259	960	24.6	W4	11	-45	-91.7515	29.5000
260	900	12.5	W4	11	-45	-91.7515	29.5000
261	900	18.4	W4	11	-45	-91.7515	29.5000
266	960	18.2	W1	11	45	-94.2467	29.5000
267	960	24.6	W1	11	45	-94.2467	29.5000
268	900	12.5	W1	11	45	-94.2467	29.5000
269	900	18.4	W1	11	45	-94.2467	29.5000
270	960	18.2	W2	11	45	-93.2833	29.5000
271	960	24.6	W2	11	45	-93.2833	29.5000
272	900	12.5	W2	11	45	-93.2833	29.5000
273	900	18.4	W2	11	45	-93.2833	29.5000
274	960	18.2	W3	11	45	-92.3167	29.5000
275	960	24.6	W3	11	45	-92.3167	29.5000
276	900	12.5	W3	11	45	-92.3167	29.5000
277	900	18.4	W3	11	45	-92.3167	29.5000
278	960	18.2	W4	11	45	-91.4135	29.5000
279	960	24.6	W4	11	45	-91.4135	29.5000
280	900	12.5	W4	11	45	-91.4135	29.5000
281	900	18.4	W4	11	45	-91.4135	29.5000
282	960	17.7	W1	6	0	-94.2244	29.5000
283	900	17.7	W1	6	0	-94.2244	29.5000
284	960	17.7	W2	6	0	-93.5575	29.5000
285	900	17.7	W2	6	0	-93.5575	29.5000
286	960	17.7	W3	6	0	-92.9600	29.5000
287	900	17.7	W3	6	0	-92.9600	29.5000
288	960	17.7	W4	6	0	-92.3178	29.5000
289	900	17.7	W4	6	0	-92.3178	29.5000
290	960	17.7	W5	6	0	-91.6522	29.5000
291	900	17.7	W5	6	0	-91.6522	29.5000
292	930	17.7	W1	6	-45	-94.2500	29.5000
293	930	17.7	W2	6	-45	-93.2650	29.5000
294	930	17.7	W3	6	-45	-92.3800	29.5000

DRAFT

Storm Number	Minimum Central Pressure (mb)	Radius To Maximum Winds (nmi)	Track	Forward Velocity (kt)	Angle (°)	Landfall Location	
						Longitude	Latitude
295	930	17.7	W4	6	-45	-91.7500	29.5000
297	930	17.7	W1	6	45	-94.2540	29.5000
298	930	17.7	W2	6	45	-93.2867	29.5000
299	930	17.7	W3	6	45	-92.3189	29.5000
300	930	17.7	W4	6	45	-91.4140	29.5000
301	930	17.7	W1	17	0	-94.2250	29.5000
302	930	17.7	W2	17	0	-93.5624	29.5000
303	930	17.7	W3	17	0	-92.9640	29.5000
304	930	17.7	W4	17	0	-92.3159	29.5000
305	930	17.7	W5	17	0	-91.6531	29.5000
306	930	17.7	W1	17	-45	-94.2567	29.5000
307	930	17.7	W2	17	-45	-93.2650	29.5000
308	930	17.7	W3	17	-45	-92.3771	29.5000
309	930	17.7	W4	17	-45	-91.7442	29.5000
311	930	17.7	W1	17	45	-94.2500	29.5000
312	930	17.7	W2	17	45	-93.2800	29.5000
313	930	17.7	W3	17	45	-92.3144	29.5000
314	930	17.7	W4	17	45	-91.4137	29.5000
315	960	17.7	W1B	11	0	-93.9253	29.5000
316	900	17.7	W1B	11	0	-93.9253	29.5000
317	960	17.7	W2B	11	0	-93.2294	29.5000
318	900	17.7	W2B	11	0	-93.2294	29.5000
319	960	17.7	W3B	11	0	-92.6065	29.5000
320	900	17.7	W3B	11	0	-92.6065	29.5000
321	960	17.7	W4B	11	0	-91.9718	29.5000
322	900	17.7	W4B	11	0	-91.9718	29.5000
323	960	17.7	W1B	11	-45	-93.7340	29.5000
324	960	17.7	W2B	11	-45	-92.8027	29.5000
325	960	17.7	W3B	11	-45	-92.0336	29.5000
326	900	17.7	W1B	11	-45	-93.7340	29.5000
327	900	17.7	W2B	11	-45	-92.8027	29.5000
328	900	17.7	W3B	11	-45	-92.0336	29.5000
331	960	17.7	W1B	11	45	-93.7278	29.5000
332	900	17.7	W1B	11	45	-93.7278	29.5000
333	960	17.7	W2B	11	45	-92.7953	29.5000
334	900	17.7	W2B	11	45	-92.7953	29.5000

DRAFT

Storm Number	Minimum Central Pressure (mb)	Radius To Maximum Winds (nmi)	Track	Forward Velocity (kt)	Angle (°)	Landfall Location	
						Longitude	Latitude
335	960	17.7	W3B	11	45	-91.9044	29.5000
336	900	17.7	W3B	11	45	-91.9044	29.5000
337	960	17.7	W1B	6	0	-93.9233	29.5000
338	900	17.7	W1B	6	0	-93.9233	29.5000
339	960	17.7	W2B	6	0	-93.2344	29.5000
340	900	17.7	W2B	6	0	-93.2344	29.5000
341	960	17.7	W3B	6	0	-92.6133	29.5000
342	900	17.7	W3B	6	0	-92.6133	29.5000
343	960	17.7	W4B	6	0	-91.9733	29.5000
344	900	17.7	W4B	6	0	-91.9733	29.5000
345	930	17.7	W1B	6	-45	-93.7267	29.5000
346	930	17.7	W2B	6	-45	-92.8000	29.5000
347	930	17.7	W3B	6	-45	-92.0350	29.5000
349	930	17.7	W1B	6	45	-93.7278	29.5000
350	930	17.7	W2B	6	45	-92.7867	29.5000
351	930	17.7	W3B	6	45	-91.9040	29.5000
352	930	17.7	W1B	17	0	-93.9225	29.5000
353	930	17.7	W2B	17	0	-93.2320	29.5000
354	930	17.7	W3B	17	0	-92.6100	29.5000
355	930	17.7	W4B	17	0	-91.9723	29.5000
356	930	17.7	W1B	17	-45	-93.7327	29.5000
357	930	17.7	W2B	17	-45	-92.8012	29.5000
358	930	17.7	W3B	17	-45	-92.0317	29.5000
360	930	17.7	W1B	17	45	-93.7300	29.5000
361	930	17.7	W2B	17	45	-92.7932	29.5000
362	930	17.7	W3B	17	45	-91.9037	29.5000
401	975	11	W1	11	0	-94.2200	29.5000
402	975	21	W1	11	0	-94.2200	29.5000
403	975	35.6	W1	11	0	-94.2200	29.5000
404	975	11	W2	11	0	-93.5575	29.5000
405	975	21	W2	11	0	-93.5575	29.5000
406	975	35.6	W2	11	0	-93.5575	29.5000
407	975	11	W3	11	0	-92.9641	29.5000
408	975	21	W3	11	0	-92.9641	29.5000
409	975	35.6	W3	11	0	-92.9641	29.5000
410	975	11	W4	11	0	-92.3165	29.5000

DRAFT

Storm Number	Minimum Central Pressure (mb)	Radius To Maximum Winds (nmi)	Track	Forward Velocity (kt)	Angle (°)	Landfall Location	
						Longitude	Latitude
411	975	21	W4	11	0	-92.3165	29.5000
412	975	35.6	W4	11	0	-92.3165	29.5000
413	975	11	W5	11	0	-91.6535	29.5000
414	975	21	W5	11	0	-91.6535	29.5000
415	975	35.6	W5	11	0	-91.6535	29.5000
416	975	18.2	W1	11	-45	-94.2600	29.5000
417	975	24.6	W1	11	-45	-94.2600	29.5000
418	975	18.2	W2	11	-45	-93.2636	29.5000
419	975	24.6	W2	11	-45	-93.2636	29.5000
420	975	18.2	W3	11	-45	-92.3845	29.5000
421	975	24.6	W3	11	-45	-92.3845	29.5000
422	975	18.2	W4	11	-45	-91.7515	29.5000
423	975	24.6	W4	11	-45	-91.7515	29.5000
424	975	18.2	W1	11	45	-94.2467	29.5000
425	975	24.6	W1	11	45	-94.2467	29.5000
426	975	18.2	W2	11	45	-93.2833	29.5000
427	975	24.6	W2	11	45	-93.2833	29.5000
428	975	18.2	W3	11	45	-92.3167	29.5000
429	975	24.6	W3	11	45	-92.3167	29.5000
430	975	18.2	W4	11	45	-91.4135	29.5000
431	975	24.6	W4	11	45	-91.4135	29.5000
432	975	17.7	W1	6	0	-94.2244	29.5000
433	975	17.7	W2	6	0	-93.5575	29.5000
434	975	17.7	W3	6	0	-92.9600	29.5000
435	975	17.7	W4	6	0	-92.3178	29.5000
436	975	17.7	W5	6	0	-91.6522	29.5000
437	975	17.7	W1	6	-45	-94.2500	29.5000
438	975	17.7	W2	6	-45	-93.2650	29.5000
439	975	17.7	W3	6	-45	-92.3800	29.5000
440	975	17.7	W4	6	-45	-91.7500	29.5000
441	975	17.7	W1	6	45	-94.2540	29.5000
442	975	17.7	W2	6	45	-93.2867	29.5000
443	975	17.7	W3	6	45	-92.3189	29.5000
444	975	17.7	W4	6	45	-91.4140	29.5000
445	975	17.7	W1	17	0	-94.2250	29.5000
446	975	17.7	W2	17	0	-93.5624	29.5000

DRAFT

Storm Number	Minimum Central Pressure (mb)	Radius To Maximum Winds (nmi)	Track	Forward Velocity (kt)	Angle (°)	Landfall Location	
						Longitude	Latitude
447	975	17.7	W3	17	0	-92.9640	29.5000
448	975	17.7	W4	17	0	-92.3159	29.5000
449	975	17.7	W5	17	0	-91.6531	29.5000
450	975	17.7	W1	17	-45	-94.2567	29.5000
451	975	17.7	W2	17	-45	-93.2650	29.5000
452	975	17.7	W3	17	-45	-92.3771	29.5000
453	975	17.7	W4	17	-45	-91.7442	29.5000
454	975	17.7	W1	17	45	-94.2500	29.5000
455	975	17.7	W2	17	45	-93.2800	29.5000
456	975	17.7	W3	17	45	-92.3144	29.5000
457	975	17.7	W4	17	45	-91.4137	29.5000
458	975	17.7	W1B	11	0	-93.9253	29.5000
459	975	17.7	W2B	11	0	-93.2294	29.5000
460	975	17.7	W3B	11	0	-92.6065	29.5000
461	975	17.7	W4B	11	0	-91.9718	29.5000
462	975	17.7	W1B	6	0	-93.9233	29.5000
463	975	17.7	W2B	6	0	-93.2344	29.5000
464	975	17.7	W3B	6	0	-92.6133	29.5000
465	975	17.7	W4B	6	0	-91.9733	29.5000
466	975	17.7	W1B	6	-45	-93.7267	29.5000
467	975	17.7	W2B	6	-45	-92.8000	29.5000
468	975	17.7	W3B	6	-45	-92.0350	29.5000
469	975	17.7	W1B	6	45	-93.7278	29.5000
470	975	17.7	W2B	6	45	-92.7867	29.5000
471	975	17.7	W3B	6	45	-91.9040	29.5000
501	975	11	E1	11	0	-91.2111	29.5000
502	975	21	E1	11	0	-91.2111	29.5000
503	975	35.6	E1	11	0	-91.2111	29.5000
504	975	11	E2	11	0	-90.4511	29.5000
505	975	21	E2	11	0	-90.4511	29.5000
506	975	35.6	E2	11	0	-90.4511	29.5000
507	975	11	E3	11	0	-89.8479	29.5000
508	975	21	E3	11	0	-89.8479	29.5000
509	975	35.6	E3	11	0	-89.8479	29.5000
510	975	11	E4	11	0	-89.2758	29.5000
511	975	21	E4	11	0	-89.2758	29.5000

DRAFT

Storm Number	Minimum Central Pressure (mb)	Radius To Maximum Winds (nmi)	Track	Forward Velocity (kt)	Angle (°)	Landfall Location	
						Longitude	Latitude
512	975	35.6	E4	11	0	-89.2758	29.5000
513	975	11	E5	11	0	-88.6467	29.5000
514	975	21	E5	11	0	-88.6467	29.5000
515	975	35.6	E5	11	0	-88.6467	29.5000
516	975	18.2	E1	11	-45	-91.3677	29.5000
517	975	24.6	E1	11	-45	-91.3677	29.5000
518	975	18.2	E2	11	-45	-90.7238	29.5000
519	975	24.6	E2	11	-45	-90.7238	29.5000
520	975	18.2	E3	11	-45	-89.9208	29.5000
521	975	24.6	E3	11	-45	-89.9208	29.5000
522	975	18.2	E4	11	-45	-89.1054	29.5000
523	975	24.6	E4	11	-45	-89.1054	29.5000
524	975	18.2	E1	11	45	-90.9941	29.5000
525	975	24.6	E1	11	45	-90.9941	29.5000
526	975	18.2	E2	11	45	-90.2138	29.5000
527	975	24.6	E2	11	45	-90.2138	29.5000
528	975	18.2	E3	11	45	-89.6380	29.5000
529	975	24.6	E3	11	45	-89.6380	29.5000
530	975	18.2	E4	11	45	-89.0471	29.5000
531	975	24.6	E4	11	45	-89.0471	29.5000
532	975	17.7	E1	6	0	-91.1978	29.5000
533	975	17.7	E2	6	0	-90.4540	29.5000
534	975	17.7	E3	6	0	-89.8470	29.5000
535	975	17.7	E4	6	0	-89.2700	29.5000
536	975	17.7	E5	6	0	-88.6490	29.5000
537	975	17.7	E1	6	-45	-91.3729	29.5000
538	975	17.7	E2	6	-45	-90.7129	29.5000
539	975	17.7	E3	6	-45	-89.9200	29.5000
540	975	17.7	E4	6	-45	-89.0971	29.5000
541	975	17.7	E1	6	45	-90.9920	29.5000
542	975	17.7	E2	6	45	-90.2100	29.5000
543	975	17.7	E3	6	45	-89.6425	29.5000
544	975	17.7	E4	6	45	-89.0500	29.5000
545	975	17.7	E1	17	0	-91.2177	29.5000
546	975	17.7	E2	17	0	-90.4437	29.5000
547	975	17.7	E3	17	0	-89.8476	29.5000

DRAFT

Storm Number	Minimum Central Pressure (mb)	Radius To Maximum Winds (nmi)	Track	Forward Velocity (kt)	Angle (°)	Landfall Location	
						Longitude	Latitude
548	975	17.7	E4	17	0	-89.2743	29.5000
549	975	17.7	E5	17	0	-88.6455	29.5000
550	975	17.7	E1	17	-45	-91.3730	29.5000
551	975	17.7	E2	17	-45	-90.7265	29.5000
552	975	17.7	E3	17	-45	-89.9205	29.5000
553	975	17.7	E4	17	-45	-89.1060	29.5000
554	975	17.7	E1	17	45	-90.9923	29.5000
555	975	17.7	E2	17	45	-90.2108	29.5000
556	975	17.7	E3	17	45	-89.6386	29.5000
557	975	17.7	E4	17	45	-89.0571	29.5000
558	975	17.7	E1B	11	0	-90.8224	29.5000
559	975	17.7	E2B	11	0	-90.1267	29.5000
560	975	17.7	E3B	11	0	-89.6000	29.5000
561	975	17.7	E4B	11	0	-88.9500	29.5000
562	975	17.7	E1B	6	0	-90.8100	29.5000
563	975	17.7	E2B	6	0	-90.1380	29.5000
564	975	17.7	E3B	6	0	-89.6000	29.5000
565	975	17.7	E4B	6	0	-88.9520	29.5000
566	975	17.7	E1B	6	-45	-91.0486	29.5000
567	975	17.7	E2B	6	-45	-90.3243	29.5000
568	975	17.7	E3B	6	-45	-89.5057	29.5000
569	975	17.7	E1B	6	45	-90.6050	29.5000
570	975	17.7	E2B	6	45	-89.9233	29.5000
571	975	17.7	E3B	6	45	-89.3500	29.5000

Figures 2-2 and 2-3 show a single storm simulation that was conducted using the 2017CPRA model, assuming the Current Conditions landscape. Figures 2-4 and 2-5 show the same storm for the Less Optimistic FWOA scenario. Finally, Figure 2-6 shows the difference between the surge levels in Current Conditions and the Less Optimistic FWOA scenario. Note in Figure 2-6 that, through much of the domain, the orange value is representative of the eustatic sea level rise applied to the model in Less Optimistic conditions. Contours other than orange represent a nonlinear storm surge response (e.g. a flood hazard change that differs from the eustatic sea level rise applied in the model).

Information from these simulations was extracted and packaged for analysis by the CLARA model. The CLARA model recieves input from the surge and waves model at four sets of locations: (1) Unprotected census blocks (UCB), (2) Semi-protected census blocks (SPB), (3) Surge and wave points (SWP), and (4) CLARA model grid points (RSP). Each set of points receives maximum surge elevation and maximum signficiant wave height information. Surge

and wave points additionaly receive the peak wave period for the maximum wave significant height, as well as time series storm surge elevation.

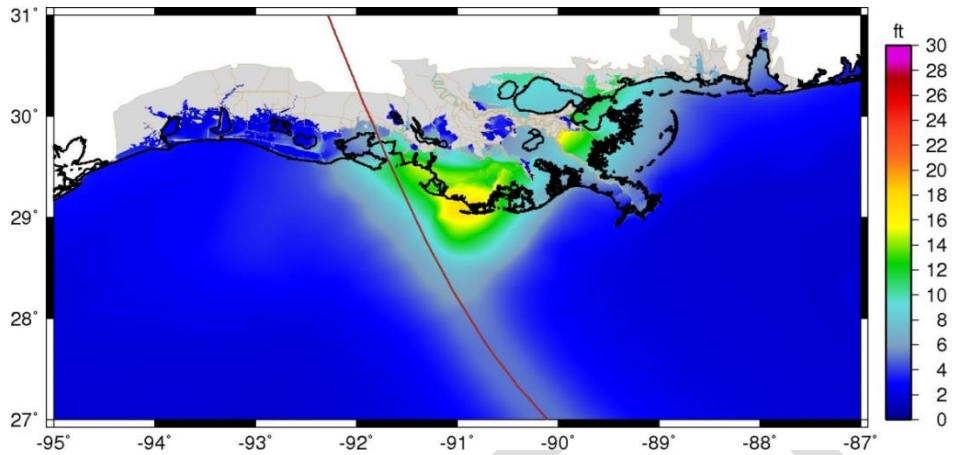

Figure 2-2: Maximum storm surge elevation (ft, NAVD88) for Storm 245 under the Current Conditions scenario. Storm track shown in brown.

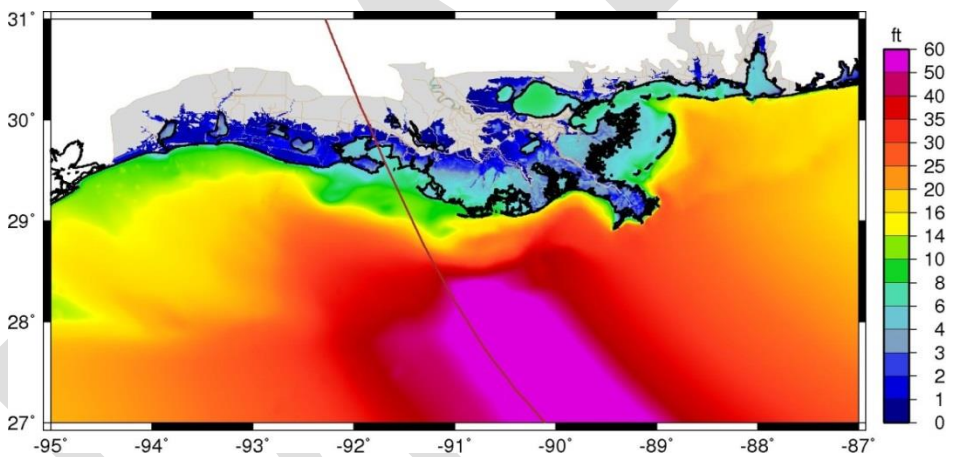

Figure 2-3: Maximum significant wave height (ft) for Storm 245 under the Current Conditions scenario. Storm track shown in brown.

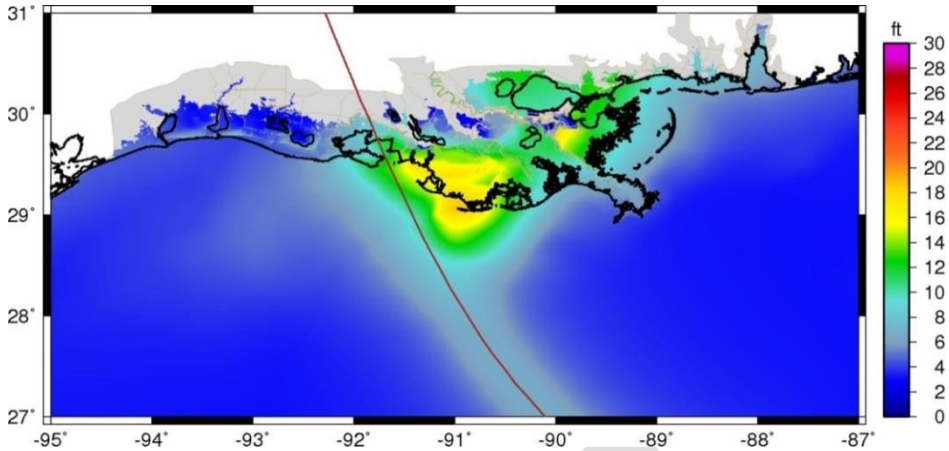

Figure 2-4: Maximum storm surge elevation (ft, NAVD88) for Storm 245 under the Less Optimistic scenario. Storm track shown in brown.

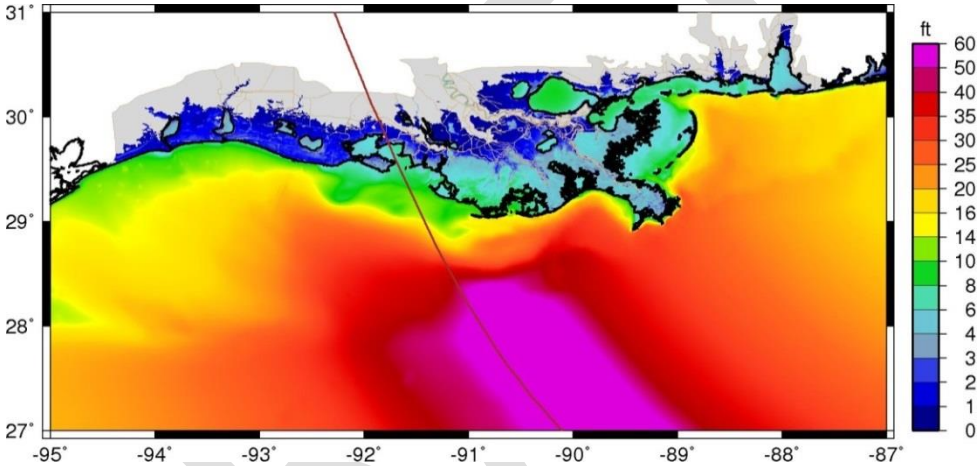

Figure 2-5: Maximum significant wave height (ft) for Storm 245 under the Less Optimistic scenario. Storm track shown in brown.

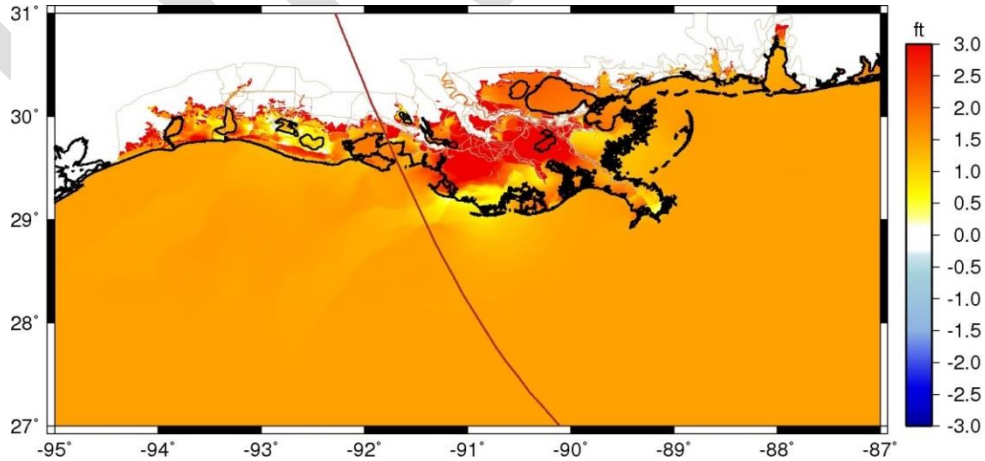

Figure 2-6: Difference in water levels (ft) between the Less Optimistic scenario and Current Conditions scenario. Positive values indicate Less Optimistic elevations higher than Current Conditions. Strom track shown in brown.

References

Powell, M.D. (2006). Final Report to the National Oceanic and Atmospheric Administration (NOAA) Joint Hurricane Testbed (JHT) Program. 26 pp.

USACE (2008b). Flood Insurance Study: Southeastern Parishes, Louisiana. Intermediate Submission 2: Offshore Water Levels and Waves. Vicksburg, Mississippi: USACE, 152 pp.

USACE (2008c). Flood Insurance Study: Southwestern Parishes, Louisiana. Intermediate Submission 2. Vicksburg, Mississippi: USACE, 697 pp.

DRAFT

Appendix 3: Raised Feature Elevation Interpolation Sensitivity Analysis

In coastal Louisiana, there are many critical features included in a storm surge model to accurately predict the movement of water throughout the system. A portion of these are frequently surveyed levees, such as federally maintained levees. The application of levee elevations in the ADvanced CIRCulation (ADCIRC)+Simulating Waves Nearshore (SWAN) model using levee crown surveys is a process that is as accurate as the survey itself. However, some critical hydraulic features (one meter or more above the surrounding landscape), such as local levees, roadways, dredge spoil mounds, and natural ridges lacksite specific survey data gathered with the intention of capturing the feature's crown elevation. When site specific survey data are not available, the crown elevations of these features must be defined using LIDAR data which do not target specific locations (e.g. feature crown locations) on the landscape. The determination of accurate representative crown elevations for these features may reduce model uncertainty.

Crown elevations for critical raised features without site specific survey data have previously been estimated from LIDAR datasets using a control volume method to normalize the selection area for elevations based upon the size of elements in the numerical model (Cobell et al., 2013; USACE, 2008a; USACE, 2008b; USACE, 2008c). A schematic is shown in Figure 3-1. In this figure, the black lines represent the triangular finite elements of the ADCIRC mesh, with the red dot representing the vertex of concern. The blue triangles represent the centers of each finite element. The red box is an example of a control volume. The LIDAR data inside this control volume are selected for analysis.

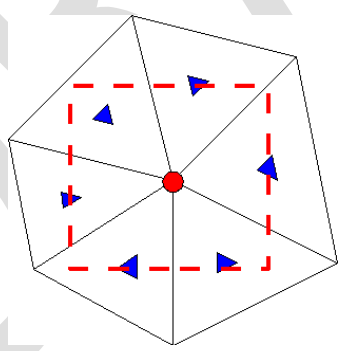

Figure 3-1: Schematic of a control volume approach for triangular finite elements.

Determining crown elevations of raised features, particularly at intersections of multiple features, can be difficult and is an ongoing research topic known as edge or ridge detection (Coggin, 2008).

For this analysis, three methods were applied to determine crown elevations of raised features that do not have individual survey data. These methods were applied in Barataria Basin and the Chenier Plain using the 2001 ATLAS LIDAR (Louisiana State University, 2004), shown in Figure 3-2. Barataria Basin has features that have relatively shorter lengths, on the order of a few miles, than

the Chenier Plain, which has many roads and natural ridges extending over the broad floodplain for 50 miles or more. This analysis assumes that the LIDAR maintains enough resolution to adequately describe the crest of the feature and, therefore, all three methods were applied without any additional post-processing.

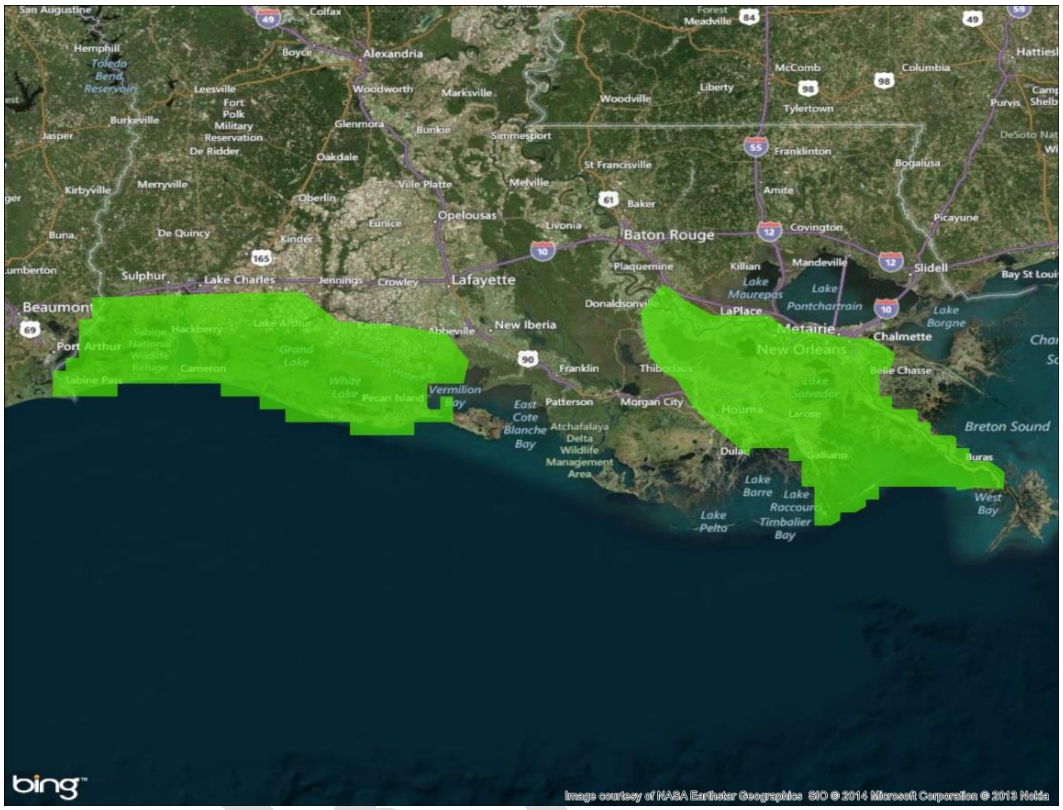

Figure 3-2: Raised feature sensitivity test domains.

Note that more recent LIDAR is available in coastal Louisiana than the 2001 ATLAS data. However, other data were not readily available during the study. Because this analysis is an evaluation of the sensitivity of interpolation methodologies and not the data themselves, these data were applied rather than more recent LIDAR.

For each of the methods, the suite of 40 storms utilized during the 2012 Coastal Master Plan was simulated on ADCIRC model meshes with modified raised feature elevations. As was done with the full suite of 446 storms from Appendix 2, information regarding storm surge and waves was extracted at discrete locations and passed to the Coastal Louisiana Risk Assessment (CLARA) model for analysis. Results are used as part of the CLARA model development tasks to assess the uncertainty related to the ADCIRC model development, specifically the translation of continuous, two-dimensional data onto linear features defined by discrete points. The appliciation of elevation data onto the model vertices is believed to be one of the largest sources of uncertainty in ADCIRC model development.

Maximum Value Method

The maximum value method extracts the maximum topographic elevation within a defined control volume around each model vertex aligned along a given raised feature. The sampling is performed on a diameter equal to the maximum finite element size that is connected to the vertex. As an example, if the vertex is connected to a 100-meter element, the searching radius will be 50 meters in any direction. The 1:1 size selection was used to ensure that the crown elevation along a suitable raised feature length is captured, even in instances where the model vertices are not aligned exactly along the raised feature crown as it is defined by LIDAR.

This method has the benefit of always finding the highest topography in the area and has generally been used for applying values to previous versions of USACE and CPRA ADCIRC models throughout Coastal Louisiana since the LACPR analysis, including the 2012 CPRA Coastal Master Plan. In this way, crown elevations are not underestimated, ensuring that hydraulic controls are fully captured. However, the risk of an approach like this is that crown elevations can be overstated by outliers in the data that are either not filtered in LIDAR post-processing or are high ground along an adjacent feature.

Based on comparisons to available site specific data, this technique has generally provided a reasonable representation of crown elevations along a feature, with the exception of feature reaches adjacent to other high land that can unintentionally set a crown elevation that is significantly higher than is actually present on the feature itself. Overstated elevations (e.g. those one foot above crown elevations determined through manual quality check procedures) have been manually adjusted in previous ADCIRC mesh development efforts. However, when numerous model scenarios are simulated, particularly for statewide analyses like the Coastal Master Plan, improved automation helps limit model setup errors and reduces the human time necessary for quality control.

Averaging Method

The averaging method, similar to the maximum value method, considers all LIDAR data within a selected control volume. LIDAR elevations within a diameter one half the maximum element size are averaged. For example, a vertex that is connected to a 100-meter element would search 25 meters in any direction. This method makes use of a smaller control volume than the maximum value method in order to reduce the number of low-lying LIDAR data (e.g., those in the floodplain immediately adjacent to the raised feature) included in the control volume. As the control volume becomes larger, the greater number of points selected from LIDAR will be from the floodplain, unintentionally lowering the crown elevation extracted at the mesh vertex.

The primary disadvantage of this approach is that some features, particularly those with narrow widths relative to the control volume size, will potentially be defined with too low of a crown elevation. However, the potential pitfall of overstating elevations in the maximum value method is addressed.

DRAFT

2σ Averaging Method

The 2**σ** averaging method was developed with the intent to leverage the benefits of the maximum value and averaging methods while limiting the impacts of the disadvantages associated with each method. The control volume size used is the same as the maximum value method.

This method assumes that the points that lie within each control volume resemble a normal distribution. To determine a representative crown elevation, only points with an elevation of 2**σ** or higher are considered, as shown in the red box in Figure 3-3. The aim is to isolate only those LIDAR points that are part of some raised features and not part of the surrounding floodplain.

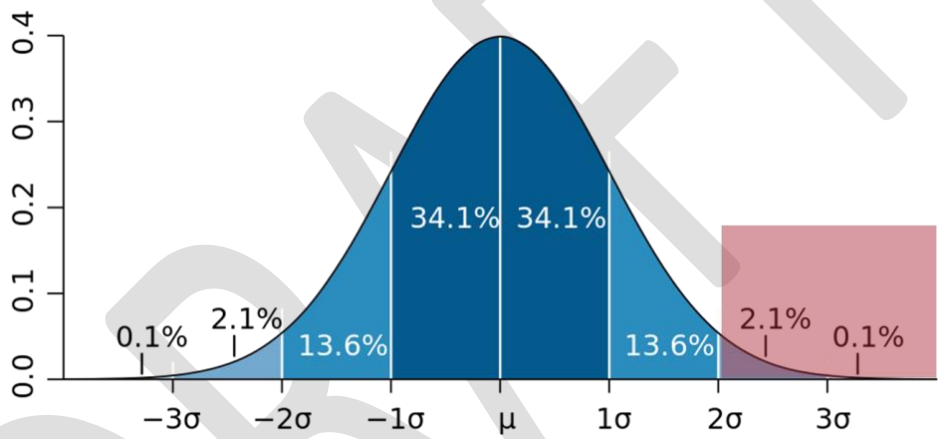

Figure 3-3: A normal distribution. Points within the control volume are assumed to follow a normal distribution with the raised features falling outside of positive 2*σ* from the mean, as shown by the red box.

Figures 3-4 and 3-6 show vertices with representative crown elevations determined through the 2**σ** averaging method and plotted with the same contour range as the LIDAR behind them. Similarly, Figures 3-5 and 3-7 show vertices with the representative crown elevations defined by the maximum value method. Figures 3-4 and 3-5 show a roadway that is higher than the surrounding topography. The applied crown elevations follow the trend of the raised feature in general for both methods. The maximum value method shows slightly higher elevations than the 2**σ** averaging method. Because the roadway has a generally consistent elevation, the slight difference in interpolation methods is expected, rather than more substantial differences.

DRAFT

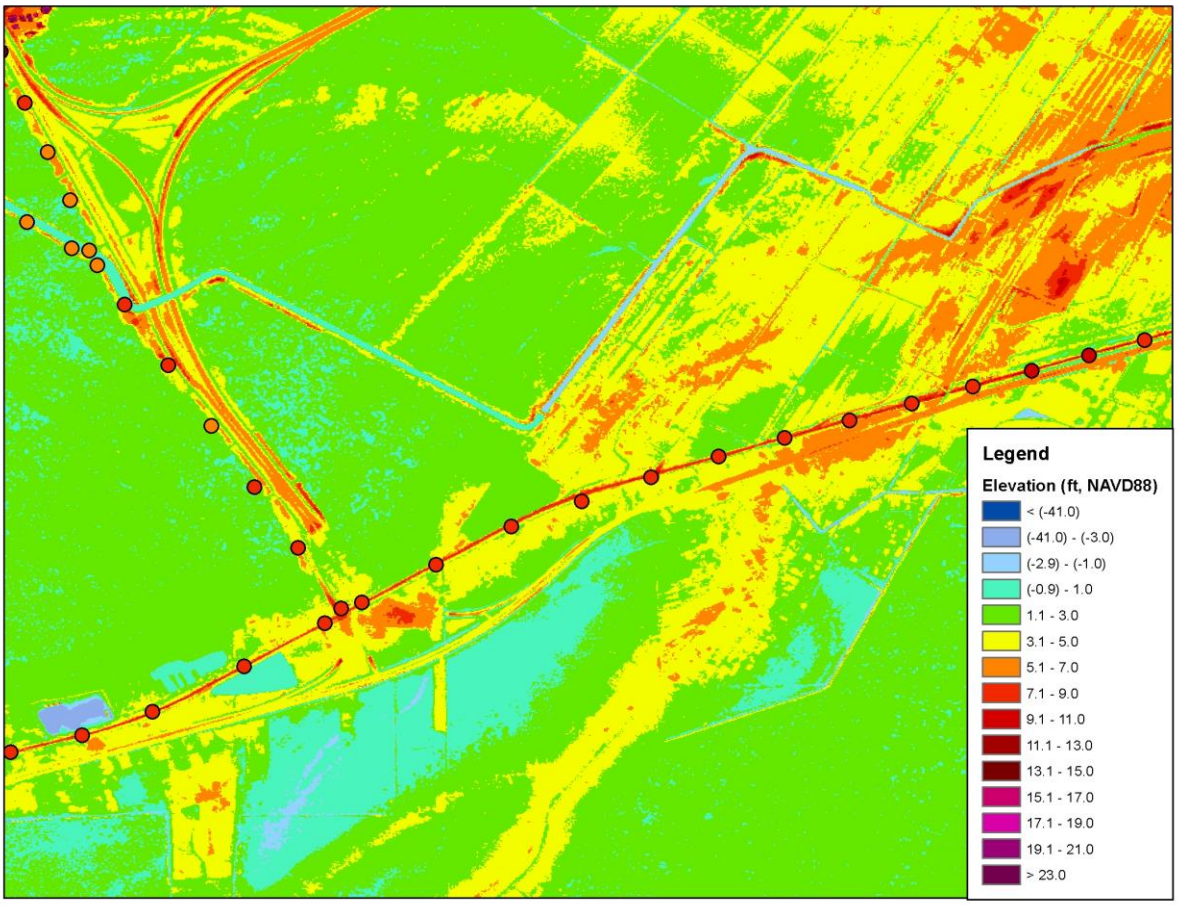

Figure 3-4: An example of an elevated roadway. LIDAR data is shown as a background. Circles show the elevations prescribed by the 2σ averaging method.

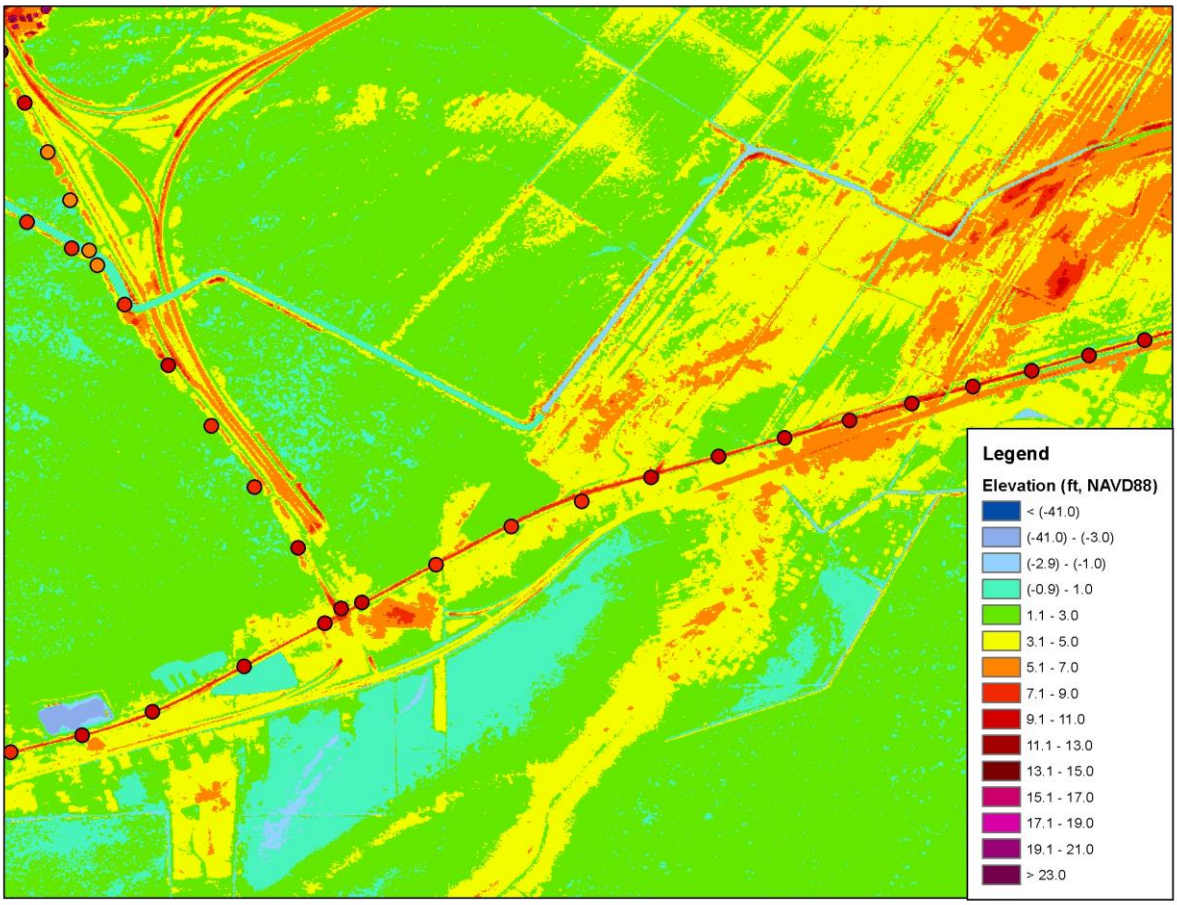

Figure 3-5: An example of an elevated roadway. LIDAR data is shown as a background. Circles show the elevations prescribed by the maximum value method.

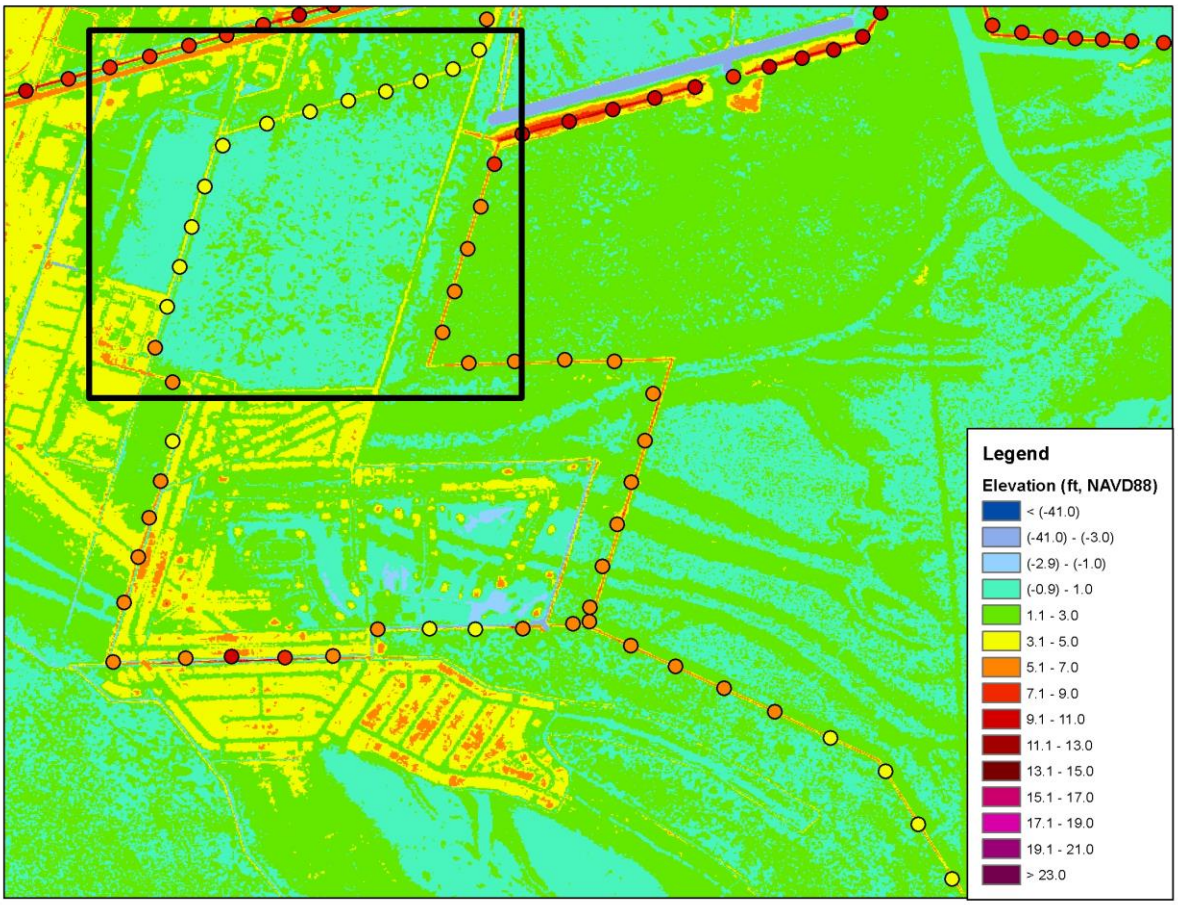

Figure 3-6: An example of a local levee with variable elevation. LIDAR data is shown as a background. Circles show the elevations prescribed by the 2σ averaging method.

DRAFT

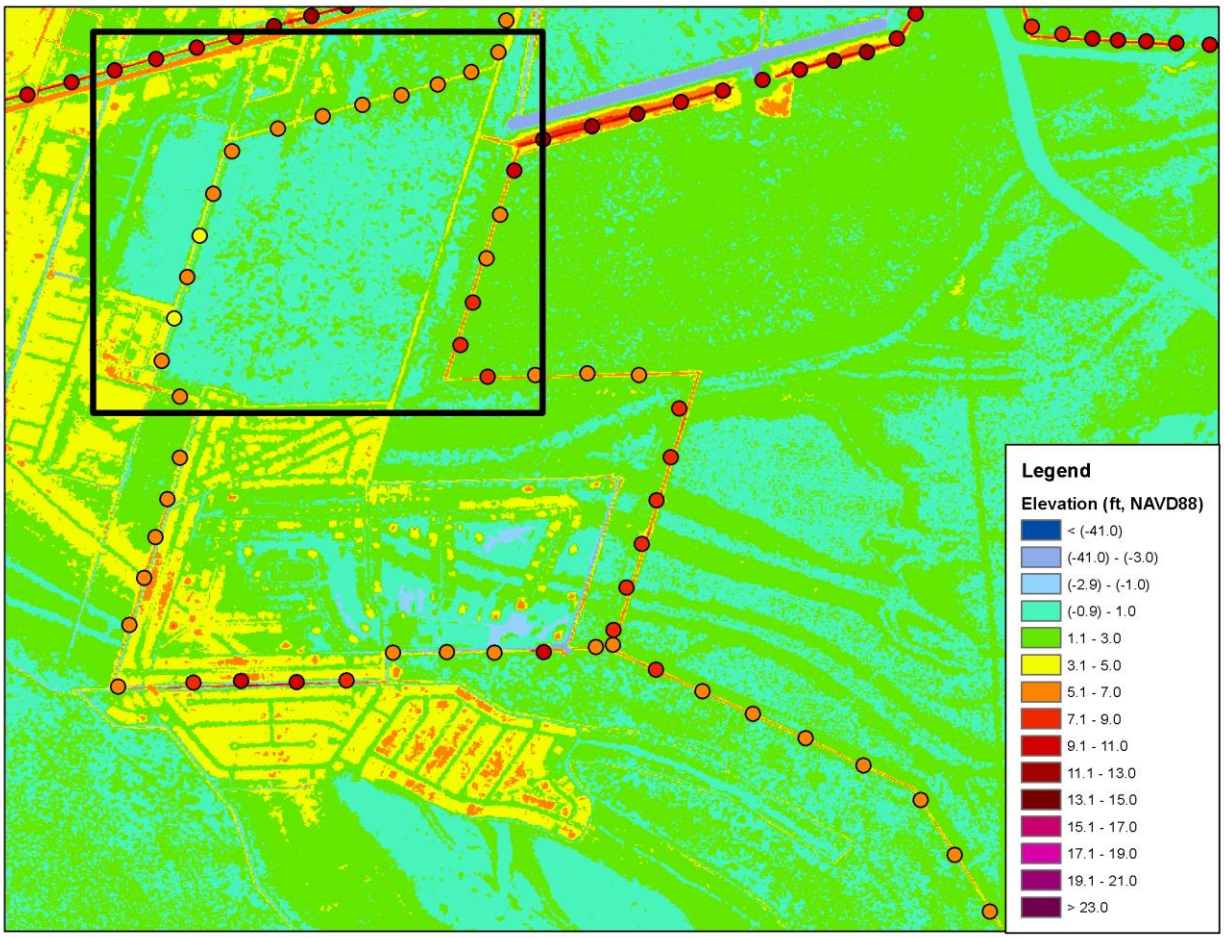

Figure 3-7: An example of a local levee with variable elevation. LIDAR data is shown as a background. Circles show the elevations prescribed by the maximum value method.

Figures 3-6 and 3-7 highlight a local levee. The LIDAR data contains high variability in topography along the feature. In the outlined region specifically, variability in LIDAR results in higher crown elevations when the maximum value approach is applied, as highlighted by the different interpolated elevations shown in Figures 3-6 and 3-7. The colored vertices in Figure 3-6 show that these high adjacent ground elevations are being filtered from the data to provide more realistic elevations for the targeted feature while Figure 3-7 shows that the maximum value overstates the elevation of the feature.

Simulation Results

Figure 3-8 shows the difference when surge elevations computed for the averaging method is subtracted from maximum value method. As expected, the averaging method increases surge behind most raised features because these features are comparatively lower. Surge is higher on the unprotected side of many raised features when using the maximum value method because the water builds up against the higher features. This comparison shows the level of difference that can be created by different methods of selecting elevation values for raised features.

The 2**σ** averaging method, however, results in only minor differences when compared to the maximum value method. Figure 3-9 shows this comparison. This is due to the small portion of data in the LIDAR that could artificially raise the elevation of a raised feature when applying a maximum value method.

The results demonstrate that the averaging method greatly understates the protection of features while the 2**σ** averaging method generates surges very near the maximum value method that had been generally applied previously. For future mesh development, the 2**σ** averaging method is recommended because it will not overstate protection. However, the simulations have shown that the maximum value method is reasonable as well, but would be a slightly more conservative estimate of protection.

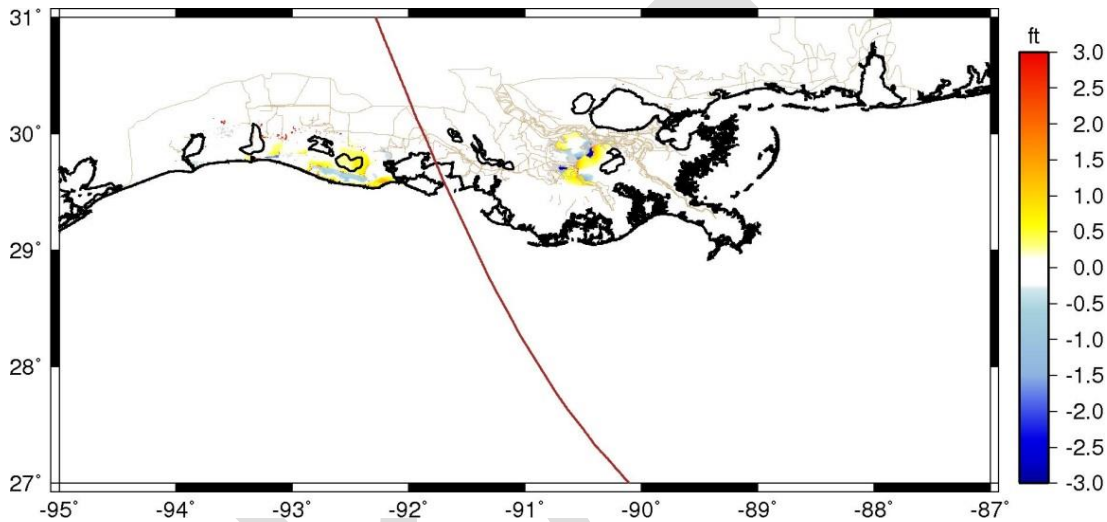

Figure 3-8: Difference in maximum surge elevation for maximum value method minus averaging method. Positive values indicate maximum value method has a higher surge in the area.

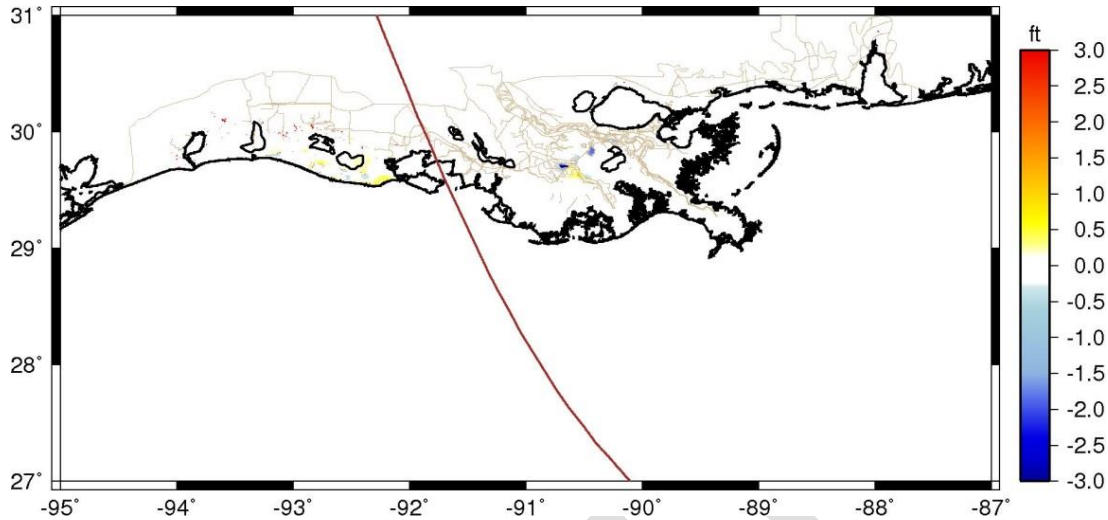

Figure 3-9: Difference in maximum surge elevation for maximum value method minus 2σ averaging method. Positive values indicate maximum value method has a higher surge in the area.

References

Cobell, Z., Zhao, H., Roberts, H.J., Clark, F.R., & Zou, S. (2013). Surge and Wave Modeling for the Louisiana 2012 Coastal Master Plan. Journal of Coastal Research: Special Issue 67 – Louisiana's 2012 Coastal Master Plan Technical Analysis, pp. 88-108.

Coggin, D. (2008). LIDAR in Coastal Storm Surge Modeling: Modeling Linear Raised Features, Unpublished Masters Thesis, University of Central Florida, Orlando, Florida.

Louisiana State University (LSU) (2004). Louisiana LIDAR. http://atlas.lsu.edu/LIDAR/.

USACE (2008a). Louisiana Coastal Protection and Restoration Technical Report. Vicksburg, Mississippi: USACE, 98 pp.

USACE (2008b). Flood Insurance Study: Southeastern Parishes, Louisiana. Intermediate Submission 2: Offshore Water Levels and Waves. Vicksburg, Mississippi: USACE, 152 pp.

USACE (2008c). Flood Insurance Study: Southwestern Parishes, Louisiana. Intermediate Submission 2. Vicksburg, Mississippi: USACE, 697 pp.

DRAFT

Appendix 4: Sector-Based Wind Drag Analysis

Until recently, storm surge and wave simulations utilizing the ADvanced CIRCulation (ADCIRC) model have applied a wind drag coefficient from Garratt (1977), as shown in Equation 1. Similarly, Simulating Waves Nearshore (SWAN) applied a nearly identical drag coefficient from Wu (1982), as shown in Equation 2.

$$C_d = \frac{1}{1000}\left(\frac{15}{20} + \frac{40}{600}U_{10}\right) \qquad (1)$$

$$C_d = \frac{1}{1000}\left(\frac{16}{20} + \frac{39}{600}U_{10}\right) \qquad (2)$$

However, Powell (2006) observed an azimuthal dependence of wind drag based upon dropsonde data. Later, Black et al. (2007) parameterized this dependence into storm sectors. This parameterization is shown in Figure 4-1.

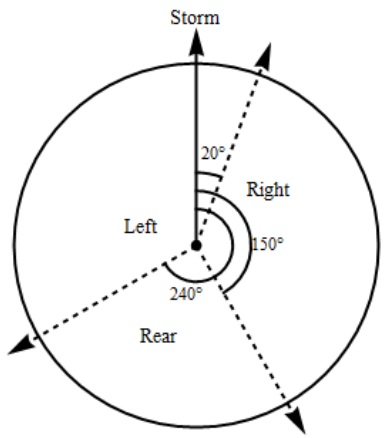

Figure 4-1: Parameterization of storm sectors

This parameterization aims to recreate the dependence of wind drag upon not only the speed of the wind but also the mean direction of wave travel. For waves that are moving in the same direction as the wind, the drag will be lower than when the waves are moving in the opposite direction as the wind. Figure 4-2 shows the wind drag scheme applied. The behavior in the right and rear sectors is similar to medium and low speed winds where the maximum drag coefficient is set at 0.002 with the right sector receiving a boost for high speed winds to 0.003. For these storm sectors, the counterclockwise winds, direction of storm travel, and mean wave directions are approximately aligned. By contrast, the left sector sees significantly increased wind drag. On the left side of the storm, the winds and waves are aligned in opposite directions. In this sector, wind drag is allowed to increase to 0.0045.

This wind drag algorithm is available to ADCIRC+SWAN versions 50 and greater.

DRAFT

Figure 4-2: Garratt Wind Drag Parameterization (left) and Parameterization of hurricane wind drag based upon storm sectors (right).

Before finalizing validations for Gustav (Dietrich et al., 2011) and Katrina, Rita, and Ike (Dietrich et al., 2012), Dietrich et al. implemented this new wind drag formulation into the ADCIRC model to optimize the validation of storm surge elevations and wave parameters. The Powell drag formulation, however, does create significant differences in storm surge response compared to the Garratt formulation. Figures 4-3 and 4-4 show the differences in storm surge elevations using the current conditions landscape created by simulating ADCIRC+SWAN considering the two wind drag formulations. For individual storms, the Powell wind drag formulation produces results that differ from both the 2012 Coastal Master Plan analysis and many other previous analyses, including the Federal Emergency Management Agency studies from 2008. However, based on model validation, described in Appendix 1, and to embrace the state of the science, the Powell sector based wind drag formulation is recommended for implementation in the 2017 Coastal Master Plan.

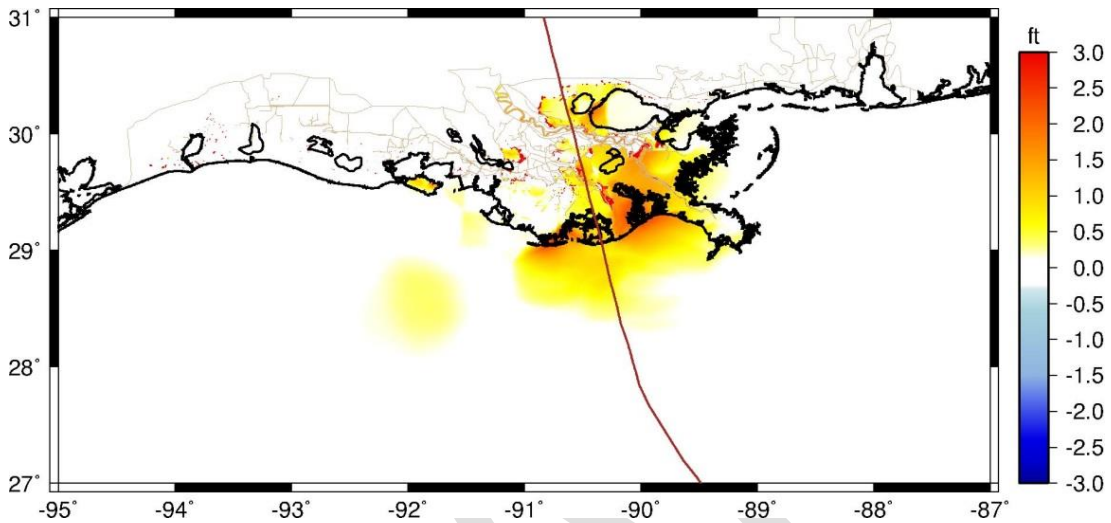

Figure 4-3: Surge elevation change for Storm 18 with Powell wind drag. Warm colors indicate greater surge when Powell wind drag is active.

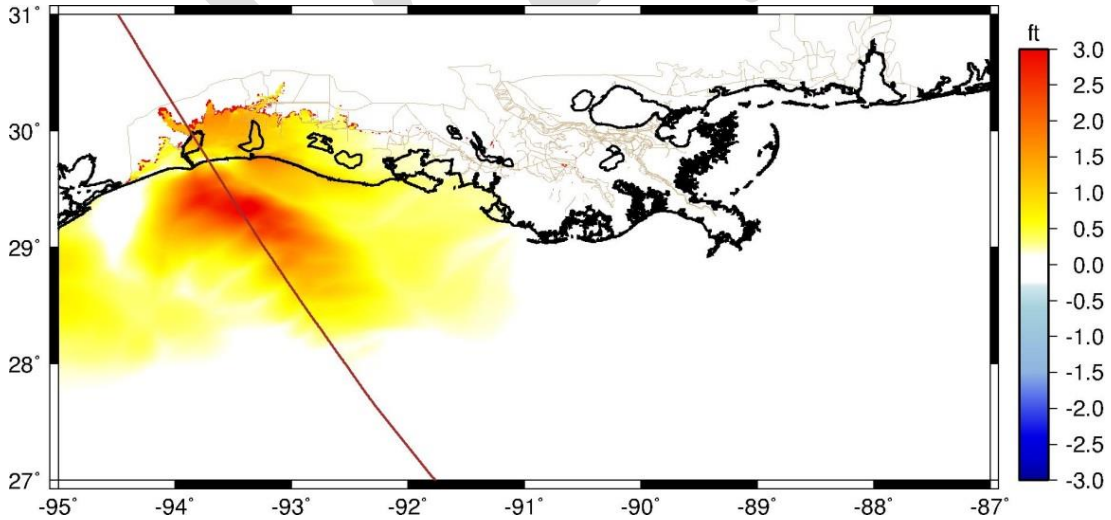

Figure 4-4: Surge Elevation Change for Storm 218 with Powell wind drag. Warm colors indicate greater surge when Powell wind drag is active.

References

Black, P.G., D'Asaro, E.A., Drennan, W.M., French, J.R., Niiler, P.P.,Sanford, T.B., Terrill, E.J., Walsh, E.J.,& Zhang. J.A. (2007). Air-Sea Exchange in Hurricanes: Synthesis of Observations from the Coupled Boundary Layer Air-Sea Transfer Experiment. Bulletin of the American Meteorological Society, Volume, 88, Issue 3, pp. 357-374.

Dietrich, J.C., Westerink, J.J., Kennedy, A.B., Smith, J.M., Jensen, R., Zijlema, M. Holthuijsen, L.H., Dawson, C., Luettich, Jr., R.A., Powell, M.D., Cardone, V.J., Cox, A.T., Stone, G.W., Pourtaheri, H., Hope, M.E., Tanaka, S., Westerink, L.G., Westerink, H.J., & Cobell.Z. (2011). Hurricane Gustav Waves and Storm Surge: Hindcast, Synoptic Analysis and Validation in Southern Louisiana. Monthly Weather Review, Volume 139, pp. 2488-2522, DOI 10.1175/2011MWR3611.1.

Dietrich, J.C., Tanaka, S., Westerink, J.J., Dawson, C.N., Luettich, Jr., R.A., Zijlema, M., Holthuijsen, L.H., Smith, J.M., Westerink, L.G., & Westerink, H.J. (2012). Performance of the Unstructured-Mesh, SWAN+ADCIRC Model in Computing Hurricane Waves and Surge. Journal of Scientific Computing, Volume 52, Issue 2, pp. 468-497.

Garratt, J.R. (1977). Review of Drag Coefficients over Oceans and Continents. Monthly Weather Review, Volume 105, pp. 915-929.

Powell, M.D. (2006). Final Report to the National Oceanic and Atmospheric Administration (NOAA) Joint Hurricane Testbed (JHT) Program. 26 pp.

Wu, J. (1982). Wind-Stress Coefficients over Sea Surface from Breeze to Hurricane. Journal of Geophysical Research, Volume 87, Issue C12, pp. 9704-9706.

DRAFT

Appendix 5: Asymmetric Hurricane Literature Review

At the 2013 ADvanced CIRCulation (ADCIRC) users meeting, Dr. Rick Luettich presented work that he has been pursuing related to asymmetric parametric hurricane wind models used in real time forecasting applications. The surge and waves team felt it would be important to understand how this related to statistical applications and better understand the treatment of asymmetry in the Planetary Boundary Layer (PBL) model used during the 2008 Federal Emergency Management Agency study in Louisiana and 2012 Coastal Master Plan.

Storm asymmetry plays an important part in determining how storm surge and waves will affect an area. Figure 5-1 shows Hurricane Isabel, which has a high level of symmetry, and Hurricane Bob, which has a high level of asymmetry. Storms with high asymmetry have greater distance to wind isotachs on one side of the storm than the other. This storm asymmetry is largely linked to the distortion that occurs due to greater translation speed (Tang and Liu, 2009). Figure 5-2 shows wind composites generated from data collected between 2000 and 2007 in the Northern Hemisphere. This data is normalized to the storm direction. The tangential component shows that, when storms have a greater translation speed, a left-right asymmetry is induced. The authors conclude that this asymmetry is an important component of hurricane weakening because it acts like a natural speed brake.

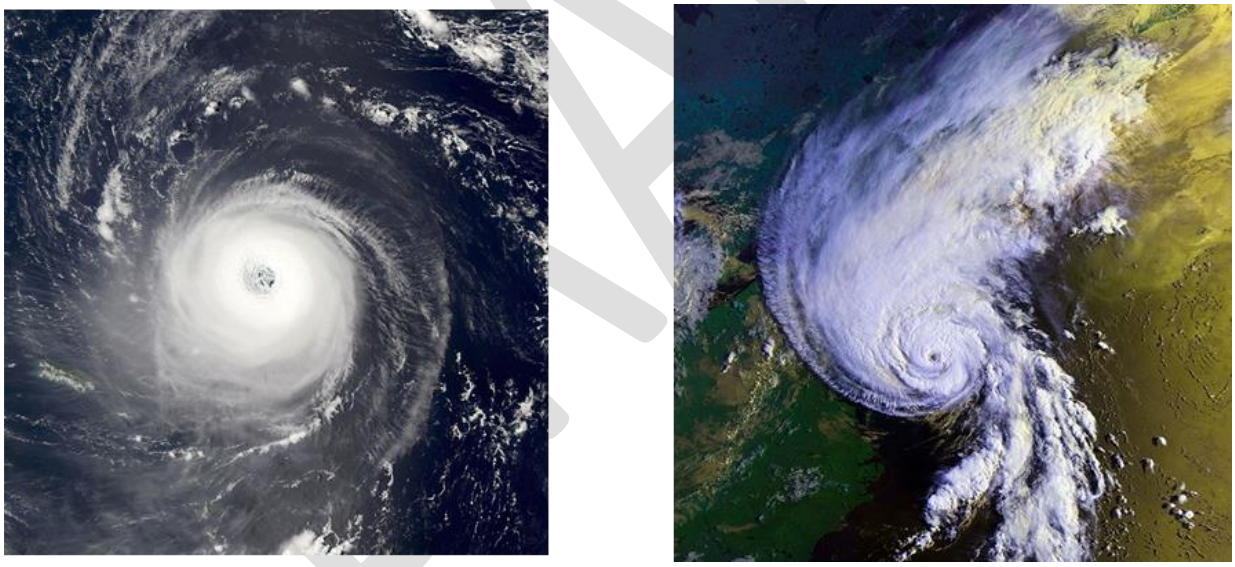

Figure 5-1: Hurricane Isabel (left), which is symmetric, and Hurricane Bob (right), which is highly asymmetric.

DRAFT

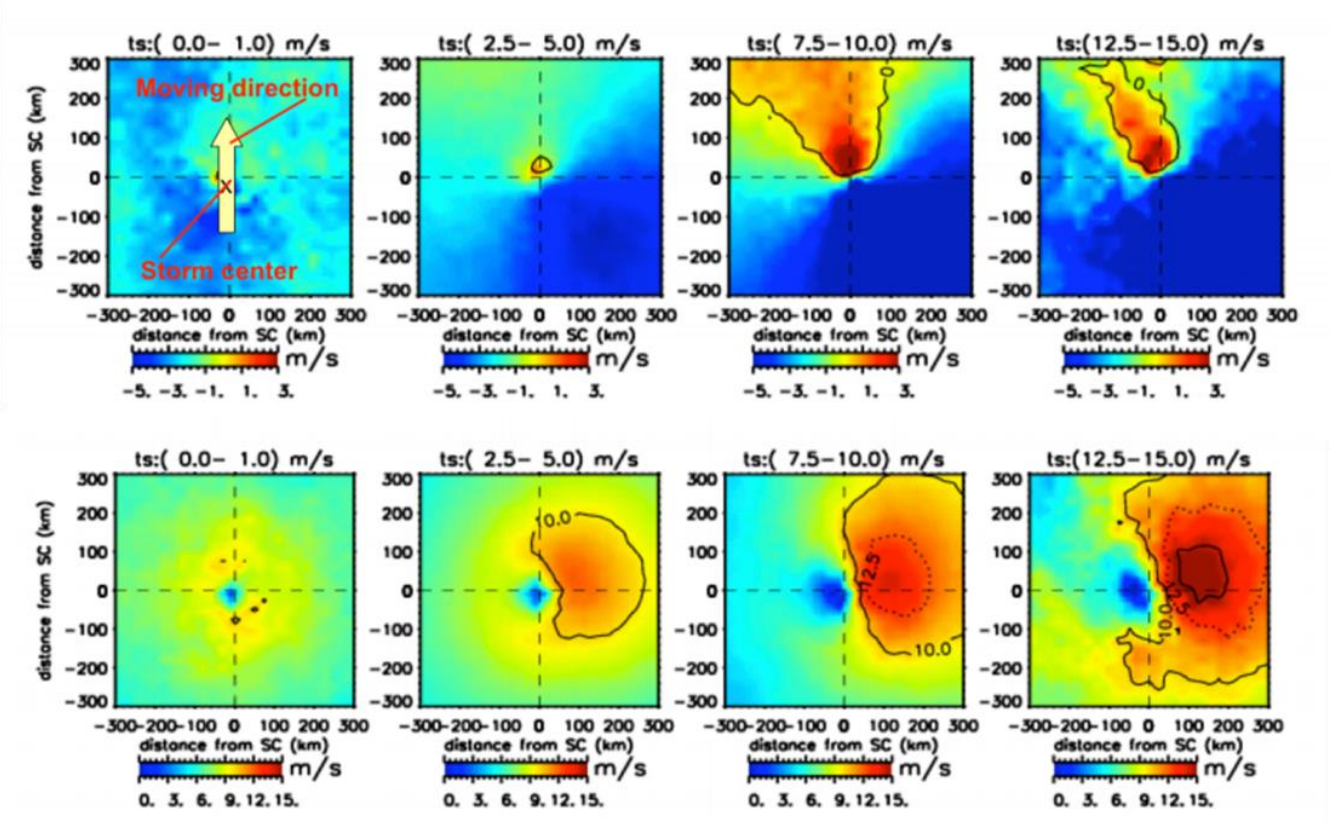

Figure 5-2: Radial (top) and tangential (bottom) wind composites for varying storm translation speeds in the Northern Hemisphere between 2000 and 2007 (Tang and Liu 2009).

Hurricane asymmetry has important implications to a hurricane storm surge model. The surge model used in the Coastal Master Plan suite of simulations is primarily driven by wind and pressure forcing. Therefore, it is important to select storms that represent the diversity of storms that can occur. For instance, a fast-moving, symmetric storm, even with identical maximum wind speeds as a slow moving, asymmetric storm, might inundate an area to a significantly lower level. The slow-moving storm will give water much more time to move through narrow channels and ultimately inundate the broader floodplain to a greater elevation, which may be accentuated in some instances due to the asymmetry.

Upon review, the PBL model takes into account some of these asymmetries. Figure 5-3 shows two storms on identical tracks within the full storm suite discussed in Appendix 2. The storm on the top is moving significantly slower than the storm on the bottom. Notice the difference in structure. The storm on the top is a near perfect set of concentric rings while the storm on the bottom is asymmetric.

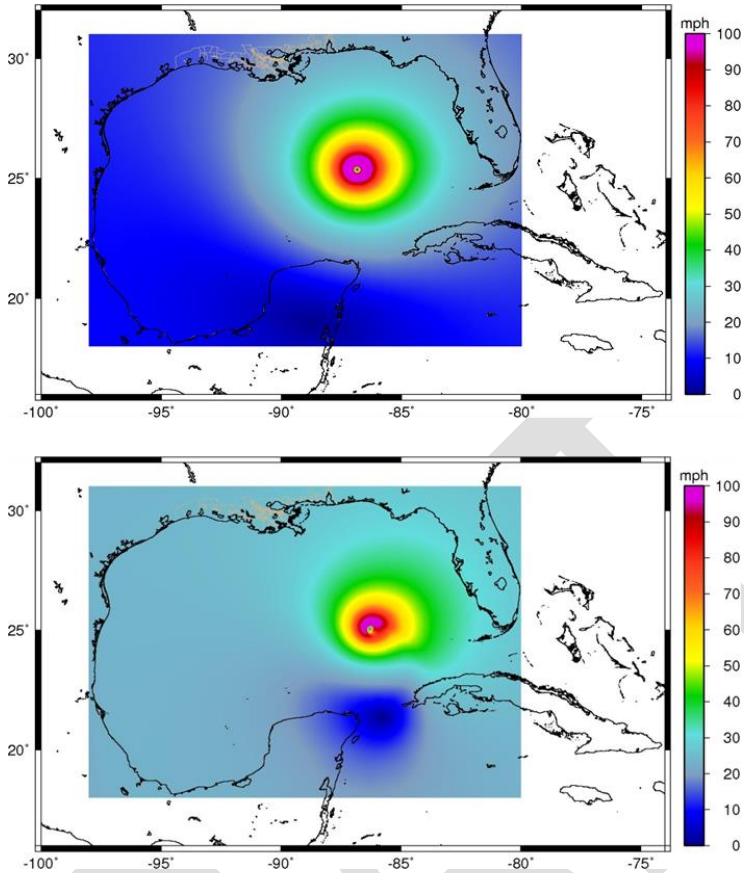

Figure 5-3: Hurricane wind symmetry (top) and asymmetry (bottom) in the PBL model.

At the onset of this task, the team assumed that all storms in the suite from the 2008 Federal Emergency Management Agency study were symmetric. The intention was to better understand the impacts of storm asymmetry to make a recommendation whether CPRA should consider regenerating wind fields with an updated wind model that better incorporates asymmetry patterns into the storm suite. However, upon evaluating the existing storm suite more closely, it has been determined that some faster moving storms already include asymmetry.

Rather than evaluating the topic of asymmetry further, it is recommended that storms with varying forward speed, and thus greater degrees of asymmetry, are incorporated into the final selected suite of storms used in the 2017 Coastal Master Plan.

References

Tang, W. & Liu, W.T. (2009). Dependence of Hurricane Asymmetry and Intensification on Translation Speed Revealed by a Decade of QuikSCAT Measurements. NASA Ocean Vector Wind Science Team Meeting, Boulder, Colorado.